Newer Physical and Chemical Methods of Generating Polymer Films with Macroscopic, Mesoscopic and Nanoscopic Patterns

A dissertation submitted to
Indian Institute of Technology Guwahati
for the degree of Doctorate of Philosophy
in Chemistry

By

Devasish Chowdhury

Department of Chemistry
Indian Institute of Technology Guwahati
Guwahati 781 039, India
February 2004

Dedicated to Baba, Ma and Bulbuli

INDIAN INSTITUTE OF TECHNOLOGY, GUWAHATI

Department of Chemistry

STATEMENT

I hereby declare that the matter embodied in this thesis is the result of investigations carried out by me in the Department of Chemistry, Indian Institute of Technology Guwahati, India under the supervision of Dr. Anumita Paul, Assistant Professor in Chemistry.

In keeping with the general practice of reporting observations, due acknowledgements have been made wherever the work described is based on the findings of other investigations.

I.I.T Guwahati — Devasish Chowdhury

February 2004

INDIAN INSTITUTE OF TECHNOLOGY, GUWAHATI

Department of Chemistry

CERTIFICATE

It is certified that the work contained in the thesis entitled " Newer Physical and Chemical Methods of Generating Polymer Films with Macroscopic, Mesoscopic and Nanoscopic Patterns" by Mr. Devasish Chowdhury, a student of the Department of Chemistry, Indian Institute of Technology, Guwahati, for the award of the degree of Doctor of Philosophy, has been carried out under my supervision and that this work has not been submitted elsewhere for a degree.

I. I. T Guwahati
February 2004

Dr. Anumita Paul
Assistant Professor
Department of Chemistry
IIT Guwahati

INDIAN INSTITUTE OF TECHNOLOGY, GUWAHATI

Department of Chemistry

COURSE CERTIFICATE

This is to certify that Mr. Devasish Chowdhury has satisfactorily completed all the courses required for the Ph. D degree programme. These courses includes:

CH 630	A Fundamental Approach to Physical Chemistry
CH 621	Newer Reagents in Organic Synthesis
CH 611	Bio-inorganic Chemistry
CH 631	Experimental Spectroscopy

Mr. Devasish Chowdhury has successfully completed his Ph. D qualifying examination in February 2001.

Dr. Jubaraj B. Baruah
Head
Department of Chemistry
I. I. T. Guwahati

Dr. Anil Kumar Saikia
Secretary
Departmental Post Graduate Program
Department of Chemistry
I. I. T. Guwahati

Acknowledgment

I am extremely thankful to my supervisor Dr. Anumita Paul for her able guidance and giving direction to my work. It was really a privilege to be her first student. I am also extremely thankful to Dr. Arun Chattopadhyay, who has also been my mentor. The energy he possesses is phenomenal and it has been a constant source of inspiration for me. He is the one who has taught me the first few steps of research. I am thankful to my Institute, Indian Institute of Technology, Guwahati for providing us with the infrastructure and facilities for research. I express my gratitude to faculty members of Department of Chemistry as well as other departments especially Prof. M. K Chowdhuri, Dr. Jubaraj B. Baruah, Dr. B. K. Patel, Dr. A. T. Khan, Dr. M. Ray, Dr. S. Adikari, Dr. D. Chakraborty, Dr. P. S. Robi and Dr. A. Srinivasan for their help and advice. I thank my lab members Tridib, Gitanjali and Lopa for extending help and support. I also take this opportunity to thank my seniors and colleagues for lending their hands of support whenever needed. I am also thankful to the technical assistants of Chemistry, Physics and Mechanical Engineering especially Amritda, Panchananda, Sidanandada, Chandanda, Lokeshda and Ramanandada for providing me with their technical expertise. Thanks are due to IACS, Kolkata and RSIC, Shillong for extending their instrumental facilities. My sincere thanks to CSIR, New Delhi for a fellowship. Last but not least, I thank my patents and sister for their moral support.

Abstract

The underlying theme of the experimental investigations carried out in the present thesis has been to find newer physical and chemical methods of generating polymer films with macroscopic, mesoscopic and nanoscopic patterns. First of all, a new method of formation of thin polyaniline film at the air-water interface is reported. It was observed that during polymerization of aniline coupled to iron (ferroin) catalyzed Beluosov-Zhabotinsky (BZ) reaction had resulted in the formation of thin film of polyaniline at the air-water interface, in addition to polymerization in the bulk. Also, film formation could be observed under non-BZ reaction conditions. The film consisted of macroscopic patterns that varied from film to film. However, each of these films contained mesoscopic patterns, observable under the microscope, which were characteristic of the reaction catalyst.

Further, a new photolithography based method of imprinting of macroscopic patterns on these polymer films was developed by simultaneous chemical and photochemical polymerization of aniline at the air-water interface. The photochemical polymerization was carried out by shining light from the top, while reagents present in the bulk catalyzed chemical polymerization. A mechanism of film formation is also discussed.

In addition, based on the above observations, a new method was developed for incorporation of TiO_2 nanoparticles (NPs) in thin films of polypyrrole. These films were subsequently used in photocalalyzing oxidation of I^- to I_3^- as well as degradation of dyes like methyl orange and methylene blue.

The thesis also reports a simple, versatile and inexpensive soft-lithographic based method of generating submicron - scale colored patterns on various surfaces. The molds used were the polycarbonate disk and aluminum foil line patterns of an ordinary compact disc (CD) and the ink was from commercially available permanent marker pen. Results on single and bi-color line patterns and cross patterns are reported.

A similar strategy was used in sub-micron scale patterning of glass surfaces by chemical reaction etching. In this method chemical etching process was carried out by simply wetting the mold (polycarbonate of compact disc) with the etching solution (aqueous HF) followed by stamping on glass substrates. Micro arrays of non-etched spots on glass substrates were also achieved by stamping twice at different angle to each other.

Abstract

Two related phenomenological investigations were also carried out and the results are reported in the thesis. One of the investigations was to study the wetting and dewetting behavior of surfactant-laden aqueous drops on glass supported alcohol films. The alcohols used were CH_3OH, C_2H_5OH and i-PrOH. It was observed that the drop spread the fastest on CH_3OH followed by C_2H_5OH and the slowest on i-PrOH. On the other hand the recoil behavior was just the opposite. In addition, concentration of surfactant in the drop played a prominent role in the spreading and recoil time of the drop with higher surfactant concentration making the drop spread and recoil faster. There was no significant fingering instability present in either spreading or recoil of the drops on the alcohol films.

Finally, the other phenomenological study discussed in the thesis deals with measuring simultaneously the pressure area isotherms, using a Langmuir – Blodgett film balance with a Wilhelmy plate and the characteristic change in the extinction coefficient of light, over a broad wavelength range in the UV-visible region, using an optical fiber probe as a function of surface pressure. It was observed that at the liquid to solid phase transition and the collapse of the monolayer an abrupt increase and then sudden fall in extinction of light had occurred. Similar extinction of light also occurred during gas to liquid phase transition in lipid monolayers. This could be used as a simple easy to use method for information about the nature of monolayer at any interface (liquid-gas, liquid-liquid), especially formation of special structures leading to monolayer collapse.

Chapter 1

Introduction

1.1 Introduction

Pattern formation is common to biological systems. Nature is full of such patterns, the patterns on the wings of butterfly, on the bodies of zebra, snake or deer. These patterns, the creations of nature, not only are aesthetically beautiful, but also serve important roles in survival such as in camouflaging. Not so apparent to the naked eye, yet under the microscope, patterns are also observed in tissues, such as in bones and muscles, and govern cell growth and cell differentiation. All these patterned growth and formations have important functional roles in the maintenance and propagation of life. Thus the success of life itself can be attributed to Mother Nature utilizing patterns. Technological applications of pattern can be seen in black and white newspaper prints of pictures, where the dot density and size determines the shade and contrast. Pattern formation can be generated spontaneously or non-spontaneously. Spontaneous patterns can be formed merely by mixing of two or more reagents. There are a number of systems where spatial patterns are observed. Pattern formation in reaction-diffusion systems has been investigated for some time and the understanding has important consequences in technological applications. Iodate-arsenous acid system[1], chlorite-thiourea-barium chloride system[2] and sodium hydroxide-copper chloride system [3] are a few known systems to exhibit spatial patterns. Even a photochemical reactions can generate patterns. For example, the photochemical reaction of photochromic and chromogenic compounds show patterns[4]. Oscillatory reactions can also lead to pattern formation. The Belousov-Zhabotinsky reaction (BZ) [5] is one such oscillatory reaction where spatial patterns are observed. Spontaneous pattern formation cannot be controlled in as far as the nature, shape and size of the patterns are concerned. On the other hand non-spontaneous pattern formation can be induced by chemical means as well as by physical means, where the growth conditions can directly influence the nature, size and shape of the patterns concerned. Self-assembled monolayers (SAM) of organic molecule on the selected parts of surface of solids such as self-assembly of organic thiols and disufides on gold, silver and copper surfaces, and carboxylic acids on alumina surface can also lead to large-scale pattern formation. Other methods include utilizing light to generate patterns. For example, a photosensitive material is coated on the surface and by making use of appropriate masks, selective photochemical reaction is achieved at select areas resulting in generation of patterns. The physical methods include soft-lithography, which is the collective name given to techniques based on self-assembly and replica molding, as a low

cost, non-photolithographic approach for generating micro and nano patterns. In this method the master containing the desired relief features is stamped onto the substrate to transfer its features on the substrates. The advantage of such patterns is that we can have control over the nature, shape and size of the patterns generated and thus have immense technological applications. Patterns can be generated on different substrates such as glass, silicon or even polymer surfaces.

As such polymer thin films are of great technological importance due to their applications in microelectronics, displays, lithography [6-13], sensors [14-19], non-linear optical materials [20-21] etc. The requirements have justifiably given rise to the development of a large number of chemical and physical methods for the growth of polymer films on solid surfaces and also at the air-water interface. In addition, various micro-molding techniques have been developed for fabrication of nanoscopically patterned polymer films on solid substrates used mainly for electronics and microfluidic device applications[22-24]. Usefulness of these devices would depend on the robustness of films deposited on a substrate for appropriate applications. This and other requirements have led to a plethora of studies on wetting and dewetting behavior of a thin film on a solid substrate. The thin film can be a polymer film or a liquid drop spread on a surface. Further, film growth at the air-water interface using especially the popular Langmuir-Blodgett (LB) technique requires the study of the properties of monomers at the interface. A large number of techniques such as LB-film balance, optical microscopic method and surface second harmonic generation are available to understand the molecular or collective properties at the interface.

With these applications in mind, I have ventured in my Ph. D. work to find newer and simpler methods of fabrication of functional thin films on substrates and study some of the relevant physical and chemical properties. The methods developed include physical as well as chemical imprinting.

Objectives of the investigations reported in this thesis are as follows:

- To find newer methods of generation of thin polymer films especially at the air-water interface.
- To imprint macroscopic patterns on these films using photolithography.

- To fabricate TiO_2 nanoparticles incorporated films for applications where the nanoparticles would be the functional moiety and the thin film would act as the support.
- To introduce the idea and to achieve sub-micron scale color lithography where a colored polymer is used as the ink.
- To fabricate glass microreactor with sub-micron scale patterns using the principle of soft lithography.
- To study the wetting and dewetting behavior of surfactant-laden aqueous drops on glass supported alcohol films.
- To investigate the collapse of a monolayer of surfactant molecules at the air-water interface using an optical fiber probe.

While pursuing polymerization of aniline coupled to iron (ferroin) catalyzed Beluosov-Zhabotinsky (BZ) reaction we observed the formation of thin film of polyaniline at the air-water interface, in addition to bulk polymerization. Upon closer examination we found that those films formed with macroscopic patterns and generally did not have any specific mesoscopic patterns. Aniline polymerization under non – BZ reaction conditions with the use of $FeSO_4$ or Mohr salt [$(NH_4)_2SO_4$, $FeSO_4.6H_2O$] in place of ferroin was also pursued. In addition, a simple mixture of $KBrO_3$ and KBr in aqueous acidic solution was also used for the polymerization. In all of the above systems we observed the formation of thin films at the air-water interface in addition to bulk polymer formation. All of those films also had macroscopic patterns. Interestingly, the thin films formed under non-BZ reaction condition consisted of distinct mesoscopic patterns, observable under the microscope. The mesoscopic patterns formed were found to be characteristics of the reaction catalyst being used. In addition, we also observed that when sodium dodecyl sulfate was present in the reaction medium within a particular range of concentration, regular circular mesoscopic patterns were formed. Also, no patterns could be observed when the reaction was carried out in the presence of ultrasonic waves. These observations we feel are significant because properties of materials at interface are expected to vary with density and orientation profiles at this scale. These studies have wide ranging technological applications in surface coatings[25-26], synthesis of nanomaterials [27], molecular-scale adhesive, lithography and microfabrication [28].

We went further in this direction and were successful in imprinting macroscopic patterns on these polymer films by simultaneous chemical and photochemical polymerization of aniline in the presence of light at the air-water interface and chemical reagents in the bulk. This is a new photolithography based method of obtaining imprinted polymer film. Herein, we have made use of light as a tool for making imprint on a growing polymer film at the air-water interface. Imprinting patterns as the polymer film grows at air-water interface offers greater control in the synthesis of functional polymer film. Moreover polymer film generated in presence of light might have or might not have the same properties as that generated simply by chemical methods. As a result there may be variations in the properties of the 'photo-grown' polymers, which can be tuned by selecting appropriate monomer, wavelength of incident light and chemical reagents that catalyze the polymerization reaction. Thus polymer film generated at interface could possibly have patterned variations in optical, electronic, chemical and even mechanical properties characterized by thickness variations or otherwise across the film. This has the unique advantage over other methods as this could lead to better control over size, shape and nature of patterns formed onto the films by controlling parameters, from above the surface for light catalyzed polymerization, and from the bulk below for the chemical polymerization. We were successful in making imprint on polymer film at air-water interface in the presence of light consisting of imprint in the shape and size of the light beam. The method makes use of simultaneous chemical and photochemical polymerization of aniline in the presence of light. The imprints could be obtained using light over a wide-range: from UV to visible wavelengths.

Encouraged by the success of thin polymer film formation at the air-water interface from chemical reagents present in the bulk and the simultaneous chemical and photochemical polymerization at the interface, we tried and successfully incorporated TiO_2 nanoparticles (NPs) in thin films of polypyrrole. We could not obtain thin film of polyaniline under the experimental condition used in the present case with the use of H_2O_2. The TiO_2 NP containing polypyrrole thin films were further used to photocalalyze oxidation of I^- to I_3^- as well as reduction of dyes like methyl orange and methyline blue. These results are reported in Chapter 4.

Although photolithography[29] has been the most successful and popular method to make patterns on various substrates for technological applications, it inherently suffers from two limitations. Firstly due to practical limitation the minimum feature size that is

obtained is equal to the wavelength of the light used even though the theoretical limit set by optical diffraction is λ/2. Secondly the technology is very expensive especially for feature sizes below 200 nm. This has resulted in exploration of other alternative cheaper methods, the prominent being soft lithography[30-32], micropen lithography, dip pen nanolithography[33] and nanosphere lithography[34]. But none of the methods emphasized the generation of color pattern that has enormous application potential in information storage, sensors and so-called " E-Paper" for display. If information could be stored in true color, the processing time for retrieval of information could be shortened considerably. Based on soft-lithography, we have introduced a simple, versatile and inexpensive method of generating submicron - scale colored patterns on various surfaces. The molds used were the polycarbonate disk and aluminum foil line patterns of an ordinary compact disc (CD). We had started making patterns on glass and plastic substrates using single color but then extended it and made bi-color patterns also. We were also successful in making micro arrays of ink positioned at angles determined by the relative angle of sequential positioning of molds.

Similar strategy was used in patterning glass surfaces following the same approach of soft lithography in making color patterns. These patterned glass surfaces have the potential of being used as microfluidic devices with applications in biological analysis[35-36], chemical assays and environmental analysis and as microreactors[37] that can manipulate and analyze materials on nano and subnano liter scales. These technological applications have stimulated us to device a new method to pattern glass. The method makes use of chemical etching process by simply wetting the mold (polycarbonate of compact disk) with the etching solution (aqueous HF) followed by stamping on glass substrates. Micro arrays of non-etched spots on glass substrates were also achieved by stamping twice at right angle to each other.

A few related phenomelogical investigations were also carried out. In this regard, we pursued the controllable spreading and recoil of surfactant containing water drops on various alcohol films supported on glass slides. The time evolution of spreading and recoil behavior was also monitored. It was observed that the drop spread the fastest on CH_3OH followed by C_2H_5OH and the slowest on i-PrOH. On the other hand the recoil behavior was just the opposite. In addition, concentration of surfactant in the drop played a prominent role in the spreading and recoil time of the drop with higher surfactant concentration making the drop spread and recoil faster. Interestingly, the drop spread and

recoiled without the formation of any fingering instability otherwise observed in many spreading and recoil phenomena.

Yet another phenomenological study discussed in the thesis deals with simultaneously measuring the pressure area isotherms, using a Langmuir – Blodgett film balance with a Wilhelmy plate and the characteristic change in the extinction coefficient of light over a broad wavelength range in the UV-visible using an optical fiber probe as a function of surface pressure. It was observed that at the liquid to solid phase transition and the collapse of the monolayer an abrupt increase and then sudden fall in extinction of light had occurred. This could be due to formation of multilayer-like structures followed by collapse and molecules going into the bulk phase thereby reducing the population of molecules per unit area for such a layer at the interface. This may have important applications for in situ studies on the formation of structures of monolayers at the air-water or other interfaces.

1.2 References

1. Pojman, J. A.; Epstein, I. R.; McManus, T. J.; Showalter, K. *J. Phys. Chem.* **1991,** 95, 1299.
2. Hauser, M. J. B.; Simoyi, R. H. *Physics Letters A*, **1994,** 191, 31.
3. Hantz, P. *J. Phys. Chem B.* **2000,** 104, 4266.
4. Gimenez, M.; Micheau, J.-C. *Naturwissenschaften*, **1983,** 70, 90.
5. Gray, P.; Scott, S. K. *Chemical Oscillations and Instabilities, Non-linear Chemical Kinetics, Oxford University Press, Oxford,* **1990.**
6. Schmid, H.; Michel, B. *Macromolecules*, **2000,** 33, 3042.
7. Chen, X.; Tolbert, L. M.; Hess, D. W.; Henderson, C.; *Macromolecules*, **2001**, 34, 4104.
8. Aoki, A.; Ghosh, P.; Crooks, R. M. *Langmuir*, **1999**, 15, 7418.
9. Denis, F. A.; Hanarp, P.; Sutherland, D. S.; Dufrene, Y. F. *Nano Lett*.**, 2002**, 2, 1419.
10. Ionov, L.; Minko, S.; Stamm, M.; Gohy, J.-F.; Jerome, R.; Scholl, A. *J. Am. Chem. Soc.***, 2003**; 125, 8302.

11. Zhang, F.; Nyberg, T.; Inganas, O. *Nano Lett.*, **2002**, 2, 1373.

12. Salavagione, H. J.; Miras, M. C.; Barbero, C. *J. Am. Chem. Soc.*, **2003**, 125, 5290.

13. Ng, H. T.; Foo, M. L.; Fang, A.; Li, J.; Xu, G.; Jaenicke, S.; Chan, L.; Li, S. F. Y. *Langmuir*, **2002**, 18, 1.

14. McQuade, D. T.; Pullen, A. E.; Swager, T. M. *Chem. Rev.*, **2000**, 100, 2537.

15. Lu, X.; Manners, I.; Winnik, M. A. *Macromolecules*, **2001**, 34, 1917.

16. Hillebrandt, H.; Tanaka, M.; Sackmann, E. *J. Phys. Chem. B.*, **2002**; 106, 477.

17. Haupt, K.; Mosbach, K.; *Chem. Rev.*, **2000**; *100*, 2495.

18. McQuade, D. T.; Hegedus, A. H.; Swager, T. M. J. *Am. Chem. Soc.* **2000**; 122, 12389.

19. Ferreira, M.; Riul, A., Jr.; Wohnrath, K.; Fonseca, F. J.; Oliveira, O. N., Jr.; Mattoso, L. H. C. *Anal. Chem.* **2003**; 75, 953.

20. Shin, Y-T.; Shin, S-W.; Shin, J.; Lee, K.; Cha, M. *Thin Solid Films* **2000,** 360, 13.

21. Alain, V.; Fort, A.; Barzoukas, M.; Chen, C-T.; Blanchard-Desce, M.; Marder, S. R.; Perry, J. W. *Inorganica Chimica Acta* **1996,** 242, 43.

22. Lahann, J.; Balcells, M.; Lu, H.; Rodon, T.; Jensen, K. F.; Langer, R.; *Anal. Chem.* **2003**, 75, 2117.

23. Hasselbrink, E. F., Jr.; Shepodd, T. J.; Rehm, J. E. *Anal. Chem.* **2002**, 74, 4913.

24. Hu, S.; Ren, X.; Bachman, M.; Sims, C. E.; Li, G. P.; Allbritton, N.; *Anal. Chem.* **2002**, 74, 4117.

25. Li, W.; Hooks, D. E.; Chiarelli, P.; Jiang, Y.; Xu, H.; Wang, H-L. *Langmuir* **2003,** 19, 4639.

26. Korbel, G. A.; Lalic, G.; Shair, *J. Am. Chem. Soc.* **2001,** 123, 361.

27. Feng, W.; Sun, E.; Fujii, A.; Wu, H.; Niihara, K.; Yoshino, K. *Bull. Chem. Soc. Jpn.* **2000,** 73, 2627.

28. Jiang, X.; Zheng, H.; Gourdin, S.; Hammond, P. T. *Langmuir* **2002,** 18, 2607.

29. Wallraff, G. M.; Hinsberg, W. D. *Chem. Rev.* **1999,** 99, 1801.

30. Xia, Y.; Whitesides, G. M. *Annu. Rev. Mater. Sci.* **1998**, 28, 153.

31. Xia, Y.; Whitesides, G. M.. *Angew. Chem. Int. Ed.* **1998,** 37, 550.

32. Xia, Y.; Rogers, J. A.; Paul, K. E.; Whitesides, G. M.; *Chem. Rev*. **1999**, 99, 1823.

33. Ivanisevic, A.; Mirkin, C. A. *J. Am. Chem. Soc.* **2001**, 123, 7887.

34. Malinsky, M. D.; Kelly, K. L.; Schatz, G. C.; Van Duyne, R. P. *J. Phys. Chem. B* **2001,** 105, 2343.

35. Wheeler, A. R.; Throndset, W. R.; Whelan, R. J.; Leach, A. M.; Zare, R. N.; Liao, Y. H.; Farrell, K.; Manger, I. D.; Daridon, A. *Anal. Chem.* **2003,** 75, 3581.

36. Khan, M. A.; Armes, S. P. *Adv. Mater*. **2000,** 12, 671.

37. Kikutani, Y.; Hibara, A.; Uchiyama, K.; Hisamoto, H.; Tokeshi, M.; Kitamori, T. *Lab Chip* **2002,** 2, 193.

Chapter 2

Thin Film Formation due to Polymerization of Aniline at Air-Water Interface

2.1 Introduction

Understanding chemistry at the interface offers rich dividends in terms of technological applications in areas such as polymer microelectronics, surface coatings[1], thin films[2], nanomaterials[3-5], molecular-scale adhesive [6], lithography and microfabrication[7] Interface tailored synthesis of materials, especially polymers, has attracted much attention because of its ability to generate oriented molecular materials [8]. Thin films with designed molecular order can exhibit properties different from the collective bulk behavior of molecules in a restricted geometry. In the past, organic thin films were considered to be too fragile and not of sufficient purity to yield reliable and consistent properties and thus were of not much use. The situation has however considerably changed with the advent of polymer thin films. Polymer thin films can have chemical inertness, mechanical strength, varying wettability and specific electrical, optical and magnetic properties. In addition, these properties could be tuned by appropriate changes at the molecular level of the monomer. The vast application potential has led to enormous growth in the methods of generation of thin polymer films and understanding of the growth processes as well as the properties of thin films as a function of their structural details at various length scales. Among the polymers studied in this regard, conducting polymers such as polyaniline (PANI), polypyrrole and polythiophene occupy a central position owing to their technological relevance.

PANI is the preeminent electrically conducting polymer that has been extensively investigated due to its application potential in microelectronics [9-12], displays[13], electrodes[14-15], sensors and actuators[16], membranes for gas separations[17-18], solar cells[19], fuel cells[20] and electro-magnetic interference (EMI) shielding[21-22]. PANI is known to undergo non-redox reversible doping / dedoping process[23] based on simple acid base chemistry, enabling control over properties like optical activity, electrical conductivity and sensor activity, thus making it unique in the class of conjugated polymers. As a natural consequence of its utility, several synthetic protocols have been developed such as functionalization of PANI backbone[24-25], enhancement of biocompatibility of the polymer using enzymes as catalysts for synthesis[26-27], synthesis of PANI nanofibers, nanotubes[28-29], metal nanoparticle-PANI composite[30] and cabon nanotube doped PANI [31]. An "insulated molecular wire"[32] inclusion complex of PANI in cyclodextrin has also been synthesized. Some of the important applications of PANI as sensor are its use as ammonia vapor sensor[33], glucose biosensor[34] and ascorbic acid sensor[35]. In general, a sensor is made in the

form of a thin film of PANI on a substrate. Typically, thin films are made by spin casting, spraying, fiber spinning, electrospinning, electrochemical polymerization on the surface, dip-coating and Langmuir-Blodgett film transfer technique. Further, PANI thin films and microtubules have been grown in porous membranes for application as sensors[4]. PANI has also been synthesized electrochemically inside ordered macroporous carbon[36].

Notwithstanding the huge growth with respect to synthesis, processing and application of PANI there remains plenty of opportunity for further investigation especially with respect to thin film formation and its properties. For example, even though enzymatic synthesis of thin film of PANI at the air-water interface has been achieved[26-27], a simple chemical means of such film formation has not been pursued so far. This has important implications in terms of it chemical, mechanical, optical, electronic and magnetic properties, especially upon incorporation of appropriate dopants. We have sought to investigate the formation of thin films of PANI due to polymerization of aniline at the air-water interface in the presence of reactants in bulk water. We have studied the growth in the presence of various chemical reagents and also probed the structural characteristics of the films grown under different conditions. One of the important observations was the macroscopic and mesoscopic pattern formation in the grown thin films. Therefore, a little bit of background with respect to pattern formation in different chemical reactions would be appropriate at this point.

Spatio-temporal pattern formation in chemical reactions is well known for a long time. Pattern formation has been observed in chemical reactions like chlorite-thiourea-barium chloride reaction, NaOH and $CuCl_2$ reaction. It has also been observed in oscillatory chemical reactions such as Beluosov-Zhabotinskii reaction.

Pattern formations in chemical reactions are usually governed by reaction-diffusion processes. A spatially extended system will often undergo a transition from a uniform state to a state with spatial variations due to non-equilibrium conditions. Non-equilibrium conditions also lead to hydrodynamic instability at the interface and are caused by a number of non-linear phenomena such as Marangoni convection, Benard - Marangoni convection, Rayleigh - Benard convection, thermocapillary convection and thermal convection. These instabilities exhibit a large variety of convection patterns, such as regular convection structures in the forms of cells and rolls, interfacial waves and chaotic convective motions in the vicinity of an interface. Pattern formation in general occurs due to coexistence of more than one type of convection. The phenomenon of convection of

fluid motion induced by buoyancy when a fluid is heated from below is called Rayleigh-Benard convection. Rayleigh-Benard convection is the instability of a fluid layer which is confined between two thermally conducting plates and is heated from below to produce a fixed temperature difference. Marangoni convection on the other hand is surface tension driven. It generally coexists with Rayleigh's buoyancy mechanism but dominates in thin layers. Instability mechanism involving gradients in surface tension coexisting with Rayleigh's buoyancy mechanism is called Benard- Marangoni convection. In this case solvent evaporation can also induce Benard- Marangoni convection [37]. In the Benard-Marangoni system, pattern formation is governed by the balance of the surface tension driven forces and dissipation due to thermal diffusion and the frictional action of viscosity. The gradient in surface tension can also be induced by variation in concentration of components leading to Marangoni convection. Other convections include thermal convection, which occurs due to temperature gradient. The patterns formed in photochemical reaction are generally due to thermal convection [38-39] although there may be other convection operating simultaneously. The driving force for thermal convection in such systems is the existence of a temperature gradient and hence the density distribution. Temperature gradient can also be caused by exothermic reaction. The evolution of heat affects the surface tension of the solutions, which, in turn may also induce convection. Thermal convection induced by in-homogeneities in surface tension always occurs if there is a free surface of the liquid against a gas or against another liquid and if there are inhomogeneities at the border surface. Since the surface tension is temperature depended ($\partial s / \partial T \neq 0$), heat produced by the chemical reaction generates surface tension gradient, which can give rise to thermocapillary convection [40]. Chemical reaction with autocatalytic or thermal feedback can combine with the diffusive transport of molecules to create a spatial or temporal pattern [41-43]. An example of spatial or temporal pattern formed due to chemical reaction is Belousov-Zhabotinskii (BZ) reaction [44-48]. It is also a classic example of 'far from equilibrium' behavior that of long lived oscillations. The BZ reaction comprises of the reduction of bromate ion (BrO_3^-) by bromide (Br^-) to bromine (Br_2) in the presence of a metal redox catalyst (usually Ce^{3+}/ Ce^{4+} or Fe^{2+}/ Fe^{3+}). The system also contains an organic substrate e.g malonic or citric acid capable of reacting with the intermediate product Br_2 and then being subsequently oxidized to return Br^-. The oscillations are characterized by a switching between the bromide ion concentration

leading to oscillations in the color of the mixture. Photochemical reaction can also induce oscillation in a reaction system[49-50].

2.1.1 Our direction

Pojman and coworkers [51-52] have reported in detail polymerization coupled to BZ reaction in a batch reactor. However, their study emphasized on the solution behavior of periodic polymerization coupled to BZ reaction. On the other hand in this chapter we report observation of patterns in thin polymer films of PANI formed at the interface coupled to reactions in the bulk medium. Although originally this work was started with the aim of possible observation of specific pattern formation due to polymerization of aniline coupled to the iron-catalyzed Belousov-Zhabotinskii (BZ) reaction in the bulk medium, our observations of similar pattern formation under non-oscillatory reaction conditions suggests that the pattern formation was not exclusive to the non-linear BZ reaction. To test the idea, we also pursued and obtained aniline polymerization under non – BZ reaction conditions in which $FeSO_4$ or Mohr salt $[(NH_4)_2SO_4.FeSO_4.6H_2O]$ had been used instead of ferroin. In addition, a simple mixture of $KBrO_3$ and KBr in aqueous acidic solution was used for polymerization. Two – dimensional macroscopic patterns formed from all reactions mentioned above and not exclusively due to BZ reaction.

We found that, if left undisturbed, anilinium sulfate in the presence of BZ reaction mixture led to the formation of polyaniline in the bulk, which finally had settled at the bottom of the solution. On the other hand there was also the formation of a thin polyaniline film at the air – water interface. While the bulk polymer was found to be devoid of any patterns, the film at the interface had rich macroscopic as well as mesoscopic patterns. This is the first report of any pattern formation in two-dimensional growth of polymeric materials at interfaces. This is important as properties of materials are expected to vary with density and orientation profiles of materials in thin films. The patterns formed in films are characteristic of the reaction conditions in the bulk and hence have the prospect of acting as markers of the chemical reaction events leading to product formation at interfaces. UV-visible and FTIR spectroscopic observations indicated the formation of low molecular weight polyaniline which was further confirmed by gel permeation chromatography. It is important to mention here that when a typical reaction was carried out in the presence of 2.02 mM sodium dodecyl sulfate regular circular mesoscopic patterns were formed in the film, while the patterns had vanished when the

reaction was carried out in the presence of ultrasonic waves. Our essential conclusion is that the polymerization at the interface occurs simultaneously at various nucleation-like centrers. As the polymer grows in two-dimensions, the centers get connected by a network, leading to the formation of mesoscopic patterns. The catalysts and reagents present at the interface generally control the nature of the patterns.

2.2 Experimental Section

Chemicals: Potassium bromate ($KBrO_3$) (Aldrich), Malonic acid (Aldrich), Potassium bromide (KBr) (Aldrich), 1,10 Phenanthroline (S.D. Fine Chemicals), Sulfuric acid (H_2SO_4) (E-Merk), Ferrous sulfate ($FeSO_4$) (EMerk), Mohr's Salt [$(NH_4)_2SO_4$. $FeSO_4.6H_2O$)] (E-Merk) and sodium dodecyl sulfate (SDS) (E-Merk) were purchased from companies mentioned in the parentheses and were used as received.

Stock solutions of Potassium bromate ($KBrO_3$), malonic acid, Potassium bromide (KBr), Ferroin, sulfuric acid (H_2SO_4), Ferrous sulfate ($FeSO_4$), Mohr's Salt and sodium dodecyl sulfate (SDS) were prepared in distilled water. The concentration of stock solution were as follows $[KBrO_3]$ = 0.3815 M, [KBr] = 0.014 M, [Malonic Acid] = 0.3005 M, $[FeSO_4.7H_2O]$ = 5.39 X 10^{-3} M, [1,10 Phen] = 0.0140 M, $[H_2SO_4]$ = 0.783 M. In general, aqueous solutions of $KBrO_3$, KBr, malonic acid, ferroin (or other catalysts and SDS as required in the study) and aniline dissolved in H_2SO_4 were mixed in a test tube and poured over a watch glass kept in contact with water in a petridish. The sequence of adding of the reagents was also in that order. The watch glass was covered with an inverted petridish to minimize the effect of air breeze on the interfacial polymerization pattern formation. The exact experimental set-up is depicted in Figure 2.1

The system studied were as follows

System 1: $KBrO_3$ + KBr +H_2SO_4 + Malonic Acid + $Fe(Phen)_3$ + aniline.

System 2: $KBrO_3$ + KBr +H_2SO_4 + Malonic Acid + $FeSO_4.7H_2O$ + aniline.

System 3: $KBrO_3$ + KBr +H_2SO_4 + Malonic Acid + Mohr's salt + aniline.

System 4: $KBrO_3$ + KBr +H_2SO_4 + aniline.

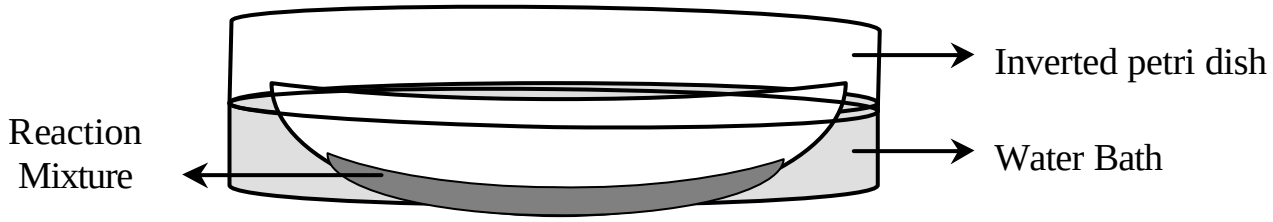

Figure 2.1: A schematic representation of the experimental set up consisting of reagents in a watch glass kept over a petridish water bath. The watch glass was further covered with an inverted petridish.

System 5: $KBrO_3$ + KBr +H_2SO_4 + Malonic acid + $FeSO_4.7H_2O$ + aniline (Vapor).

System 6: $KBrO_3$ + KBr +H_2SO_4 + Malonic acid + Mohr's salt + aniline (Vapor).

In certain set of studies aniline was also introduced into the reaction mixture from the vapor phase. In these cases the inverted petridish cover was replaced by an inverted funnel from where a vial containing aniline had been kept hanging, above the water level as shown in Figure 2.2. The opening of the inverted funnel was covered to minimize the effect of any breeze. The temperature of the bath was generally between 23^o and 27^{o}C during the course of all the reactions.

Film formation at the air – water interface was generally observed in about 15 minutes of mixing reactants. Films formed with aniline reactant in aqueous phase were sufficiently thick for transfer to microscope slides after about 1½ hour of reaction. On the other hand the polymer films obtained via introduction of aniline from vapor phase were ready for transfer in about 3 hours. The films once deemed ready to transfer were made to float above the watch glass by pouring water carefully into the petridish. After a few cycles of water draining and refilling, the films were carefully transferred to microscope slides. The film thickness was measured with the help of an optical microscope by focusing at the top surface of the film and the top surface of the slide. The difference in height was taken to represent the approximate film thickness.

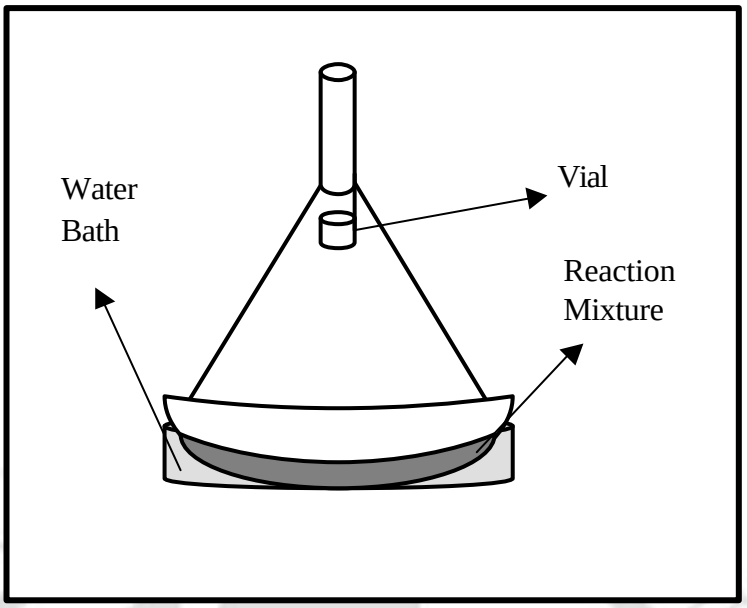

Figure 2.2: A schematic diagram of the experimental set up for vapor phase introduction of aniline to the reaction. All other reagents were in a watch glass kept over a petridish. water bath. Aniline was kept in a vial hanging from an inverted funnel that covered the reagent watch glass.

To carry out reaction in presence of ultrasonic waves, the watch glass containing reaction mixture of $KBrO_3$, KBr and aniline in H_2SO_4 was kept in contact with water in an ELMA (Model Transonic 460 / H, 35 KHz) ultrasonicator bath for about 1½ hour. The film grown at the interface was transferred to a microscope slide as above.

The macroscopic patterns were recorded either by taking photograph and then scanning the photographs by a HP5200C scanner or by using the scanner only. The optical micrographs were recorded by a Carl Zeiss (Axiotech) microscope. The colors in the micrographs are not due to any color of the film material but due to interference of light in the thin polymer layers. UV-visible spectra of films transferred on to sapphire discs were recorded by a Hitachi 2001 UV-visible spectrophotometer. To record Fourier Transform Infrared spectra of polymers, a batch of films grown under identical reaction condition were collected and washed with water and filtered. The solid was then collected and dried in a Silica Gel desicator for five hours before recording spectra in KBr pellet. A Nicolet IMPACT 410 FTIR spectrophotometer was used for recording IR spectra. Samples prepared for FTIR analysis were also used for recording Gel Permeation Chromatography data in a Waters HPLC-GPC system.

2.3 Results and Discussion

2.3.1 Film formation

When the reagents were mixed and poured in a watch glass and left undisturbed, a film formation at the interface was observed along with the product formation in the bulk. The film formation was not observed in absence of aniline in the reaction mixture. The film was transferred to a microscopic slide when it was sufficiently thick to be transferred and examined. For a typical film 1½ hr of reaction time was needed to elapse before the film could be transferred. Figure 2.3 shows photographs of four films that were transferred to microscopic slides. As evident from the photographs, macroscopic two - dimensional patterns were present in all the films that were formed from aniline introduced either directly into the solution phase or from the vapor phase. The patterns formed in the films did not have any specific symmetry. On the other hand they were rather random in their growth profile. In some cases, smaller regions of growth of particular shapes were separated by wide gaps consisting of simple growth with no specific observable patterns. These could be seen in the case of B-Z reaction mixture or $KBrO_3$ / KBr reacting system. On the other hand, continuous long - range growth of specific patterns with relatively narrower gaps were also observed, as is the case with $FeSO_4$ containing reaction mixture.

It is also important to note that such patterns were also seen in the case of films grown from aniline introduced from the vapor phase (Mohr's salt containing mixture as in Figure 2.3). In all cases probably multiple layers of patterned film growth took place based on the formation of patterns at the initial stages. In other words, if the pattern of a film between two consecutive layers were different, the film patterns would have been smoother than it appears. It is conceivable that patterns generated at the initial stages of film formation act as templates for further growth and thus patterns remain constant once it is formed even if further growth of polymer takes place. Further, there is no diffusion of products across the surface once the films are formed, otherwise destruction of pattern formed initially would have occurred. In other words, the nature of pattern formed is "frozen" at the interface in the initial stages of film formation. It is important to mention here that we have not been able to reproduce exact macroscopic patterns even under identical experimental condition. This non - uniformity in macroscopic pattern formation suggests that no simple or single mechanism of patterned growth of polymers at the

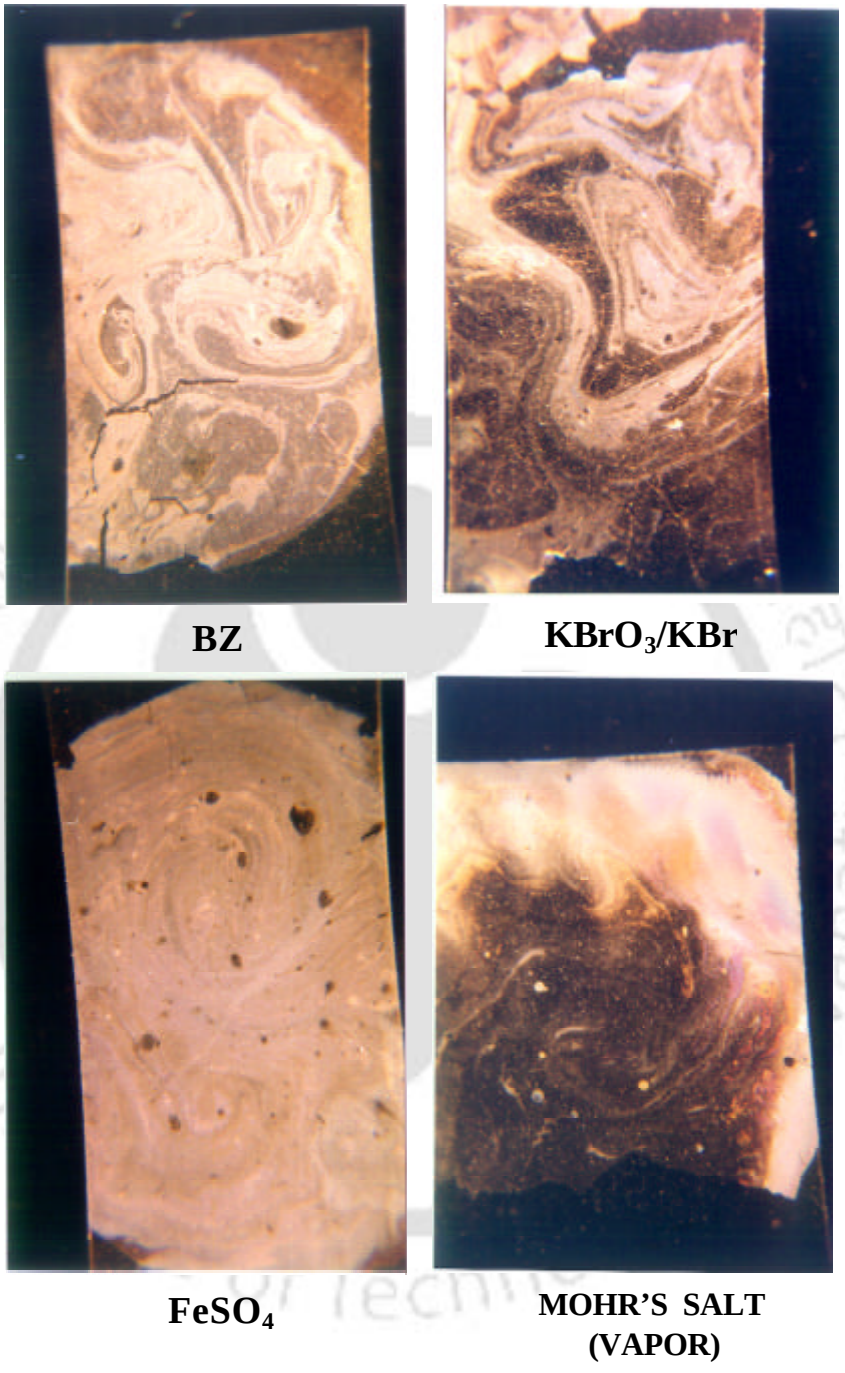

Figure 2.3: Photographs of a few films taken after transferring them to microscope slides (1.0 in.). **BZ:** 1.0 mM $[Fe(Phen)_3]^{3+}$, 0.12 M $KBrO_3$, 0.1 mM KBr, 0.3 M H_2SO_4 0.01 M Malonic Acid and 4.07 mM aniline. **$KBrO_3$ / KBr:** 0.12 M $KBrO_3$, 0.1 mM KBr, 0.3 M H_2SO_4 and 4.07 mM aniline **$FeSO_4$:** 1.0 mM $FeSO_4$, 0.12 M $KBrO_3$, 0.1 mM KBr, 0.3 M H_2SO_4 0.01 M Malonic Acid and 4.07 mM aniline. **Mohr's Salt (vapor):** 1.0 mM $(NH_4)_2SO_4$. $FeSO_4.6H_2O$, 0.12 M $KBrO_3$, 0.1 mM KBr, 0.3 M H_2SO_4 0.01 M Malonic Acid and aniline vapor

interface is involved. However, right now we are not in a position to explain the exact origin of macroscopic pattern formation from the above observations.

Although the reaction also took place in the bulk, our experimental observations suggest that the polymer film formation was due to reaction at the interface and not due to products initially formed in the bulk followed by migration to the surface by diffusion or convection. This is supported by the observation that when a glass slide was kept in contact with the water surface, the polymer film formation was not observed underneath the glass slide at the glass-water interface. When the glass slide was lifted after films were formed at other parts of the interface, no film could be observed on the surface that was beneath the glass slide. Also, there was no film on the glass surface. On the other hand the polymer film formed at other parts of the air – water interface and in the bulk. In addition, when the reaction was carried out in a 25μm cuvette, which was made by placing a Teflon spacer in between two glass slides, there was no film formation at the glass - water interface, whereas bulk reaction occurred to produce the polymer. In addition, similar patterns were observed in the film formed at the interface when the reaction was carried out in a chamber previously purged with gaseous nitrogen indicating that the pattern formation could also occur in presence of an inert atmosphere above the solution.

We also report that when the polymerization reaction in the bulk in presence of BZ reaction condition was followed by UV-visible spectroscopy (in an ordinary optical cuvette), continuous growth of polymers was observed. There was no oscillation in the absorbance in the spectra. Hence the BZ reaction must have been in a non-oscillatory domain for the polymerization of aniline.

2.3.2 UV – visible spectroscopic studies

UV – visible absorption spectra of a few films formed under various reagent conditions are shown in Figure 2.4. Absorption spectra were taken after transferring the film onto a sapphire disk. Figure 2.4 E represents the UV – visible absorption spectrum of polymeric film developed by vapor phase introduction of aniline. All other spectra are due to films grown from aniline introduced directly into the solution phase. It is noteworthy that the major absorption peaks of all films fall below 400 nm. There is though a little variation in the peak positions depending on the nature of the reagents used. For example,

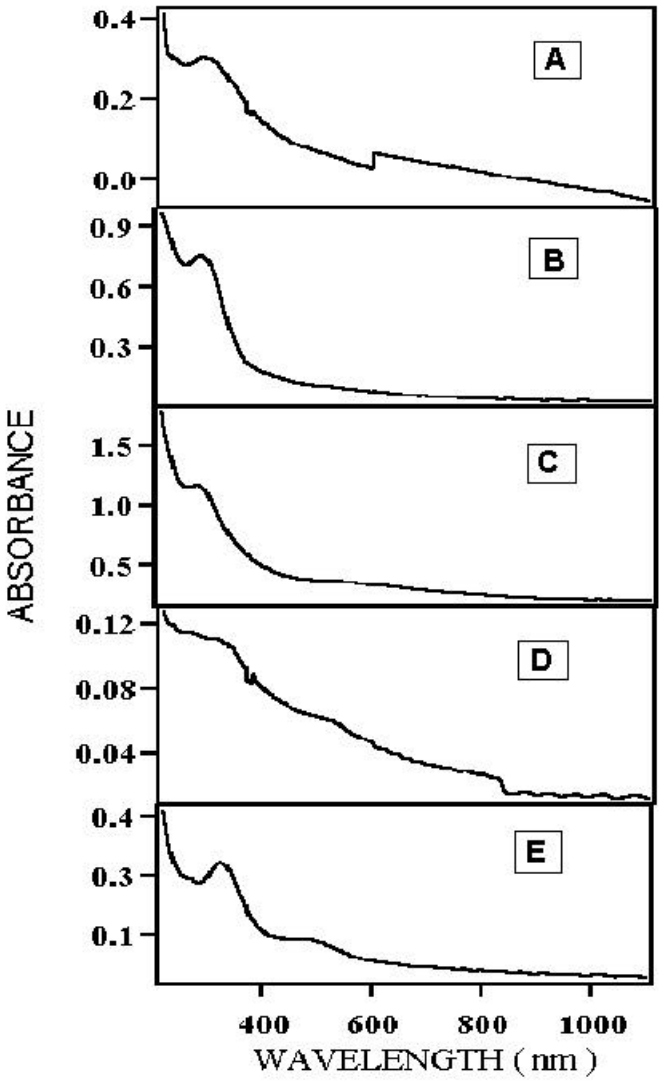

Figure 2.4: UV-visible absorption spectra of polyaniline films produced from different reagent mixtures as given below. Absorption spectra were taken after transferring the film onto a sapphire disk. **[A]** Mohr's Salt: 1.0 mM $(NH_4)_2SO_4$, $FeSO_4.6H_2O$, 0.12 M $KBrO_3$, 0.1 mM KBr, 0.3 M H_2SO_4, 0.01 M Malonic Acid and 0.011M aniline. **[B]** $KBrO_3$ / KBr: 0.12 M $KBrO_3$, 0.1 mM KBr, 0.3 M H_2SO_4 and 0.011M aniline. **[C]** $FeSO_4$: 1.0 mM $FeSO_4$, 0.12 M $KBrO_3$, 0.1 mM KBr, 0.3 M H_2SO_4, 0.01 M Malonic Acid and 0.011M aniline. **[D]** BZ: 1.0 mM $[Fe(Phen)_3]^{2+}$, 0.12 M $KBrO_3$, 0.1 mM KBr, 0.3 M H_2SO_4, 0.01 M Malonic Acid and 0.011M aniline. **[E]** BZ (Vapor): 1.0 mM $[Fe(Phen)_3]^{2+}$, 0.12 M $KBrO_3$, 0.1 mM KBr, 0.3 M H_2SO_4, 0.01 M Malonic Acid and aniline introduced from Vapor phase

when Mohr's salt was used the absorption maximum in the 200 – 400 nm region appeared red - shifted compared to that of the film from $FeSO_4$.

This variation may be due to difference in molecular weight and or branching of the polymers formed. In some cases, peak between 400 and 600 nm could also be observed (Figure 2.4C through E), albeit weak, typically corresponding to branched, low molecular weight form of polyaniline[27].

2.3.3 FTIR spectroscopic studies

A typical FTIR spectrum of a polymer film grown in presence of acidic $KBrO_3$ / KBr reagents is shown in Figure 2.5. A broad peak due to quinoid and benzenoid ring deformations in the region of 1570 - 1500 cm^{-1} could be observed. A band at 1160 cm^{-1}, characteristic of polyaniline emaraldine base could also be observed [53]. There is no indication of Br incorporation in the polymer as the characteristic peaks due to C-Br stretch in the region 600 – 500 cm^{-1} is absent. FTIR spectra of films formed under other reaction conditions appeared similar to that in Figure 2.5.

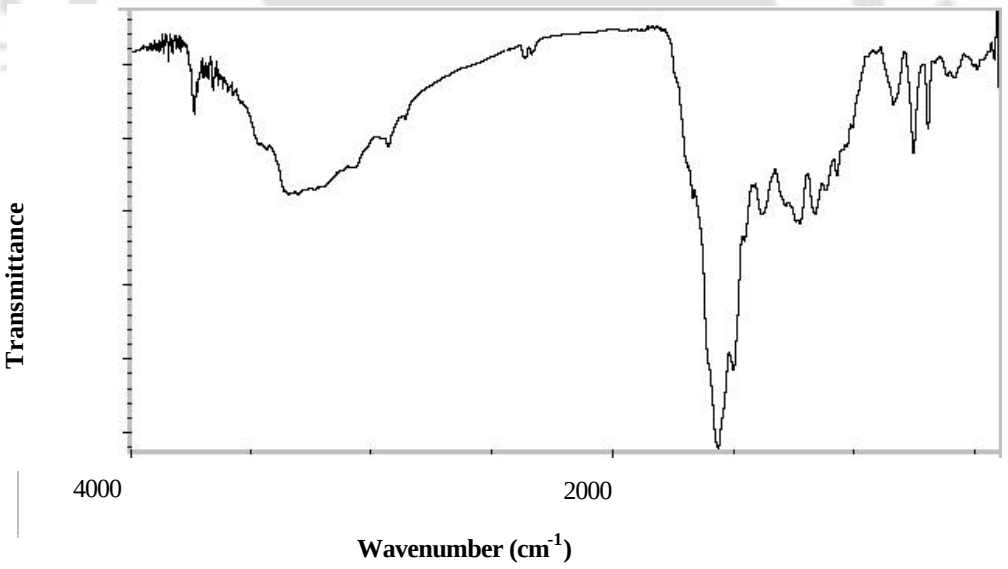

Figure 2.5: FTIR spectrum of thin polymer film grown in presence of acidic $KBrO_3$ / KBr and recorded in KBr pellet. The concentration of different reagents are 0.12 M $KBrO_3$, 0.1 mM KBr, 0.3 M H_2SO_4 and 0.011M aniline.

2.3.4 Gel Permeation Chromatography

Gel Permeation Chromatographic (GPC) data of the polymer films generated from all of the above reactions consisted of a single peak (for each polymer film) with typical

molecular weight in the range of 2500 – 2800 Dalton. The molecular weight determined by GPC of the system studied is tabulated in Table 2.1.

Table 2.1: The molecular weight distribution of the various systems studied.

	M_n(Daltons)	M_w(Daltons)	M_p(Daltons)
System 1(BZ)	2597	2674	2504
System 2(Mohr salt)	2679	2932	2474
System 3($FeSO_4$)	2771	2977	2633
System 4(Br^-/BrO_3)	2839	3134	2728

BZ = $KBrO_3$ + KBr +H_2SO_4 + Malonic Acid + $Fe(Phen)_3$ + aniline.

Mohr's salt = $KBrO_3$ + KBr +H_2SO_4 + Malonic Acid + $FeSO_4.7H_2O$ + aniline.

$FeSO_4$ = $KBrO_3$ + KBr +H_2SO_4 + Malonic Acid + Mohr's salt + aniline.

Br^-/BrO_3 = $KBrO_3$ + KBr +H_2SO_4 + aniline.

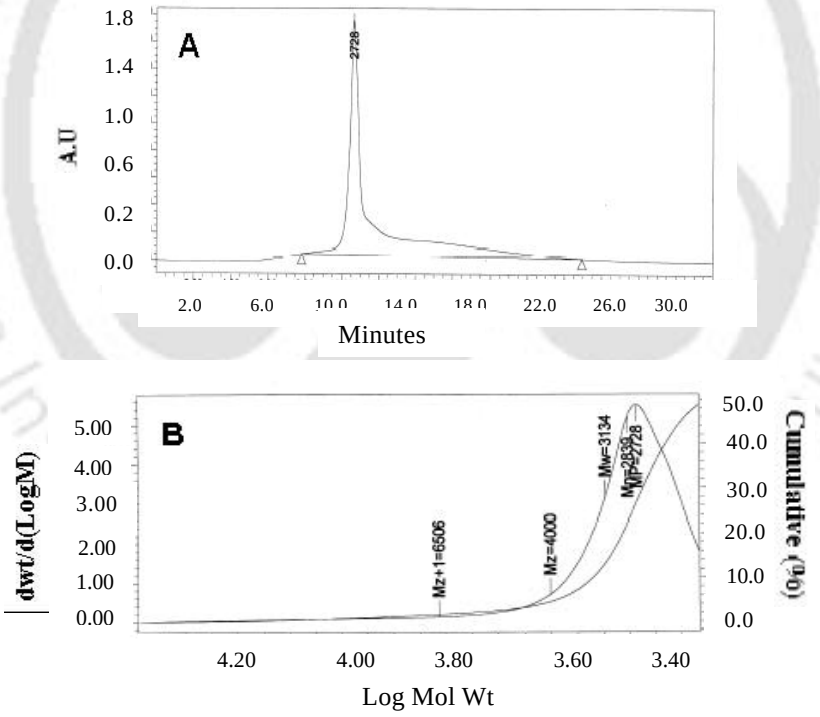

Figure 2.6: (a) Gel Permeation of Chromatogram of the polymer produced at the interface from the reaction with $KBrO_3$ / KBr. (b) Molecular weight distribution plot of the same . The calibration was done using polymethyl methacrylate as the reference standard.

A typical GPC chromatogram is shown in Figure 2.6. The eluting solvent used in the experiment is tetrahydrofuran (THF). The calibration was done using polymethyl methacrylate as the reference standard.

2.3.5 1H Nuclear Magnetic Resonance (NMR)

A typical ^1H NMR spectrum of a film (polymer) grown in the presence of $KBrO_3$ / KBr, as shown in Figure 2.7, contained multiplets between δ values of 7.25 and 7.5. This may be due to the combination of benzenoid and quinoid forms of the "emeraldine salt", the primary doped form of PANI, in which two structures coexist: the polaronic form and the bipolaronic structure[54].

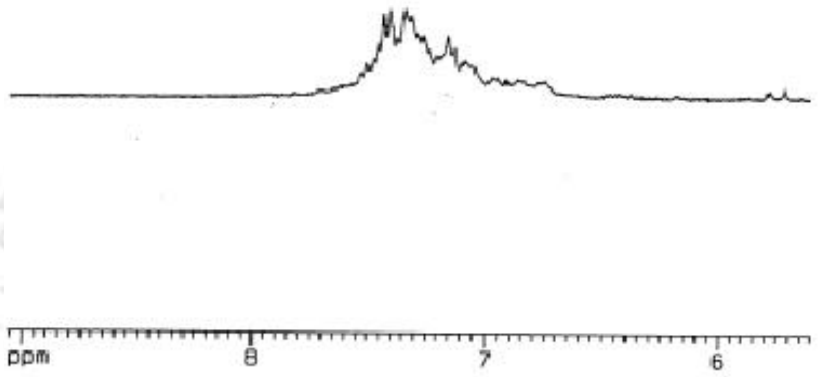

Figure 2.7: A typical proton NMR spectrum of a film grown in presence of $KBrO_3$ / KBr recorded in CD_3OD solvent.

2.3.6 Resistivity measurement

The resistivity measurements of the samples of different system (in the form of films transferred to glass slides) were carried out at room temperature (298 K) using the two-probe method and are tabulated in Table 2.2. It is evident from the values in the table that resistivity of the sample is quite high with typical value varying between 14 – 3 MΩ cm. The typical resistivity value for a conducting form of PANI is about 10 Ω cm. From the resistivity data we conclude that non-conducting form of the polymer was formed as the film at the air-water interface.

Table 2.2: Resistivity values obtained using two-probe method at 298° K

System	Resistivity(W cm)
BZ	4.14×10^6
$FeSO_4$	1.80×10^7
Mohr's salt	1.41×10^7
Br^-/BrO_3^-	3.15×10^6

2.3.7 Thickness measurement

Typical film thickness varied between a few microns to more than 100 microns. The film thickness was measured using optical microscope. The method employs focusing at the top surface of the film and the top surface of the slide. The difference in height was taken to represent the approximate film thickness. For example, in Figure 2.3, the thickness of the film produced from BZ reaction was about 2 μm and that from Mohr's salt was 58 μm, while the thickness of the film generated by the reaction with $KBrO_3$ / KBr was about 120 μm. The thickness variation is probably due to various rates of reaction and concentration of reacting species at the interface. This is expected considering the different mechanisms with different initiating and terminating species that are likely to be involved in polymer formation from different reagents.

2.3.8 Mesoscopic investigation of polymer film

Further investigation of the polymer films by optical microscopy revealed the formation of various two-dimensional repeated geometrical forms at the microscopic level. Some typical optical micrographs obtained are shown in Figures 2.8 and 2.9. The films obtained using $FeSO_4$ and $KBrO_3$ / KBr containing reagents have repeated circular patterns of growth spaced by gaps. These circular patterns were also observed to have merged with each other. When Mohr's salt containing reagents were used the polymer growth patterns had units of polygons of various shapes and sizes. In general, films grown from B-Z coupled reactions were devoid of any observable shapes of units, except at certain positions where random growth patterns have been observed. This was observed for both cases of aniline introduction, from solution phase and from vapor phase. When aniline was introduced from vapor phase and Mohr's salt was used as catalyst, spots of film where circular forms merged to form lumps could be seen. Mesoscopic pattern formation at the interface might occur due to nucleation-like process where polymerization takes place simultaneously at different nucleation sites. With the growth of polymers the areas of sites grow bigger and finally merge with each other. Once the network of grown pattern forms at the interface further growth of polymer takes place underneath the surface, using the initial pattern as a template. The nature of patterns formed depends on both the reactants and catalysts used. Thus for different reagent conditions we observed different mesoscopic patterns. We would also like to point out here that the reagent specific mesoscopic patterns were quite reproducible in terms of their shapes and not sizes.

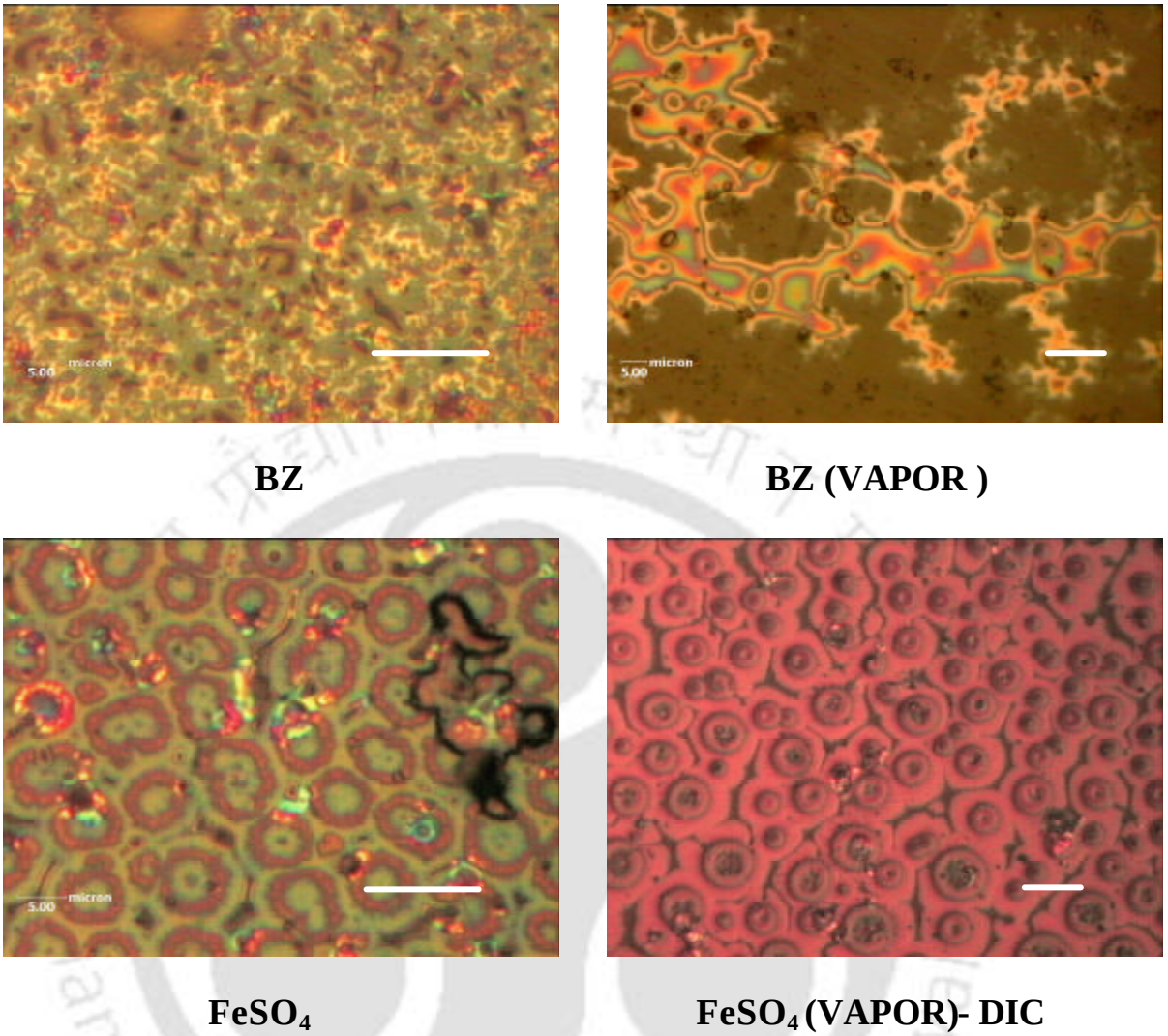

Figure 2.8: Optical Micrographs of a few films on microscope slides. Bar is 10? m. **BZ:** 1.0 mM $[Fe(Phen)_3]^{2+}$, 0.12 M $KBrO_3$, 0.1 mM KBr, 0.3 M H_2SO_4, 0.01 M Malonic Acid and 0.011M aniline. **BZ (VAPOR):** 1.0 mM $[Fe(Phen)_3]^{2+}$, 0.12 M $KBrO_3$, 0.1 mM KBr, 0.3 M H_2SO_4, 0.01 M Malonic Acid and aniline introduced from vapor phase. **$FeSO_4$:** 1.0 mM $FeSO_4$, 0.12 M $KBrO_3$, 0.1 mM KBr, 0.3 M H_2SO_4, 0.01 M Malonic Acid and 0.011M aniline. **$FeSO_4$ (VAPOR)-DIC:** 1.0 mM $FeSO_4$, 0.12 M $KBrO_3$, 0.1 mM KBr, 0.3 M H_2SO_4, 0.01 M Malonic Acid and aniline introduced from vapor phase. DIC: Differential Interference Contrast.

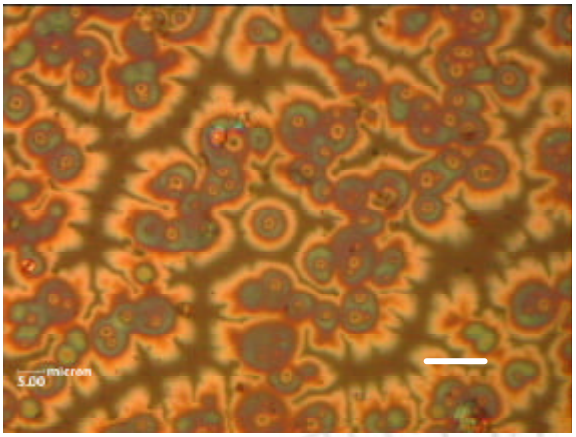

MOHR'S SALT (VAPOR)

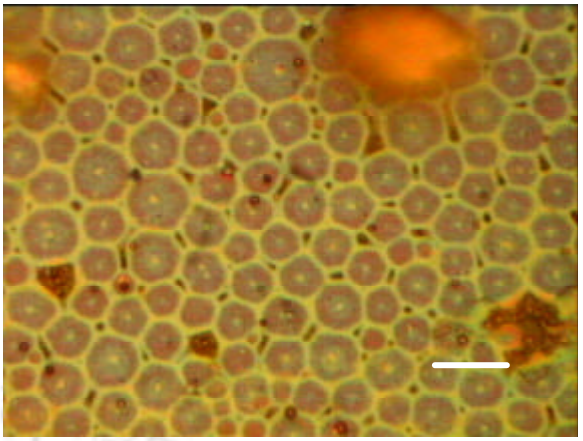

MOHR'S SALT

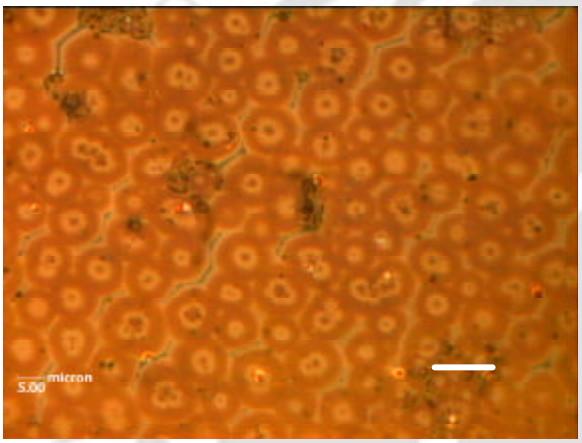

$KBrO_3$/KBr

Figure 2.9: **MOHR'S SALT (VAPOR):** 1.0 mM $(NH_4)_2SO_4$, $FeSO_4.6H_2O$, 0.12 M $KBrO_3$, 0.1 mM KBr, 0.3 M H_2SO_4, 0.01 M Malonic Acid. Aniline was introduced from the vapor phase. **MOHR'S SALT:** 1.0 mM $(NH_4)_2SO_4$, $FeSO_4.6H_2O$, 0.12 M $KBrO_3$, 0.1 mM KBr, 0.3 M H_2SO_4, 0.01 M Malonic Acid and 0.011M aniline. **$KBrO_3$/KBr :** 0.12 M $KBrO_3$, 0.1 mM KBr, 0.3 M H_2SO_4 and 0.011M aniline.

For example, various identical runs of the film formation with $FeSO_4$ containing reaction condition produced films with circular mesoscopic structures of various diameters while the patterns obtained from Mohr salt condition were of polygonal shapes with varying sizes. In addition, similar variations were also observed in the same films but at different locations of the slide.

2.3.9 Effect of surfactant on the mesoscopic structures

One of the remarkable observations in optical micrograph of the thin polymer film was the growth of repeated filled circular units of various diameters when 2.02 mM sodium dodecyl sulphate (SDS) was added to B-Z reaction mixture with aniline in the solution. The optical micrograph of such a film is shown in Figure 2.10. At higher concentration of SDS either films were to fragile to be transferred for observation or film formation did not take place. Aniline is immiscible with water. However we have found that it is soluble in water in presence of SDS (in our experiments we could dissolve 50 mM of aniline in water in presence of 200 mM of SDS). This is possibly due to the "solvation" of aniline in the hydrophobic core of SDS micelles. At the air-water interface the aniline molecules might also reside in between SDS molecules in a fashion similar to that of micellar dissolution of aniline prior to polymerization. A two-dimensional analog of the spherical micelle would have circular form due to minimum surface free energy requirement. Thus the film would contain patterns of circular form of growth occurring at various length scales. The merging of the surfaces of these circular patterns would make the film continuous and hence might explain the circular form of film growth. At higher concentration of surfactants, when the surface is fully covered with SDS only, there would be no surface aniline and hence no surface nucleation site and thus no surface polymerization. It is also possible that a minimum concentration of aniline at the interface is needed to form a film. With high concentration of SDS molecules at the interface, the minimum number of aniline molecules needed to form film might not have been present and hence the film formation did not take place. This may be the reason for the longer time required for film formation when aniline was introduced from the vapor phase. The above result indicates that it may be possible to control the formation of thin film and the contour of two – dimensional patterns at the interface by surface – active reagents.

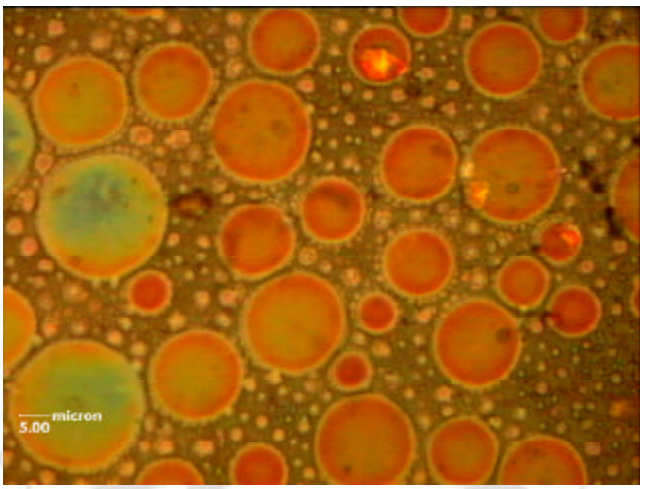

Figure 2.10: Optical Micrographs of the film generated by BZ reaction in the presence of 2.02mM SDS. Bar is 10μm. The different concentration of reagents are 1. 0mM $[Fe(Phen)_3]^{2+}$,0.12 M $KBrO_3$, 0.1 mM KBr, 0.3 M H_2SO_4, 0.01 M Malonic Acid, 0.011M aniline and 2.02 mM sodium dodecylsulfate.

2.3.10 Effect of sonication on macroscopic and microscopic patterns of film

We also investigated the effect of ultrasonic waves on the macroscopic and mesoscopic patterns of the film formed at the interface. For this purpose we carried out the polymerization reaction in an ultrasonicator bath. The procedure is discussed in the experimental section. We found that the macroscopic and mesoscopic patterns present in earlier figures were absence in the present case. A more uniform film growth took place in the presence of ultrasonic waves. A typical film growth profile both at the macroscopic and mesoscopic scales is shown in Figure 2.11.

The smoothness of the film may arise due to destruction of the normal patterned template at the initial stages of the reaction. As the reactants are vigorously shaken, pattern formation is inhibited and the reaction is no more diffusion limited. Also, specific nucleation centers might have been destroyed due to vigorous shaking by ultrasonic waves. Occasional hole formation observed in the film is probably due to gas bubble evolution from the bulk solution during sonication. The hole formation was clearly visible when the ultrasonicator bath had been used and was not so evident when reactions were performed without the bath.

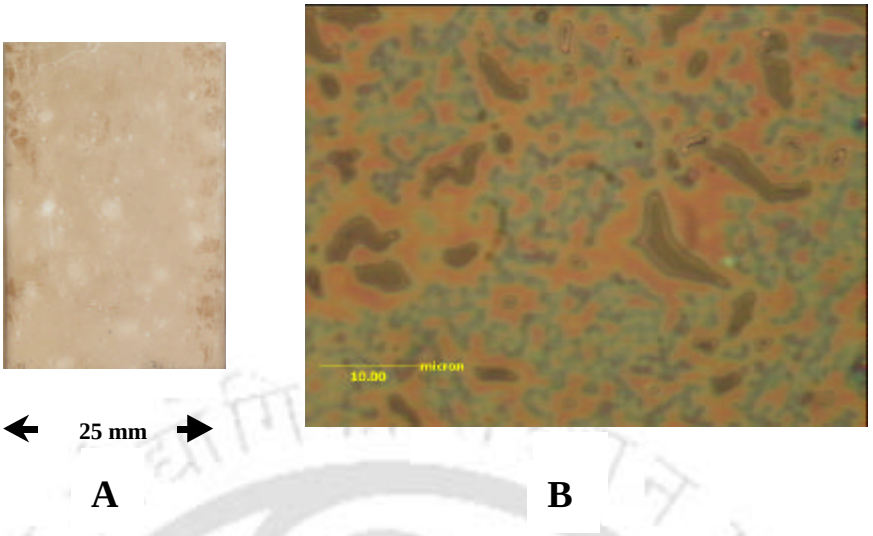

Figure 2.11: Polyaniline film generated in an ultrasonicator bath. The reaction conditions are $KBrO_3$ / KBr: 0.12 M $KBrO_3$, 0.1 mM KBr, 0.3 M H_2SO_4 and 0.011M aniline. A: Photograph of the film recorded by a HP5200C scanner. B: Optial micrograph of the film. Bar is 10 µm.

From the above observations it is clear that pattern formation in the polymerization of aniline at the interface is not exclusive to the BZ reaction. In fact, any radical species that can start initiation is enough to generate patterned polymer at the interface;

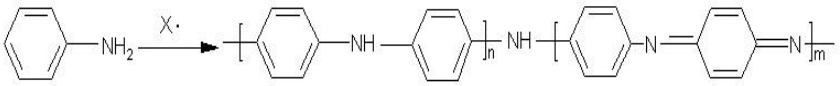

where $X^{\cdot}$ is the initiator. We also have observed similar pattern formation when polymerization was carried out in presence of Ce(III) catalyzed BZ reaction. With different reagents different nucleation sites for pattern formation might be formed and hence the observation of different mesoscoic patterns for different systems. In presence of ultrasonic waves these nucleation sites are altered and spatial uniformity in the distribution of reacting species leads to smoother film formation. This is also consistent with our observation of circular patterned growth in presence of SDS.

2.4 Conclusion

In this chapter we have reported the formation of thin films during the polymerization of aniline at the air-water interface. We also have reported the spontaneous formation of mesoscopic and macroscopic patterns in the films formed at the interface. On the other hand the polymers formed in the bulk were devoid of any patterns and finally settled at the bottom of the reaction vessel. The macroscopic patterns formed in the films were rather random and could not be reproduced in different runs. On the other hand, the mesoscopic patterns formed were different for different reagent conditions. The shapes of polymer growth pattern constituting the films were reproducible under the same reaction (reagent) condition, but their sizes varied from reaction to reaction (run to run). Our observations suggest that both macroscopic and mesoscopic pattern formation took place from the reagents in the bulk that had reacted in the non-oscillatory regime, even though we had started with the aim of observing patterns in the film formed at the interface due to polymerization coupled to BZ reaction in the bulk. We did not observe any pattern in the growth of polymers in the bulk in any of the cases mentioned above. There might be several nucleations - like sites at the interface from where polymer growth begins. The growing polymers sites at the interface finally merge to form a film. The formation of patterns in the multiple - layered growth might be controlled by the pattern formed initially. The pattern formation in the growth of thin polymer films at the interface may depend on various factors like diffusion of reactants to the interface from the bulk, concentration and orientation of aniline at the interface, dynamic surface tension during the formation of products and mixing of reactants at the interface, templates formed at the beginning of the film formation etc. An important point to note here is that the films must be sufficiently porous to allow growth of layers of films in the case of aniline coming from the vapor phase. Even though, the time taken of film formation is longer, there is enough porosity in the film to allow thick film formation with time. Most of our observations suggest that the dynamics of film formation is irregular and exact macroscopic pattern in the film formation may not be reproducible. Even then the result observed with polymer grown in presence of SDS suggests that the ultimate pattern formation may be affected by the nature of the species present at the interface. The pattern formation might still be influenced by controlling the nature and concentration of reactants present at the interface. We also observed that the macroscopic and mesoscopic patterns present in earlier cases were absence in case when reaction was performed in the presence of ultrasonic waves.

Convective patterns caused by gradient of interfacial tension may also play a key role in the pattern formation. This might have been well reflected in the pronounced role of SDS and ultrasound waves in pattern formation. Different mesoscopic pattern formation under different experimental condition indicates the role of nucleation-like process in the pattern formation in the microscopic scale. The macroscopic pattern is probably a reflection of film growth (thickness) process. Evaporation of water during the growth process might also influence the structures of the films formed. Polyelectrolyte and micellar template systems are known to be useful in guided growth of polyaniline. Also, controlled organization of nanoparticles has been achieved using interfacial properties of reverse micelles and microemulsions. Spatial pattern formation is well known in various non – oscillatory reaction systems. In the present case, the initial structure of the thin film formed by mixing of reactants is affected by the presence of the species at the interface followed by formation of multiple layers of film using the initial layer as the template.

2.5 References

1. Maoz, R.; Matlis, S.; Dimasi, E.; Ocko, B. M., Sagiv, J. *Nature* **1996,** 384,150.
2. Aksay, I. A.; Trau, M.; Manne, S.; Honma, L.; Yao, N.; Zhou, L.; Fenter, P.; Eisenberger, P. M.; Gruner, S. M. *Science* **1996,** 273, 892.
3. Li, M.; Schnablegger, H.; Mann, S. *Nature* **1999,** 402, 393.
4. Sleytr, U. B.; Messner, P., Pum, D.; Sára, M. *Angew. Chem. Int. Ed*. **1999,** 38, 1034.
5. Ramos, L.; Lubensky, T. C.; Dan, N., Nelson, P.; Weitz, D. A. *Science* **1999,** 286, 2325.
6. Davey, R. J.; Williams-Seton, L.; Lieberman, H. H.; Blagden, N. *Nature* **1999,** 402, 797.
7. Xia, Y.; Whitesides, G. *Angew. Chem. Int. Ed*. **1998,** 37, 550.
8. Bruno, F. F.; Akkara, J. A.; Samuelson, L. A.; Kaplan, D. L.; Mandal, B. K.; Marx, K.A.; Kumar, J.; Tripathy, S. K. *Langmuir* **1995,** 11, 889.

9. Sirringhaus, H.; Tessler, N.; Friend, R. H. *Science* **1998**, 280, 1741.

10. Burroughes, J. H. *Nature* **1990,** 347, 539.

11. Wohlgenannt, M.; Tandon, K.; Mazumdar, S.; Ramsesha, S.; Vardeny, Z. V. *Nature* **2001,** 409, 494.

12. Yu, G.; Gao, J.; Hummelen, J. C.; Wudl, F.; Heeger, A. J. *Science* **1995,** 270, 1789.

13. Pages, H.; Topart, P.; Lemordant, D. *Electrochimica Acta* **2001,** 46, 2137.

14. Bartlett, P. N.; Simon, E. *J. Am. Chem. Soc.* **2003,** 125, 4014.

15. Kang, X.; Jin, Y.; Cheng, G.; Dong, S. *Langmuir*, **2002,** 18, 10305.

16. Sukeerthi, S.; Contractor, A. Q. *Anal. Chem*. **1999,** 71, 2231.

17. Kaner, R. B. *Synth. Metals*, **2002,** 125, 65.

18. Stolarczyk, A.; Lapkowski, M. *Synth. Metals*, **2001,** 121, 1385.

19. Chen, S. A.; Fang, Y. *Synth. Metals*, **1993,** 60, 215.

20. Kitani, A.; Akashi, T.; Sugimoto, K.; Ito, S. *Synth. Metals*, **2001,** 121, 1301.

21. Koul, S.; Chandra, R.; Dhawan, S. K. *Polymer*, **2000**, 41, 9305.

22. Joo, J.; Lee, C. Y. *J. Applied Phys.* **2000,** 88, 513.

23. Heeger, A. J. *Angew. Chem. Int. Ed*. **2001,** 40, 2591.

24. Yue, J.; Wang, Z. H.; Cromack, K. R.; Epstein, A. J.; MacDiarmid, A. G. *J. Am. Chem. Soc*. **1991,** 113, 2665.

25. Wei, X. L.; Wang, Z. H.; Long, S. M.; Bobeczko, C.; Epstein, A. J. *J. Am. Chem. Soc*. **1996,** 118, 2545.

26. Liu, W.; Kumar, J.; Tripathy, S.; Senecal, K. J.; Samuelson, L. *J. Am. Chem. Soc*. **1999,** 121, 71.

27. Liu, W.; Cholli, A. L.; Nagarajan, R.; Kumar, J.; Tripathy, S.; Bruno, F. F.; Samuelson, L. *J. Am. Chem. Soc*. **1999,** 121, 11345.

28. Huang, J.; Virji, S.; Weiller, B. H.; Kaner, R. B. *J. Am. Chem. Soc*. **2003**, 125, 314.

29. Wei, Z.; Zhang, Z.; Wan, M. *Langmuir*, **2002,** 18, 917.

30. Sarma, T. K.; Chowdhury, D.; Paul, A.; Chattopadhyay, A. *Chem. Commun*. **2002,** 1048.

31. Zengin, H.; Zhou, W.; Jin, J.; Czerw, R.; Smith Jr., D. W.; Echegoyen, L.; Carroll, D. L.; Foulger, S. H.; Ballato, J. *Adv. Mater*. **2002,** 14, 1480.

32. Yoshida, K.; Shimomura, T.; Ito, K.; Hayakawa, R. *Langmuir*, **1999,** 15, 910.

33. Lee, Y-S; Joo, B-S; Choi, N-J; Lim, J-O; Huh, J-H; Lee, D-D *Sens. Actuators B* **2003**, 93, 148.

34. Sirkar, K.; Revzin, A.; Pishko, M. V. *Anal. Chem*. **2000,** 72, 2930.

35. Bossi, A. I.; Piletsky, S. A.; Piletska, E. V.; Righetti, P. G.; Turner, A. P. F. *Anal. Chem*. **2000,** 72, 4296.

36. Lei, Z.; Zhang, H.; Ma, S.; Ke, Y.; Li, J.; Li, F. *Chem. Commun*. **2002,** 676.

37. Mitov, Z.; Kumacheva, E. *Phys. Rev. Lett*. **1998,** 81, 3427.

38. Gimenez, M.; Micheau, J. C *Naturwissenschaften* **1983,** 70, 90.

39. Micheau, J. C.; Gimenez, M.; Borckmans, P.; Dewel, G. *Nature* **1983,** 305, 43.

40. Epstein, I. R. *J. Phys. Chem*. **1984,** 88, 187.

41. Hauser, M. J. B.; Simoyi, R. H. *Chem. Phys. Lett*. **1994,** 227, 593.

42. Hauser, M. J. B.; Simoyi, R. H. *Physics Letters A.* **1994,** 191, 31.

43. Martincigh, B. S.; Simoyi, R. H. *J. Phys. Chem A.* **2002,** 106, 482.

44. Vanag, V. K.; Zhabotinsky, A.M.; Epstein, I. R. *J. Phys. Chem. A.* **2000,** 104, 1566.

45. Tóth, R.; Gáspár, V.; Belmonte, A.; O' Connell, M. C.; Taylor, A.; Scott, S. K. *Phys. Chem. Chem. Phys.* **2000,** 2, 413.

46. Johnson, B. R.; Scott, S. K.; Taylor, A. F. *J. Chem. Soc., Faraday Trans.* **1997,** 93, 3733.

47. Berenstein, I.; Agreda, J.; Barragán, D. *Phys. Chem. Chem. Phys.* **1999,** 1, 4601.

48. Taylor, A. F.; Gaspar, V.; Johnson, B R.; Scott, S. K. *Phys. Chem. Chem. Phys.* **1999,** 1, 4595.

49. Laplante, J. P.; Potter, R. H. *J. Phys. Chem*. **1982,** 86, 4759.

50. Epstein, I. R.; Morgan, M.; Steel, C.; Valdes-Agullera, O. *J. Phys. Chem*. **1983,** 87, 3955.

51. Pojman, J. A.; Epstein, I. R. *J. Phys. Chem.* **1990,** 94, 4966.

52. Washington, R. P.; West, W. W.; Misra, G. P.; Pojman, J. A. *J. Am. Chem. Soc.* **1999,** 121, 7373.

53. Moon, D. K.; Osakada, K.; Maruyama, T.; Yamamoto, T. *Makromol. Chem.*, **1992,** 193, 1723.

54. Cochet, M.; Maser, W. K.; Benito, A. M.; Callejas, M. A.; Martinez, M. T.; Benoit, J. M.; Schreiber J.; Chauvet, O., *Chem. Commun*., **2001**, 1450.

Chapter 3

Lithography by Simultaneous Chemical and Photo-chemical Polymerization of Aniline at the Air-Water Interface

3.1 Introduction

Photochemical pattern generation plays a key role in various fields of modern technology such as lithography, microelectronics and microfluidics [1-4]. Photo-patterning of organic photoresist is a standard method for structure generation in microelectronics industry. Another important consequence of photolithography is soft lithography [5-9], which has made considerable impact in the generation of sub-micron scale structures at a lower cost. In this case, the master is made by photolithography. Further, functionalized patterned surfaces in conjunction with light can be used for controlled wetting[10], devising futuristic micro and nanostructure technology affinity assays, cell assays and DNA devices for on-chip rapid screening purposes [11]. It has also been demonstrated that fabrication using microlithographic patterning can be used in making DNA based devices where electrodes are defined by the first mask or layer and oligonucleotides are aligned and immobilized covalently in desired patterns during the second step [12]. Even patterned surfaces can acts as templates for DNA arrays. The key step here is to photopattern self-assembled monolayers to form hydrophobic and hydrophilic regions on a metal surface [13]. Laser photopatterning of polymer monoliths inside glass microchannels is used to fabricate mobile fluid control elements, which are open and closed by electrokinetic pressure [14]. These can be used for multiple chromatographic separations on a single microchip. Moreover, tailored modification of polymeric surfaces has engendered wide interest with respect to application of these materials [15], for example, micropatterned polymer lipid bilayers with potentially important biomedical applications [16].

3.1.1 Some of the Existing methods of photo-chemical pattern generation

Photo-chemical pattern generation has been used for the last several decades for fabrication of semiconductor devices. With the increasing demand of obtaining structures with higher resolution, deep ultraviolet (DUV) and X-ray light have been used for fabrication[17-21]. In this approach a polymer film is spin-cast on a surface, which is then selectively exposed to light using a mask. Another method that has been successfully used is the Laser ablation (LAB) [22-23] which is a flexible microfabrication technique suitable for surface structuring of polymers with high UV absorption and non-thermal ablation behavior. Photo patterning of polymer Langmuir-Blodgett film[24-25] by cross-linking is a useful technique where polymers are amphiphilic in nature. On the other hand, photo patterning of amphiphilic molecules has also be been achieved using self-assemble

property, as it offers a superior path for forming stable monolayer films[26-31]. Self-assembly in amphiphilic molecular monolayer formation is thermodynamically favorable and hence requires less special attention or equipment than the preparation of a LB monolayer. In brief, all the methods mentioned above involve preparation of a film on a substrate followed by exposure to light of particular wavelength for pattern formation required for a particular application.

3.1.2 Our approach

We discuss below a method of generating patterns on a polymer film using light as the polymer grows at the air-water interface catalyzed by chemical reagents present in the bulk. Our method allows greater control in the synthesis of patterned polymers films as the patterns are "imprinted" onto a growing polymer film at an interface. One of the ways of achieving this is to carry out the polymerization reaction at an interface, simultaneously in presence of light from above and chemical reactions from below. There are several advantages of this method as it offers achieving greater control over the variation of properties of the polymer across the film due to its growth profile. Polymer generated in the presence of light might have or might not have the same properties as that generated by chemical methods. Further, there may be variations in the properties of the photo-grown polymers across the film, which can be tuned by selecting appropriate monomer, wavelength of incident light and chemical reagents that catalyze the polymerization reaction. The polymer film thus generated could possibly have patterned variations in optical, electronic, chemical and even mechanical properties characterized by thickness variations or otherwise across the film. This has the unique advantage over other methods as one could have a better control over size, shape and nature of patterns formed onto the films by controlling parameters, from above the surface for light catalyzed polymerization, and from the bulk below for the chemical polymerization. Potential applications of such a system include designed polymer surfaces with controlled wettability or porosity, incorporation of catalysts inside a polymer film, arrays of sensors in polymer films, lithographic pattern formation, generation of patterned polymers for electronic display systems, oriented film generation using appropriately polarized light. There is one report in literature in which thermally induced convection patterns were frozen in the polymer film generated by UV induced polymerization [32], but as far we know, this is the first report

of generating patterns on polymer film by simultaneous chemical and photo-chemical polymerization at the air-water interface.

With these objectives in mind we introduce a new method of generation of patterned polymer thin films, at the air – water interface, that attempts to address a first issue of the above idea. Our choice of synthesis of polyaniline films[33-34], at the air-water interface, was guided by application potential owing to its electrical conductivity. It is well known that the synthesis of polyaniline can be catalyzed by oxidizing chemical reagents [35-39]. We have recently found that polymerization of aniline in aqueous acidic $KBrO_3$ / KBr solution occurred with thin film formation at the air – water interface, in addition to bulk polymerization. The films consisted of mesoscopic nucleation patterns that were characteristic of the catalysts used. For example when the reaction was carried out in presence of acidic $KBrO_3$ / KBr, the nucleation patterns were polygonal, whereas circular patterns were formed when $FeSO_4$ was used as catalysts in addition to the above reagents. The results of the detail study have already been discussed in Chapter 2. Here we report air – water interface polymerization of aniline coupled to reaction with acidic $KBrO_3$ / KBr in the bulk from below and in the presence of UV or visible light impinging from above on a select part of the interface. The polymer film formed at the interface in the presence of light consisted of a macroscopic imprint of the shape and size of the light beam within the otherwise usual film formed in the remaining part of the interface as observed in absence of light. In other words, a polymer film was formed with an imprint in a part of the film in the shape and size of the light beam. Observation under optical microscope revealed that the characteristic nucleation pattern of growth was absent in that part of the film where light was impinged. The imprinted patterns could be observed over a wide range of UV and visible incident light wavelengths. We propose that in absence of light, radicals like BrO_2•, generated by chemical reaction in the bulk aqueous phase, catalyze the polymerization reaction. On the other hand our observations of the absence of patterns on illuminated part could be explained to have happened due to simultaneous polymerization of aniline at the interface in the presence of Br• radicals generated by photodissociation reactions and BrO_2• catalyzed polymerization as above. A detailed mechanistic treatment is discussed in section 3.3.6

3.2 Experimental

Chemicals: Potassium bromate ($KBrO_3$)(Aldrich), Potassium bromide (KBr) (Aldrich) and sulfuric acid (H_2SO_4)(Merk) were purchased from the companies mentioned in the parentheses and used as received. The monomer used for polymerization was aniline (MERK) and it was distilled before use. HPLC grade Tetrahydrofuran (THF) (Merk) was used as the solvent in Gel Permeation Chromatography.

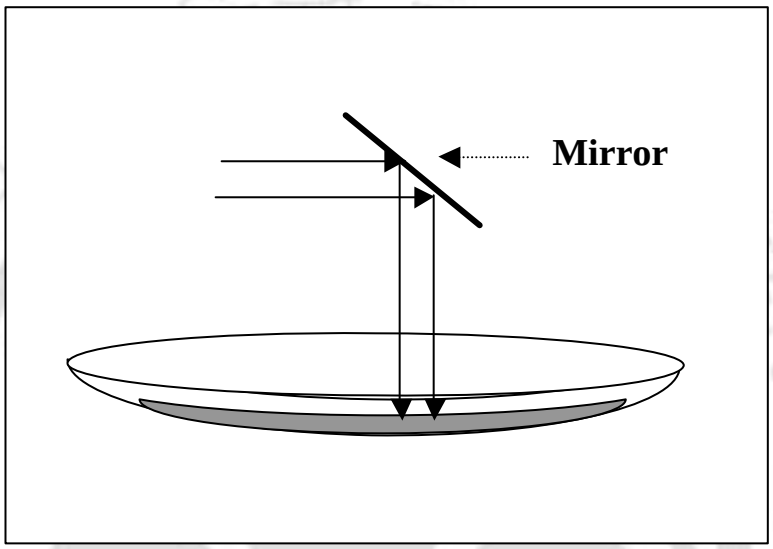

Figure 3.1: A schematic view of the experimental set-up. The output beam from the excitation monochromator was reflected from a plane mirror and impinged onto the reaction mixture kept in a watch glass.

A schematic view of the experimental set up is shown in Figure 3.1. Stock solutions of Potassium bromate ($KBrO_3$), Potassium bromide (KBr) and sulfuric acid (H_2SO_4) were prepared in Milli-Q water. The concentration of stock solution were as follows $[KBrO_3]$ = 0.3815 M, [KBr] = 0.014 M and $[H_2SO_4]$ = 0.783 M. Appropriate amounts of reagents were taken from the stock solutions and then mixed in a test tube.

The final concentrations of various reagents were as follows: 0.12 M $KBrO_3$; 1 x 10^{-4} M KBr; 0.3 M H_2SO_4 and 0.15 M of aniline. The mixture was then poured into a watch glass that was kept inside the sample compartment of the Shimadzu RF-5301PC spectrofluorometer, whose light beam was used as the light source. The exit beam of the excitation source, with 20 nm slit width, was reflected by a plane mirror onto the surface of the solution. The exit beam generally has rectangular shape. For generating desired

shape, the beam was masked with black paper. The film was allowed to grow for about 1 hour. For photo polymerization at various incident wavelengths, the excitation monochromator was tuned to the desired wavelength.

Afterwards, the film was made to float above the watch glass by pouring water carefully into a petridish where the watch glass was placed. After a few cycles of water draining and refilling, the film was carefully transferred to a microscope slide. The film thickness was measured with the help of an optical microscope by focusing at the top surface of the film and the top surface of the slide. The difference in height was taken to represent the approximate film thickness. The macroscopic patterns were recorded by using a HP5200C or HP5370 optical scanner. The optical micrographs were recorded by a Carl Zeiss (Axiotech) microscope. The colors in the optical micrographs are not due to any color of the film material but due to interference of light in the thin polymer layers. Typical film thickness varied between 30 and 200 μm. Room temperature, during growth of the film, was between 20-25^{0}C.

UV-visible spectra of films on slides and polymer forming solution were recorded by a Hitachi U – 2001 UV-visible spectrophotometer. To record FTIR spectra of the polymers, photo illuminated and non-illuminated parts of films were scraped off from the slide and transferred separately for making KBr pellets. A Nicolet IMPACT 410 FTIR spectrophotometer was used for recording IR spectra. The molecular weight of the film was recorded using Gel Permeation Chromatography data in a Waters HPLC-GPC system. The eluting solvent used was tetrahydrofuran (THF). The calibration was done using polymethyl methacrylate (PMMA) as the reference standard.

3.3 Results and Discussion

We have discussed in Chapter 2 the film formation at the air-water interface due to polymerization of aniline. We have carried out the experiments reported here in much the same way except that only $KBrO_3$ / KBr reagents were used for polymerization and also in the presence of light of various wavelengths at some desired regions of the film. The films formed at the interface were transferred to microscope slides in 90 min after the reaction mixture was poured into the watch glass. Photographs of three such films, generated at the air – water interface in presence of 320 nm light followed by transferring to microscope slides are shown in Figure 3.2 A, B and C. The horizontal dimension of each slide is about 25 mm.

The illuminated parts appeared as "I I T" of English alphabet (abbreviation of the name of our institute " Indian Institute of Technology") and were clearly discernible against the other parts, where the polymer had grown in absence of light, as the background film. The " T " letter was formed by masking the light appropriately so that it had shone on the interface in the shape of the letter " T". It is important to note here that the films formed were stable enough to be able to transfer to slides. They were also continuous in their growth profile such that there were no apparent discontinuity in film formation between the parts that grew in presence and absence of light.

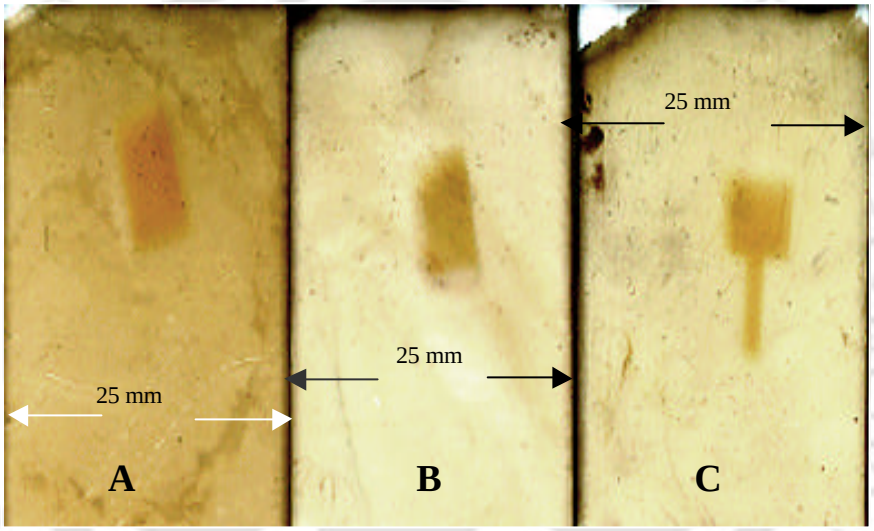

Figure 3.2: Photographs of polymer films taken after transferring to microscope slides. The three pictures (I I T) on three separate 25 mm slides (A, B, C) were recorded by HP5200C Scanner. Here the rectangular impressions, referred to as the letter "I" and T-shaped impression referred to as the letter "T" are the 320 nm light illuminated parts of the films with non-illuminated parts of the films as the background.

Our next aim was to investigate the effect of various incident wavelengths of light on the nature of imprints on the films. A UV-visible absorption spectrum of a mixture of $KBrO_3$, KBr and aniline in aqueous H_2SO_4 in the concentration ratio used for polymer thin film formation and recorded 7 min after mixing showed a strong absorption with two peaks in the region of 300 nm to 650 nm. This is shown in Figure 3.3. We have taken advantage of this absorption range and could obtain imprints at several incident light

wavelengths ranging between 320 nm to 650 nm. We however did not observe any significant imprint when the incident light wavelength was beyond 650 nm.

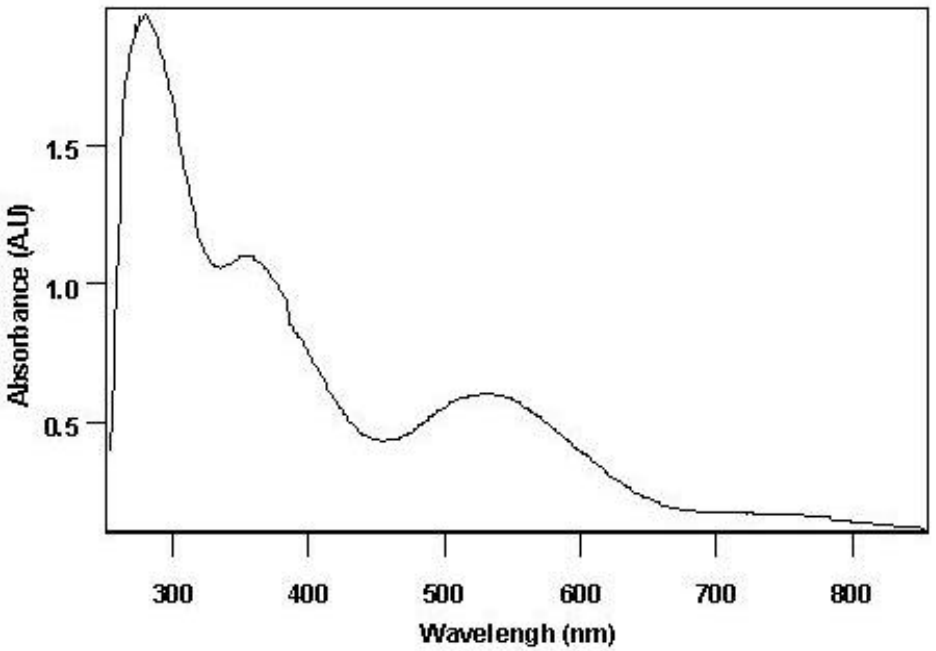

Figure 3.3: UV-visible absorption spectrum of a mixture (diluted from the original mixture) of $KBrO_3$, KBr and aniline in aqueous H_2SO_4 recorded about 7 min after mixing.

Figure 3.4 shows a collection of pictures of polymer films generated at the interface in presence of incident light of different wavelengths. The wavelengths of light used were 320, 350, 400, 450, 500 and 650 nm. The illuminated part in each film appeared as rectangular shape surrounded by the polymer film grown in absence of light. As evident from the figure, the clarity of the rectangular mark went down with increasing wavelength with nearly vanishing mark at 650 nm. Even then, the imprints could easily be identified up until an incident wavelength of 500 nm.

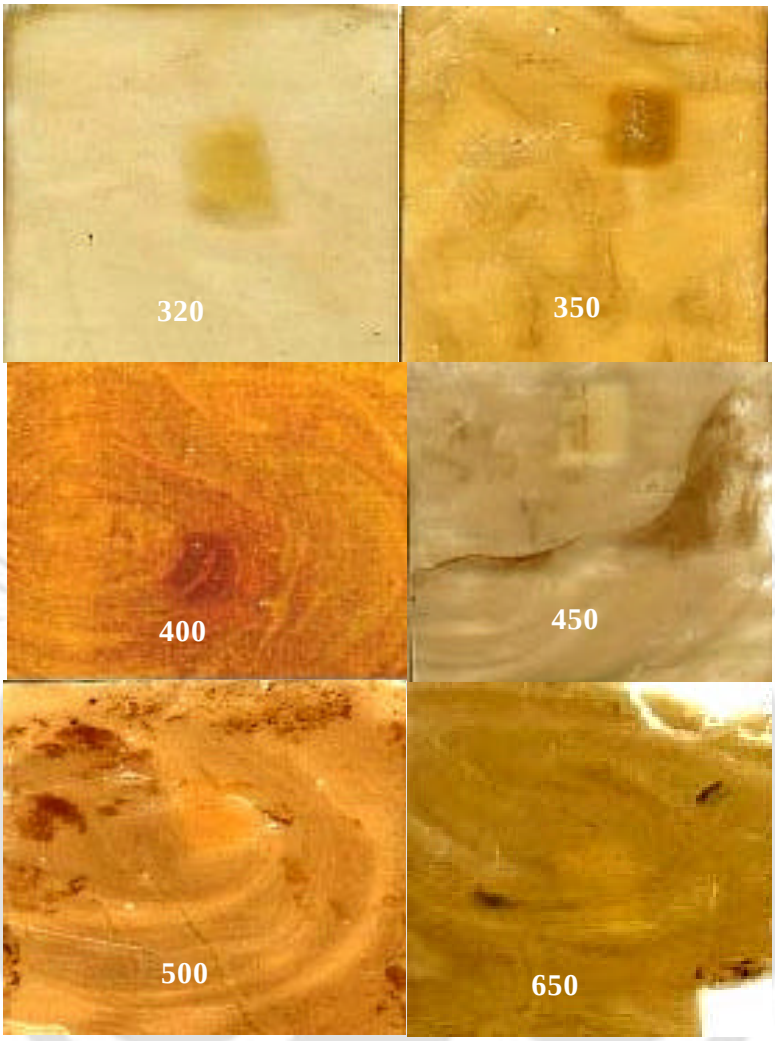

Figure 3.4: Pictures of polymer films generated under illumination of incident light at various wavelengths. The impressions appear in the form of rectangles. Films transferred to microscope slides were scanned using a HP5370C scanner. The contrasts of the pictures were changed (equally for all) for more dear views. The number written on each plate corresponds to the wavelength of light (nm) used for imprints. The horizontal dimension of each plate is 25 mm and the same scale length is applicable to vertical dimension.

3.3.1 Characterization of polymer film by Fourier Transform Infra-Red spectroscopic (FTIR) studies

We then pursued FTIR spectroscopic investigation of the polymer film for characterization, especially the difference between the nature of polymer formed in the photo illuminated and non-illuminated regions. For this purpose FTIR spectra of

illuminated and non-illuminated parts of a film grown in presence of 320 nm light were recorded. The FTIR Spectra are shown in Figure 3.5. Both the spectra show a broad peak due to quinoid and benzenoid ring deformations in the region of 1570 and 1500 cm^{-1}, respectively. A band at 1160 cm^{-1}, characteristic of polyaniline emaraldine base[37] could also be observed. Thus FTIR spectroscopic results of the polymer film grown in presence and absence of light indicated that the polymers formed were identical in nature. It is possible that even though the mechanism of polymerization in presence and absence of light are different, the polyaniline formed in both cases are of the same chemical form.

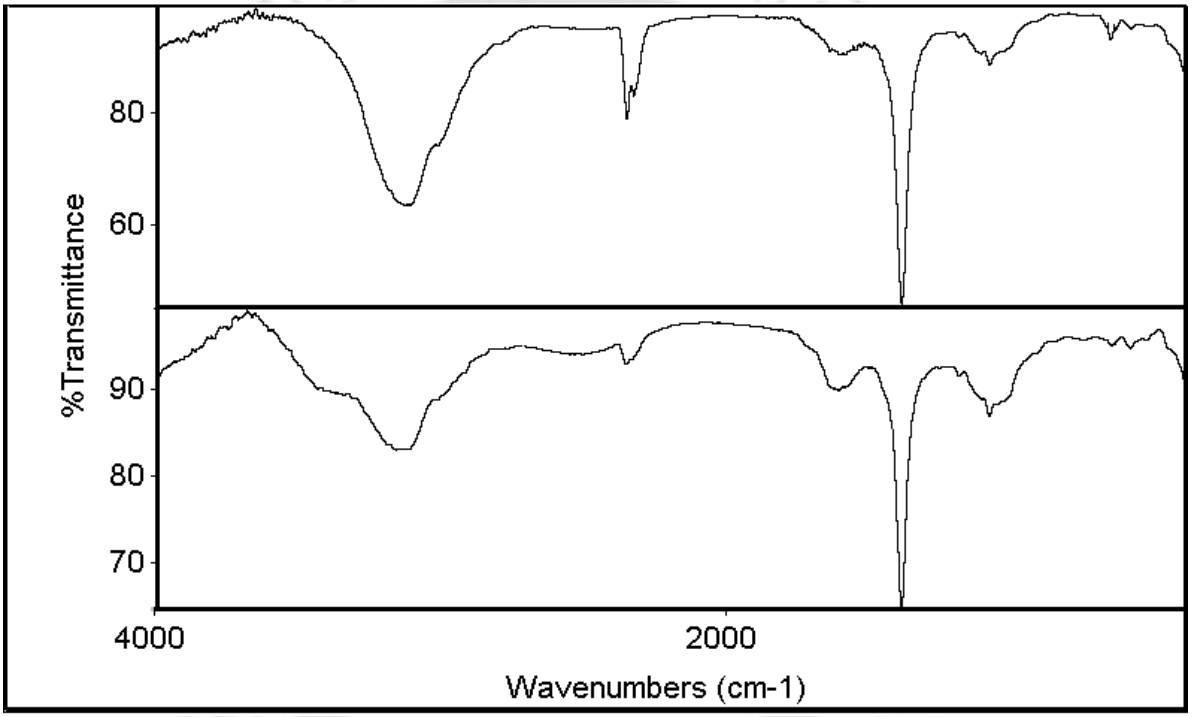

Figure 3.5: FTIR spectra of 320nm illuminated (top) and non-illuminated (bottom) parts of a film recorded in KBr pellets.

3.3.2 UV-Visible spectroscopic studies

The UV-vis spectra of the polymer film grown at air/water were also recorded. Figure 3.6 shows the UV-vis spectra of the photo illuminated and non-illuminated parts of the film after transferring it onto a sapphire window. The noteworthy observation was that the ratio of optical density between the illuminated part and the non – illuminated part was about 2 measured at the absorption maxima of 320 nm.

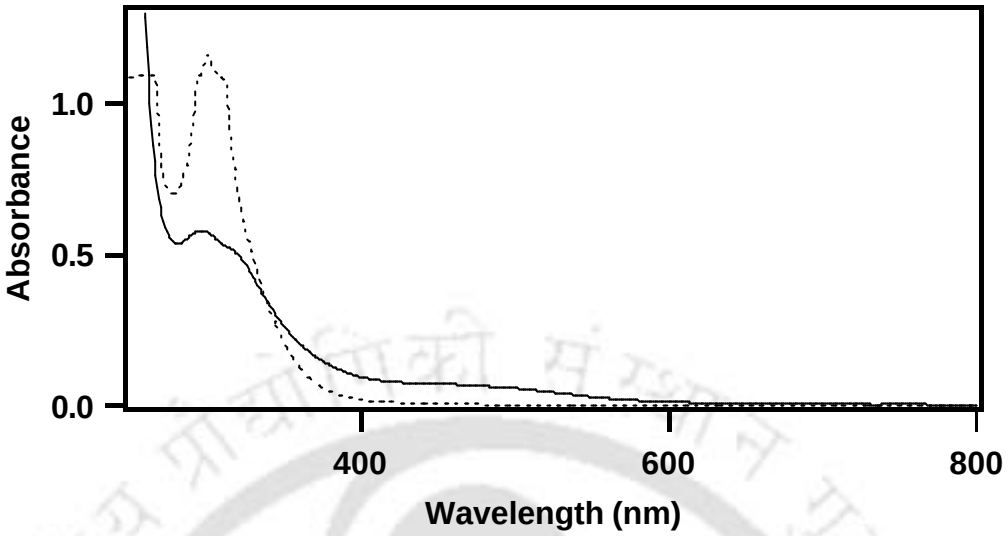

Figure 3.6: UV-visible absorption spectrum of polymer film after transferring on sapphire window of (_____) non-illuminated part (--------) illuminated part (illuminated with 320 nm).

3.3.3 Gel Permeation Chromatography

Gel Permeation Chromatographic (GPC) data of the polymer films was taken of the illuminated as well as non-illuminated part. The molecular weights are tabulated in Table 3.1. The average molecular weight of the polymer film was around 2400-2700 daltons. The molecular weight distribution plots of both illuminated (at 320nm) and non-illuminated parts of the film are depicted in Figure 3.7 and 3.8 respectively. It is quite evident from the table that there is not much difference in molecular weight of the polymer in illuminated and non-illuminated parts of the film.

Table 3.1: Molecular weight distribution of the polymer film.

Sample	Mn (Daltons)	Mw (Daltons)	Mp (Daltons)
illuminated part	2787	3039	2577
Non-illuminated part	2723	2996	2619

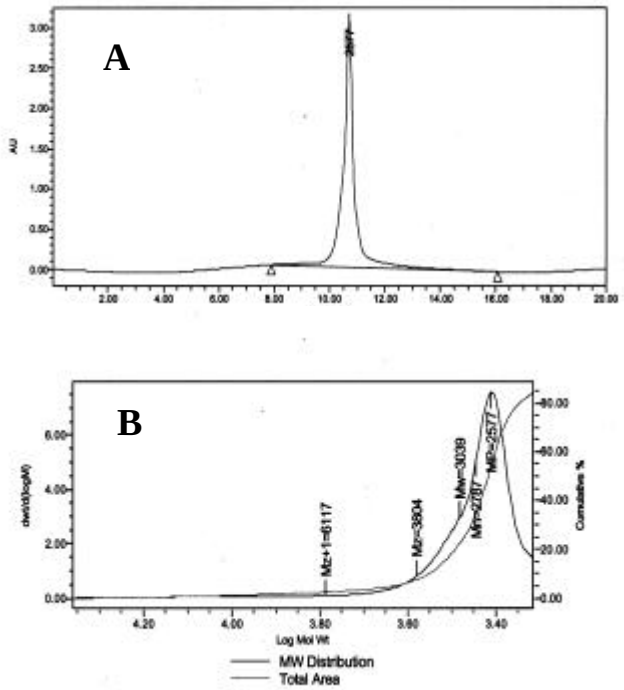

Figure 3.7: (A) Gel Permeation of Chromatogram of the polymer produced at the interface from the reaction with $KBrO_3$ / KBr which was illuminated by 320nm light. (B) Molecular weight distribution plot of the same. The calibration was done using polymethyl methacrylate as the reference standard.

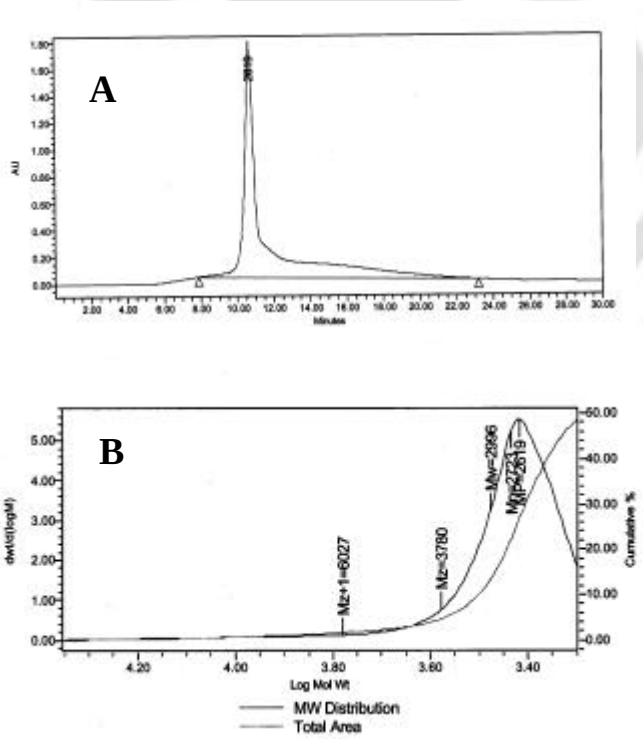

Figure 3.8: (A) Gel Permeation of Chromatogram of the polymer produced at the interface from the reaction with $KBrO_3$/ KBr (non-illuminated part) (B) Molecular weight distribution plot of the same. The calibration was done using polymethyl methacrylate as the reference standard.

3.3.4 Thickness measurement

The thickness of a typical film was measured using an optical microscope. It was done by focusing at the top surface of the film and the top surface of the slide. The difference in height was taken to represent the approximate film thickness. The thickness of the film grown at various incident wavelength and determined by this method are tabulated in Table 3.2

Table 3.2: Thickness of polyaniline films: non-illuminated parts and illuminated at different wavelength. The numbers in the same column are from the same film grown at air-water interface.

	320nm	350nm	400nm	450nm	500nm	600nm
Non-illuminated (mm)	46.2	92.4	61.6	30.8	30.8	23.1
Illuminated (mm)	77.0	154.0	92.4	38.5	35.4	23.1

As clear from the table, the part of the polymer film grown in presence of light generally had a higher thickness than that grown in absence of light. However, the thickness difference gradually decreased with increase in the incident wavelength of light. At 320 and 350 nm the illuminated part of the film was about 67% greater than the non-illuminated part. At 600 nm there was no difference between the two parts of the film. The increase in the relative thickness is probably due to higher rate of growth of film in presence of light that is formed in addition to chemically catalyzed reaction.

3.3.5 Investigation of mesoscopic structures of the illuminated and non-illuminated parts of films

Investigation under optical microscope revealed that characteristic polygonal nucleation sites of growth of polymer film were present in the film that formed in absence of light. These are shown in Figure 3.9 A and B. The two optical micrographs are of non-illuminated part with different resolution. The characteristic patterns could easily be identified from the occasional presence of spots of dried up films that appear to have been formed at some parts of the films. On the other hand these characteristic nucleation patterns of growth of film were absent in the illuminated part of the film. A typical optical micrograph is shown in Figure 3.9 C.

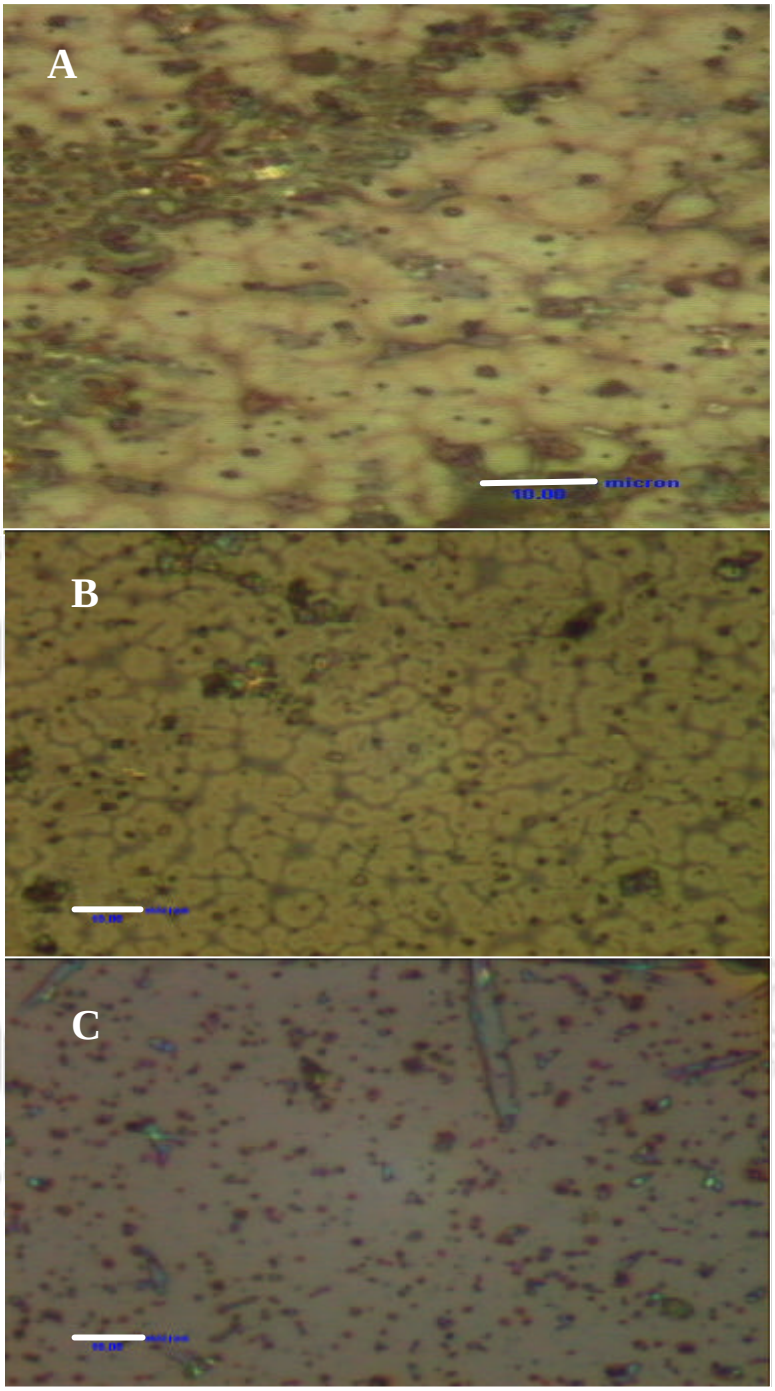

Figure 3.9: A and B are micrographs of non – illuminated parts of with characteristic polygonal nucleation pattern. C is the 320 nm light illuminated part of the first "I" part of Figure 3.6 A. The micrographs were recorded by Carl Zeiss (Axiotech) microscope. Bar is 10 μm.

This means when light of appropriate wavelength is illuminated on a part of the interface where the film is grown, the mesoscopic nucleation patterns are not formed in that part where the light beam is present. A relatively smoother film formation takes place in the

presence of light. On the other hand, the rest of the film grows with characteristic nucleation pattern. A more clear picture of this difference in patterns as well as film formation characteristics can be seen at the border of illuminated and non-illuminated region of growth. This is shown in Figure 3.10 at two different magnifications.

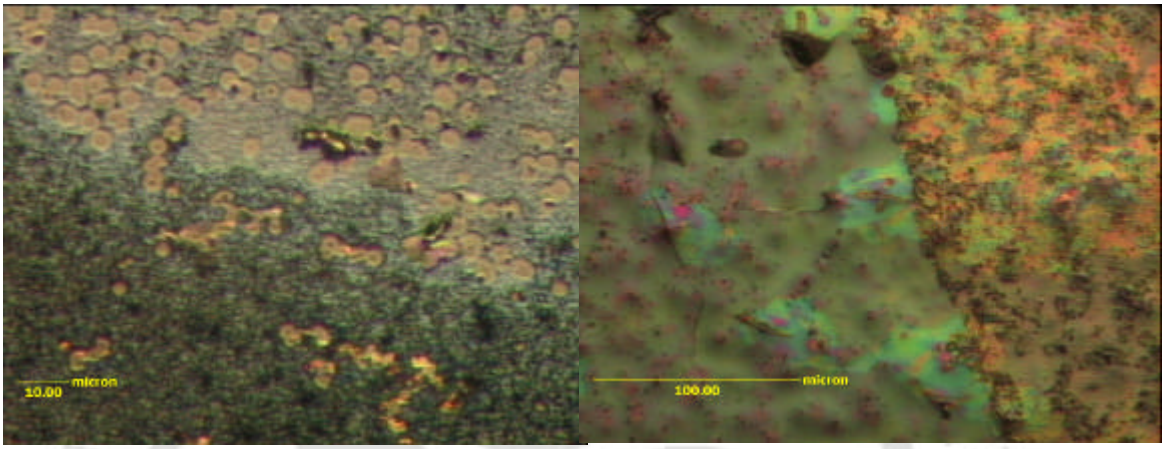

Figure 3.10: The film growth characteristics at the border region of illuminated and non-illuminated parts of a film. The wavelength of incident light for growth was kept at 320 nm.

A noteworthy feature is that the imprint of light beam on the film had the same size as the original beam. This suggests that the film structure formed initially was "frozen" for the rest of the growth of the film. There was no diffusion of film or parts of it along the interface after initial formation. Also, the initial film template formed at the interface remained the same all through the reaction that lead to thicker film formation, as the mesoscopic patterns would not have been otherwise observed. We also note a negative result. When a film was grown in the absence of light and subsequently illuminated with 320 nm light, after transferring to a microscope slide for about 1½ hr no imprint was observed. This result indicates that the imprint on the film resulted due to polymerization reaction in presence of light and not due to degradation of the polymer film upon UV radiation. Also, when aniline dissolved in H_2SO_4 was poured onto a glass slide and then dried up, which was further followed by placing the slide under UV irradiation (320 nm) for about 1½ hr no observable film formation took place. This suggests that in order to have imprints on a film simultaneous photochemical (from the top) and chemical polymerization (from the reagents present in the bulk) was necessary.

3.3.6 Mechanism

Based on our observation and previous related studies we propose the following as a possible mechanism resulting in the formation of pattern in the film. There are two competing catalytic polymerization reactions that are responsible for the polymerization of aniline in the present system. One is due to chemical reaction in presence of light and the other is due to chemical reaction only.

It is known that $KBrO_3$ and KBr in acidic medium produce BrO_2• radical

$BrO_3^- + Br^- + 2H^+ \rightarrow HBrO_2 + HOBr$

$HBrO_2 + Br^- + H^+ \rightarrow 2HOBr$

$HOBr + Br^- + H^+ \rightarrow Br_2 + H_2O$

$BrO_3^- + 5Br^- + 6H^+ \rightarrow 3Br_2 + 3H_2O$

$BrO_3^- + HBrO_2 + H^+ \rightarrow 2BrO_2\bullet + H_2O$

In absence of light, BrO_2• may play the key role as the radical initiator necessary for polymerization of aniline (ANI), so we have

$ANI + BrO_2\bullet + H^+ \rightarrow PANI\bullet + HBrO_2$

$PANI\bullet + PANI\bullet \rightarrow PANI$

PANI• is the polyaniline polymer radical.

But, in presence of light, Br_2 dissociates into Br• atoms [40] that probably initiate the polymerization in addition to BrO_2• initiator.

$Br_2 + h\nu \rightarrow 2\ Br\bullet$

$Br\bullet + ANI \rightarrow PANI\bullet + HBr$

$PANI\bullet + PANI\bullet \rightarrow PANI$

This reaction would be wavelength dependent, depending on the dissociation cross section of Br_2 upon absorption of light at various wavelengths. Radicals or other species generated by the chemical reaction plays a key role in the product formation in presence of

light. That may be the reason for obtaining mark even beyond the wavelength where aniline typically absorbs. In absence of light, mesoscopic nucleation pattern in the polymer formation at the interface formed is characteristic of the polymerization initiator. In presence of light Br• radicals act as initiators in addition to BrO_2• radical. This probably destroys the nucleation pattern that occurs in absence of light. The polymer growth is more in the photo-irradiated region of the interface and thus thickness is more as compared to non-illuminated part.

We have already mentioned that the clarity of the rectangular mark went down with increasing wavelength and was a nearly vanishing mark at 650 nm. At lower wavelengths of incident light, the photochemical reaction dominates over chemical reaction where light is impinged and the imprint is clearer as the nucleation patterns are not grown. On the other hand, with increasing wavelength of the incident light beam, the photochemical reaction becomes less and less important while the chemical catalyzed polymerization becomes predominant and as a result the imprint becomes increasingly nebulous. This is evident from the continuous macroscopic patterns observed in both the illuminated and non-illuminated parts of the film, when the wavelengths of light were longer (Figure 3.4).

3.4 Conclusion

In this chapter we have described a method for generating lithographic patterns on thin polyaniline films grown at the air-water interface, simultaneously in the presence of light over a wide incident wavelength range and chemical reagents in the bulk. The method takes advantage of the simultaneous chemical and photochemical reaction leading to polymerization of aniline. Our observation suggests that the polymer formed in the illuminated and non-illuminated parts of the films are chemically same. Radicals or other species generated by the chemical reaction plays a key role in the product formation in presence of light. That may be the reason for obtaining mark even beyond the wavelength where aniline typically absorbs. When light of appropriate wavelength is illuminated on a part of the interface where the film is grown, the mesoscopic nucleation patterns are not formed in those parts where the light beam is present. On the other hand, the rest of the film grows with characteristic nucleation pattern. The growth of the polymer film is more on photo-illuminated part as compared to non-illuminated region thus having more thickness. This results in light induced imprints with a darker appearance in the film.

The new technique of photolithography reported here in thin polymer films formed at the air – water interface may have certain advantage over other methods as the imprint is embedded in the film of the same material and a wide range of wavelengths of incident light can be used. This method does not involve removing any part of the formed film and hence is non destructive. Even though the resolution of the imprints is low in our case, in principle the resolution can be made much higher with appropriate light source and optical masks. In addition, the contrast in optical density of the films could be tuned with appropriate choice of polymer forming materials. Also, one can envision the generation of polymer doped with chemical sensors whose chemical nature could be altered by light. Thus an array of molecules with different chemical structures can be imprinted in the polymer thin film.

3.5 References

1. Zhao, B.; Moore, J. S.; Beebe, D. J.; *Science* **2001**, 291, 1023.
2. Fodor, S. P.; Reid, J. L.; Pirrung, M. C.; Stryer, L.; Lu, A. T.; Solas, D. *Science* **1991**, *251*, 767.
3. Doshi, D. A.; Huesing, N. K.; Lu, M.; Fan, H.; Lu, Y.; Simmons- Potter, K.; Potter, B. G., Jr.; Hurd, A. J.; Brinker, J. *Science* **2000**, 290, 107.
4. Kenis, P. J. A.; Ismagilov, R. F.; Takayama, S.; Whitesides, G. M. *Acc. Chem. Res.* **2000**, 33, 841.
5. Zhao, X. M.; Xia, Y.; Whitesides, G. M., *J. Mater. Chem.* **1997**, 7, 1069.
6. Xia, Y.; Whitesides, G. M., *Angew. Chem. Int. Ed.* **1998,** 37, 550.
7. Xia, Y.N.; Rogers, J.A.; Paul, K.E.; Whitesides, G.M. *Chem. Rev*. **1999,** 99, 1823.
8. Xia, Y.; Whitesides, G. M., *Annu. Rev. Mater. Sci.* **1998,** 28, 153.
9. Odom, T. W.; Thalladi, V. R.; Love, J. C.; Whitesides, G. M. *J. Am. Chem. Soc.* **2002**, 124, 12113.
10. Wang, R.; Hashimoto, K.; Fujishima, A.; Chikuni, M.; Kojima, E.; Kitamura, A.; Shimohigoshi, M.; Watanabe, T. *Nature* **1997**, 388, 431.
11. Urban, G.; *Sens. Actuators* **1999,** 74, 219.

12. Pathak, S.; Dentinger, P. M. *Langmuir* **2003**, 19, 1948.

13. Gillmor, S. D.; Thiel, A. J.; Strother, T. C.; Smith, L. M.; Lagally, M. G. *Langmuir* **2000**, 16, 7223.

14. Kirby, B. J.; Shepodd, T. J.; Hasselbrink Jr., E. F. *J. Chromatogr. A* **2002**, 979, 147.

15. Kumar, A.; Biebuyck, A. B.; Whitesides, G. M. *Langmuir* **1994**, 10, 1498.

16. Morigaki, K.; Baumgart, T.; Offenhauser, A.; Knoll, W. *Angew. Chem. Int. Ed. Engl.* **2001,** 40, 172.

17. Wallraff, G. M.; Hinsberg, W. D. *Chem Rev.* **1999,** 99, 1801.

18. Nonogaki, S.; Ueno, T.; Ito, T. *Microlithography fundamentals in semiconductor devices and fabrication technology,* Marcel Dekker Inc, New York, **1998.**

19. Hatzor, A.; Weiss, P. S. *Science,* **2001**, 291, 1019.

20. Toyota, E.; Washio, M. *J. Vac. Sci. Technol B.* **2002**, 20, 2979.

21. Romanato, F.; Businaro, L.; Di Fabrizio E.; Passaseo, A.; De Villorio, M.; Cingolani, R.; Patrini, M.; Galli, M.; Bajoni, D.; Andreani, L. C. *Nanotechnology* **2002**, 13, 644.

22. Naessens, K.; Van Daele en Poel, P. *Proceedings Symposium IEEE/LEOS Benelux Chapter,* **2000,** 99.

23. Schäfer, D.; Ihlemann, J.; Marowsky, G.; Herman, P. R. *Appl. Phys. A* 72, 377.

24. Aoki, A.; Miyashita, T. *Polymer*, **2001**, 42, 7307.

25. Miyashita, T.; Nakaya, M.; Aoki, A. *Thin Solid Films,* **1998,** 327, 833.

26. Böhme, P.; Vedantham, G.; Przybycien, T.; Belfort, G. *Langmuir* **1999,** 15, 5323.

27. Prucker, O.; Rühe, J. *Macromolecule* **1998**, 31, 592.

28. Rozsnyai, L. F.; Wrighton, M. S. *J. Am. Chem. Soc.* **1994,** 116, 5993.

29. Huang, J.; Hemminger, J. C. *J. Am. Chem. Soc*. **1993**, 115, 3342.

30. Huang, J.; Dahlgren, D. A.; Hemminger, J. C. *Langmuir* **1994**, 10, 626.

31. Tarlov, M. J.; Burgess, R. F.; Gillen, G. *J. Am. Chem. Soc*. **1993**, 115, 535.

32. Li, M.; Xu, S.; Kumacheva, E. *Langmuir* **2000,** 16, 7275.

33. Riede, A.; Helmstedt, M.; Riede, V. *Langmuir* **2000**, 16, 6240.

34. Zhao, B.; Neoh, K. G.; Liu, F. T.; Kang, E. T.; Tan, K. L. *Langmuir* **1999,** 15, 8259.

35. Trivedi, D. C. *Bull. Mater. Sci.* 1999, 22, 447.

36. Gospodinova, N.; Mokreva, P.; Terlemezyan, L. *Chem. Commun.* **1992,** 923.

37. Moon, D. K.; Osakada, K.; Maruyama, T.; Yamamoto, T. *Makromol. Chem.* **1992,** 193, 1723.

38. Moon, D. K.; Osakada, K.; Maruyama, T.; Kubota, K.; Yamamoto, T. *Macromolecules* **1993,** 26, 6992.

39. MacDiarmid, A. G. *Synth. Metals* **1997,** 84, 27.

40. Oldman, R. J.; Sander, R. K., Wilson, K. R. *J. Chem. Phys.* **1975**, 63, 425.

Chapter 4

Polypyrrole TiO_2 Nanoparticles Composite Thin Film Formation at the Air-Water Interface

4.1 Introduction

The promise of Nanotechnology with application potential in sensing devices[1], photonic materials, molecular electronics and advanced oxidation techniques [2] has propelled intense research activity, among others, in finding methods of synthesis and functionalization of semiconductor [3-5] and metal nanoparticles (NPs) [6-11]. Moreover, size and shape depended optical and electronic properties of NPs make them attractive for exploitation in photochemical reactions. For example, photoassisted organic pollutant degradation using semiconducting oxide material is attracting great attention as an alternative technology to waste water treatment [12]. Generally under photo-excitation semiconductors undergo charge separation and initiate oxidation of the organic compound at the interface. Thus nanostructured semiconducting oxides with their size dependent band gap are practically useful for photodegradation of organic compounds [13-14]. Therefore, photocatalytic electron and hole redox potentials of size quantized semiconductor nanocrystals can be tuned to achieve increased catalytic efficiency for selective photochemical reaction. Moreover as photocatalytic reaction occurs at the surface, nanosized semiconductor's high surface to volume ratio will contribute to increase in the decomposition rate. In other words decreasing the sizes of nanoparticles will bring about increased rate of decomposition of organic contaminant. In this regard one of the useful and well-studied materials is titanium dioxide. Its choice is borne by the fact that TiO_2 is a photocatalyst, which among numerous applications aids in the decomposition of organic materials. TiO_2 has been used extensively in dye-sensitized solar cells [15-25.] Also, TiO_2 is chemically stable and biologically inert, making it environment friendly. The advantages mentioned above call for finding ways of generation and incorporation of TiO_2 NPs in appropriate host depending on the nature of applications.

An ideal scenario of device fabrication would be NPs well dispersed in a matrix for structural integrity along with accessibility of the NPs to the reacting molecules in a medium. An array of NPs made immobile on a solid substrate surface would seem to fulfill the promises of best of both worlds – the catalytic efficiency of NPs and the possibility of repeated use upon immobilization. The challenge, however, lies in the ability to incorporate NPs on the surfaces of such a substrate. An intriguing option in this regard is the incorporation of NPs such as hat of TiO_2 in a polymer thin film. The application potential

would increase manifold if the polymer in question would be a conducting one. Metal and semiconductor NPs embedded conducting polymers have the advantage of flexibility and conductivity of the film along with the optical, electronic and catalytic property of the NPs.

The last three decades have witnessed an enormous growth in the literature on "synthetic metal" i.e. conducting polymers[26] as they represent best of two worlds; the properties of metal and flexibility of organic materials. Enormous amount of studies have been devoted to develop methodologies for their synthesis[27-29] study their properties and applications [30-31]. Polymer thin films are of great technological importance due to their applications in microelectronics, displays, lithography, sensors and as non-linear optical materials. The idea that films of conducting polymers on electrodes could be switched electrochemically between the insulating and conductive states with a corresponding change in the electrical, optical and chemical properties, while retaining the attractive mechanical properties of the polymer, is quite remarkable. In general, these polymers are doped to enhance the electrical conductivity over the full range from insulator to metal. Semiconductors have also been incorporated in polymer matrix to achieve the desired objectives.

We were interested in the possibility of incorporation of TiO_2 NPs in thin films of the well-studied conducting polymer polyaniline (PANI). We have already described in Chapter 2 a new method of thin PANI film formation at the air-water interface. We have however been unsuccessful in incorporating TiO_2 NPs in the thin film of PANI using a method similar to that described in Chapter 2. We tried in vain in making thin film with the incorporation of TiO_2 NPs, using H_2O_2 for the polymerization of aniline. On the other hand we were successful in fabricating thin film of TiO_2 NPs incorporated polypyrrole (PPy). Polypyrrole can be easily synthesized by reaction with H_2O_2. We discovered that just like PANI, a thin PPy film was formed at air-water interface when A simple UV-visible spectroscopic probe for observing collapse of Langmuir-Blodgett monolayers at air-water interface had been treated with H_2O_2.

In this chapter we report a new method of PPy thin film generation at the air-water interface. We also report a method of incorporation of TiO_2 NPs in these films. The TiO_2 containing PPy films when transferred onto glass substrates were able to photocatalytically oxidize iodide ions in potassium iodide solution to triiodide. Further, the same films could

photocatalyze the decomposition of methyl orange and methylene blue. UV-visible spectroscopic, electron microscopic and X-ray diffraction methods were used to characterize the TiO_2 incorporation into of the film. The photocatalysis was followed by UV-vis spectroscopy.

4.2 Experimental Section

Materials and Instrumentation: The materials used in the experiment are as follows. Titanium isopropoxide (Aldrich), iso- propanol (MERK), hydrogen peroxide (MERK), hydrochloric acid (MERK), sulfuric acid (MERK), pyrrole (Aldrich), potassium iodide (CDH), potassium dichromate (CDH), methylene blue (Qualigen). The substrates used for depositing thin polymer film are microslides procured from Blue Star, India. Mili Q water (resistivity 18.2 MΩcm) was used for all the experiments.

Reactions were monitored using UV-visible spectrophotometer (Shimadzu U-2001). Transmission electron microscope (TEM) studies of the samples were carried out using JEOL; JEM 100 CX II where the accelerating voltage used was 80 KV. For this experiment a drop of TiO_2 solution was placed on a carbon grid and then evaporated before recording the micrograph. Scanning Electron Microscope studies were carried out in JEOL instrument (model JSM-35CF). The accelerating voltage used was 20kV. The sample slide containing TiO_2 embedded PPy film was coated with Au before recording the micrograph. A Seifert powder X – Ray diffractometer (XRD 3003 TT) with Cu - a source with wavelength 1.54 Å was used for recording XRD data at room temperature.

4.2.1 Preparation of TiO_2 nanoparticles

A stock solution of 10% (v/v) titanium isopropoxide in iso-propanol was prepared. 1000 µL of the isopropoxide stock solution was added, with continuous stirring, to a round bottom flask containing 10 mL of 0.5 M hydrochloric acid. The resultant solution was heated to 60 °C with continuous stirring was for 3 hours. The NPs formation was further confirmed by UV-vis spectroscopic, TEM and XRD.

4.2.2 Preparation of thin polymer film containing TiO_2 NPs

The experimental setup consisted of a watch glass placed on a petri dish containing water, which served as the water bath. The setup was the same as that described in Chapter 2.

The TiO_2 nanoparticles prepared separately, as described in the previous section, and 30% hydrogen peroxide were mixed in a test tube. The resultant solution turned yellow which is known to be due to the formation of titanium peroxide. The solution was then poured onto the watch glass. Pyrrole was introduced to the reaction mixture as vapor by hanging a small beaker containing pyrrole. The beaker was kept hanging from an inverted funnel, similar to the experimental setup already described in chapter 2 (Figure 2.2). It took about 3 hr to form a film at the air-water interface. The film thus formed was washed carefully by repeated addition and draining of water from the sides of the watch glass and then transferred onto a clean glass slide.

4.2.3 Photocatalysis of the polypyrrole film containing TiO_2 NPs

It is well known that TiO_2 photocatalyst is a strong oxidizing agent, having the ability to oxidize water to hydroxyl radicals, which in turn decomposes organic compounds. The photo-oxidation reaction occurs on the surface of TiO_2 and hence NPs form is expected to be more efficient as catalyst. In the present case, NPs embedded PPy films were transferred onto glass substrates and used as photocatalyst for the degradation of organic dye. In all the experiments conducted to study the photocatalytic properties of NPs embedded thin PPy film, the glass plate containing the thin film was immersed in a small beaker containing the reactant, before irradiating it with UV light. The general experimental set up is shown in Figure 4.1.

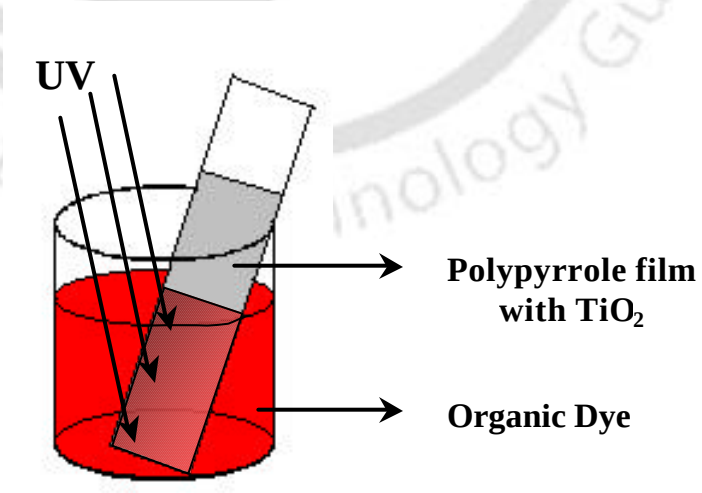

Figure 4.1: The general strategy adopted in studying the photocatalyst properties of the polypyrrole film embedded with TiO_2 NPs. *(See color plates, page 136)*

4.3 Result and Discussions

When titanium isopropoxide was heated at 60^0C for 3 hr a partially cloudy solution was obtained which had strong optical absorption below 250 nm typical of that of colloidal TiO_2 NPs. A typical UV-vis spectrum of such a solution is shown in Figure 4.2. TEM measurement (Figure 4.3) showed the evidence of formation of NPs with particle size of about 200-300 nm. The solution containing the same NPs turned yellow upon treatment with H_2O_2. The yellow color is generally attributed to the formation of titanium peroxide. When pyrrole was introduced from the vapor phase to this solution a dark brown colored thin film as well as bulk precipitate were obtained. The thin film was formed at the air-water interface and after 3 hr of reaction time the film was sufficiently thick for transfer to microscope slides for further analysis. Scanning electron micrograph (SEM) of the films showed formation of clusters of particles of similar sizes in the film. These clusters were separated from each other but many particles appeared to have been merged with each other in the film. A typical SEM picture of a film is shown in Figure 4.4, which clearly demonstrates the formation of clusters of 200-300 nm particles.

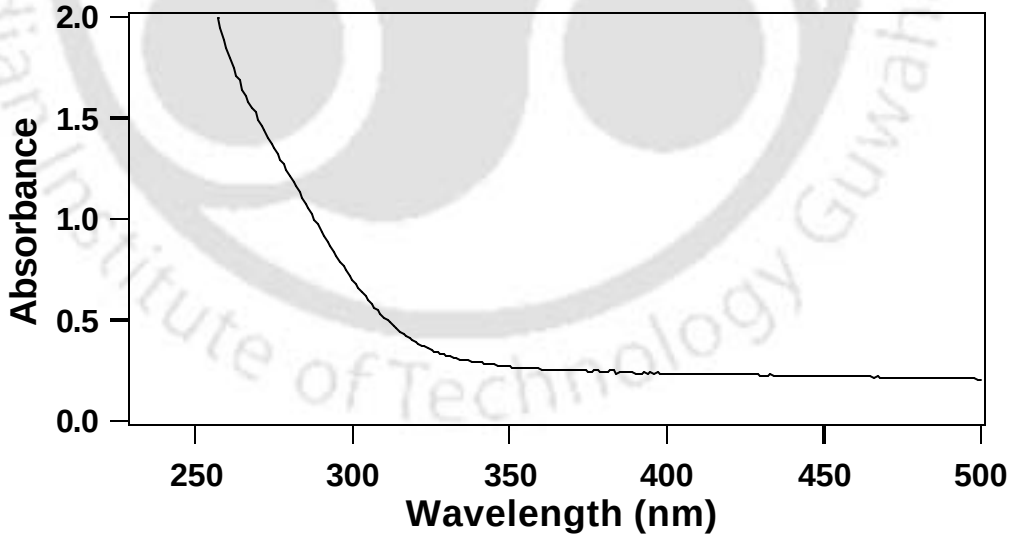

Figure 4.2 UV-visible of TiO_2 nanoparticles formed by the hydrolysis of titanium isopropoxide.

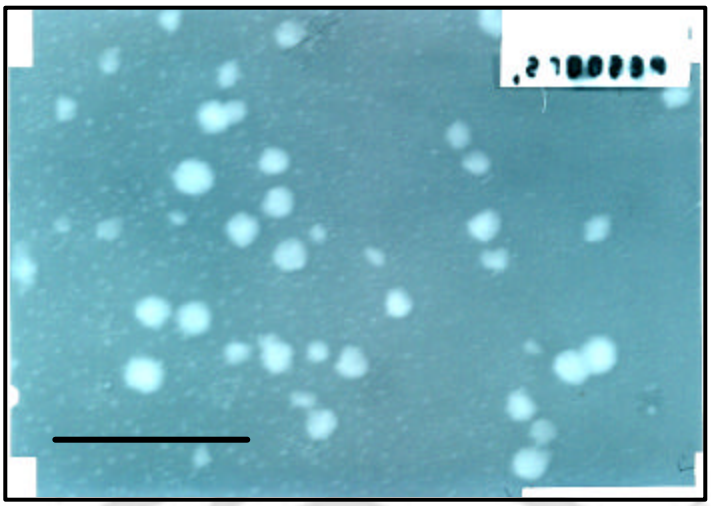

Figure 4.3 The transmission electron micrograph image of the TiO_2 nanoparticles formed in aqueous solution by hydrolysis of titanium isopropoxide. The scale bar is 1.6µm.

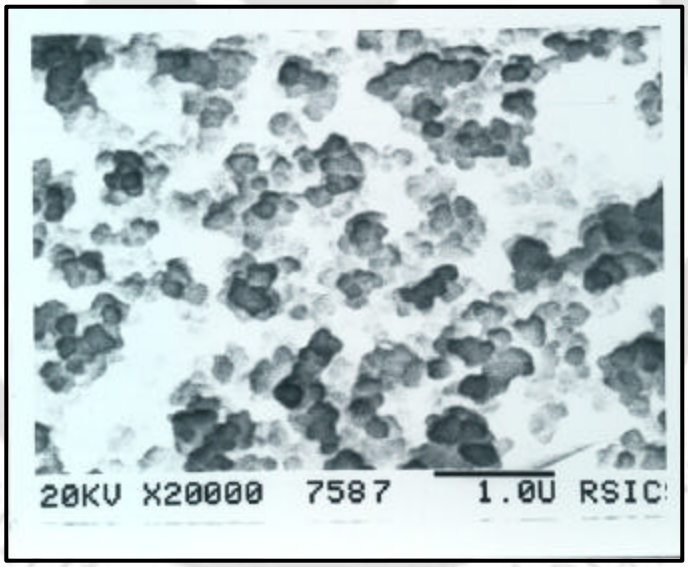

Figure 4.4 Scanning electron micrograph of the polypyrrole film containing TiO_2 nanoparticles.

We further pursued powder X-ray diffraction measurements to confirm the presence of TiO_2 in the film. Unfortunately the signal from a single such film with respect to XRD of TiO_2 was too weak to be observed. To overcome this problem a set of 5 such films were grown independently in different reaction batch under identical condition. The films were then lifted from their respective solutions, cleaned with water and air-dried. Finally, these films were ground into powders for recording XRD.

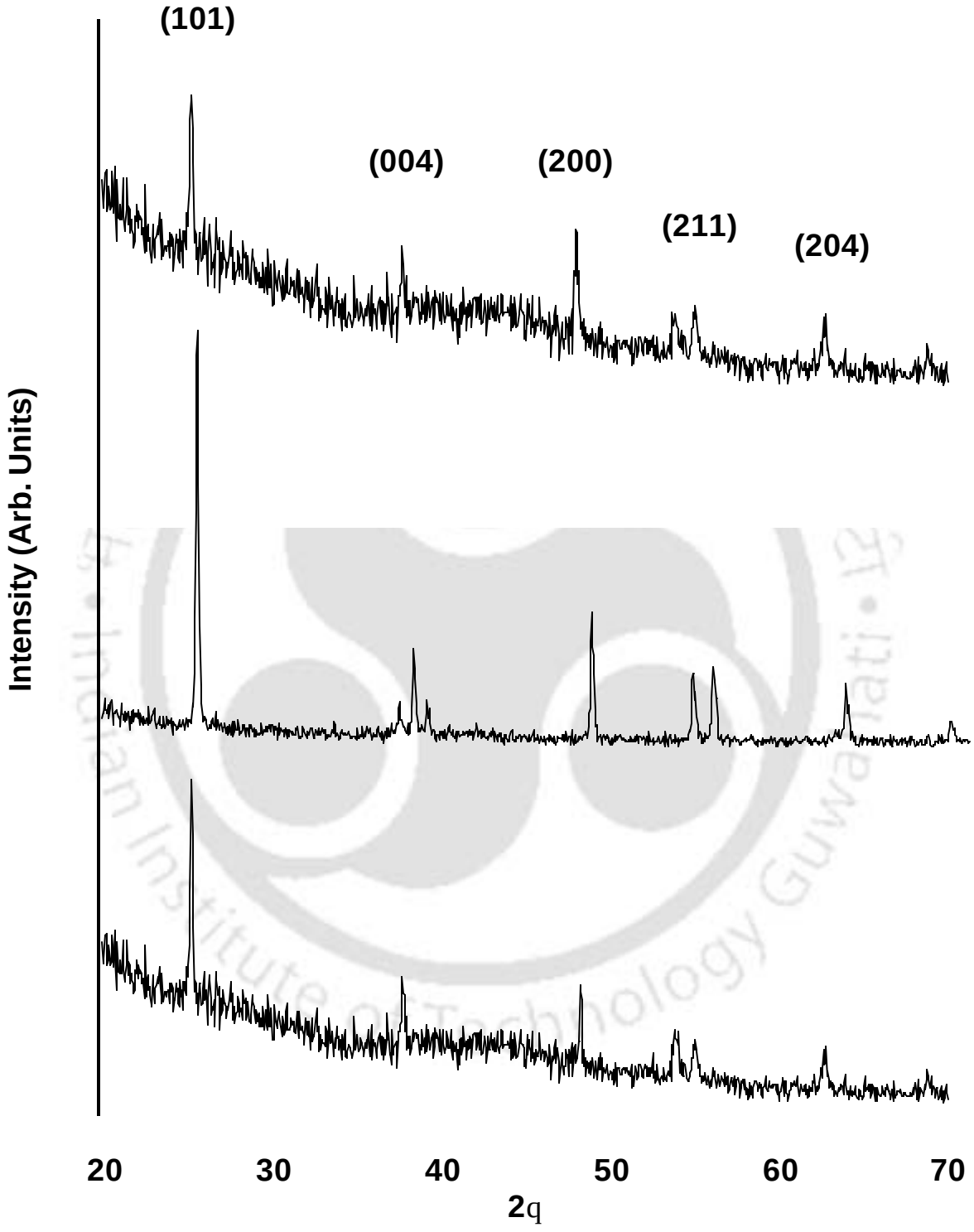

Figure 4.5: X-ray diffraction patterns of (a) polypyrrole film containing TiO_2 NPs (b) TiO_2 particles deposited on glass slide (c) bulk polypyrrole TiO_2 composite precipitate.

We could obtain clear signal due to XRD diffraction pattern, which is shown in Figure 4.5a. The X-Ray diffraction pattern had peaks at $2\theta = 25.32^o$ 37.86^o, 48.06^o, 53.97^o, 55.09^o,62.75^o and 68.87^o (PDF 86-1157), which correspond to (101) (004), (200), (105), (211), (204) and (116) respectively of anatase-syn form of TiO_2. Also shown, as a reference in Figure 4.5b is the XRD patterns of TiO_2 particles. These particles were prepared by hydrolysis of a concentrated solution of titanium isopropoxide. For this the solution containing TiO_2 was centrifuged followed by decantation of the solvent. The solid was transferred to a slide and dried in an oven before recording the XRD. Further, XRD pattern of the bulk polymer shown in Figure 4.5c shows similar characteristic peaks. The only difference in XRD patterns between the TiO_2 (Figure 4.5b) and the polymer TiO_2 composite (in film as well as in the bulk; Figure 4.5a and 4.5c) is the absence of two weak peaks at 38 and 39^0, which is probably due to inherent weakness of the signal itself rather than any other effect.

Next, we were interested in finding the photocatalytic properties of the thin polypyrrole film containing TiO_2 NPs. A sample study was performed with iodide ions in potassium iodide solution to oxidize to triiodide using the film**.** Three beakers, each

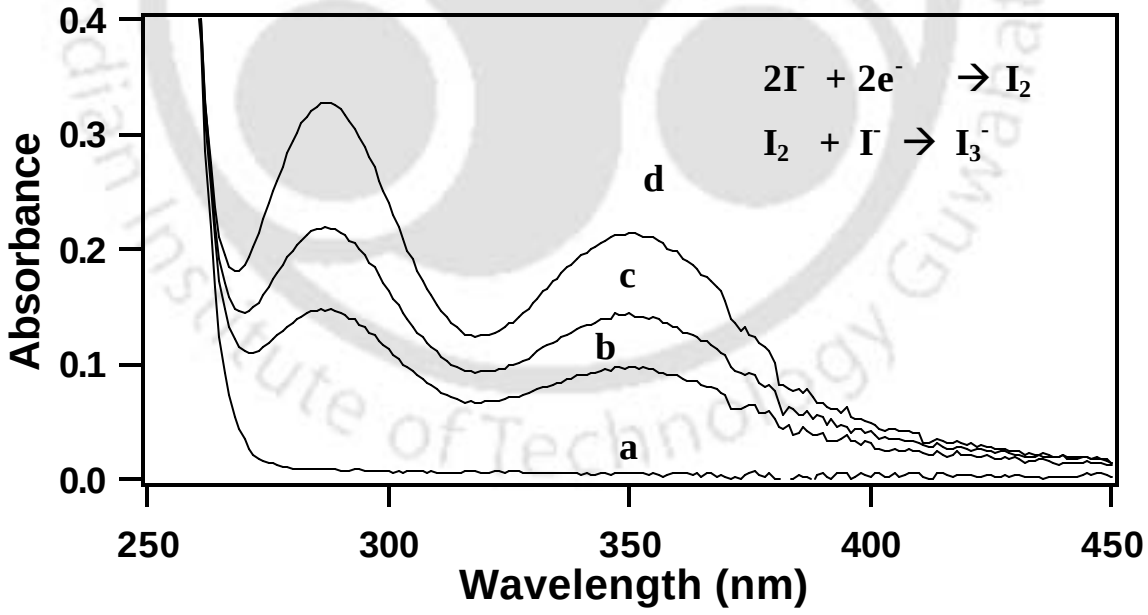

Figure 4.6 UV-vis spectra of potassium iodide solution (a) at 0 hrs, (b) irradiated for 2 hrs, (c) irradiated for 2 hours in the presence of a polypyrrole film, (d) irradiated for 2 hours in the presence of thin polypyrrole film containing TiO_2. The light source used was an ordinary TLC plate UV lamp at 254 nm.

containing 10 mM potassium iodide solution, were taken. In the first beaker, polypyrrole film containing TiO_2 NPs was immersed, in the second beaker plain polypyrrole film was immersed and the in the third beaker there was no film. These three solutions were irradiated with 254nm UV light simultaneously and kept for 2 hr. It is well known that photocatalytic oxidation of iodide ions (I^-) produces iodine molecules (I_2), which combine with iodide ions (I^-) yielding tri-iodide ions (I_3^-) that absorbs light at 352 nm. Therefore, upon photo irradiation, the appearance of the 352nm peak in UV-vis spectrum is taken to be indicative of the formation of the photo-oxidation product, I_3^-. Figure 4.6 shows the UV-vis spectra of the results of the catalytic oxidation of iodide ions to tri-iodide in the presence of UV light.

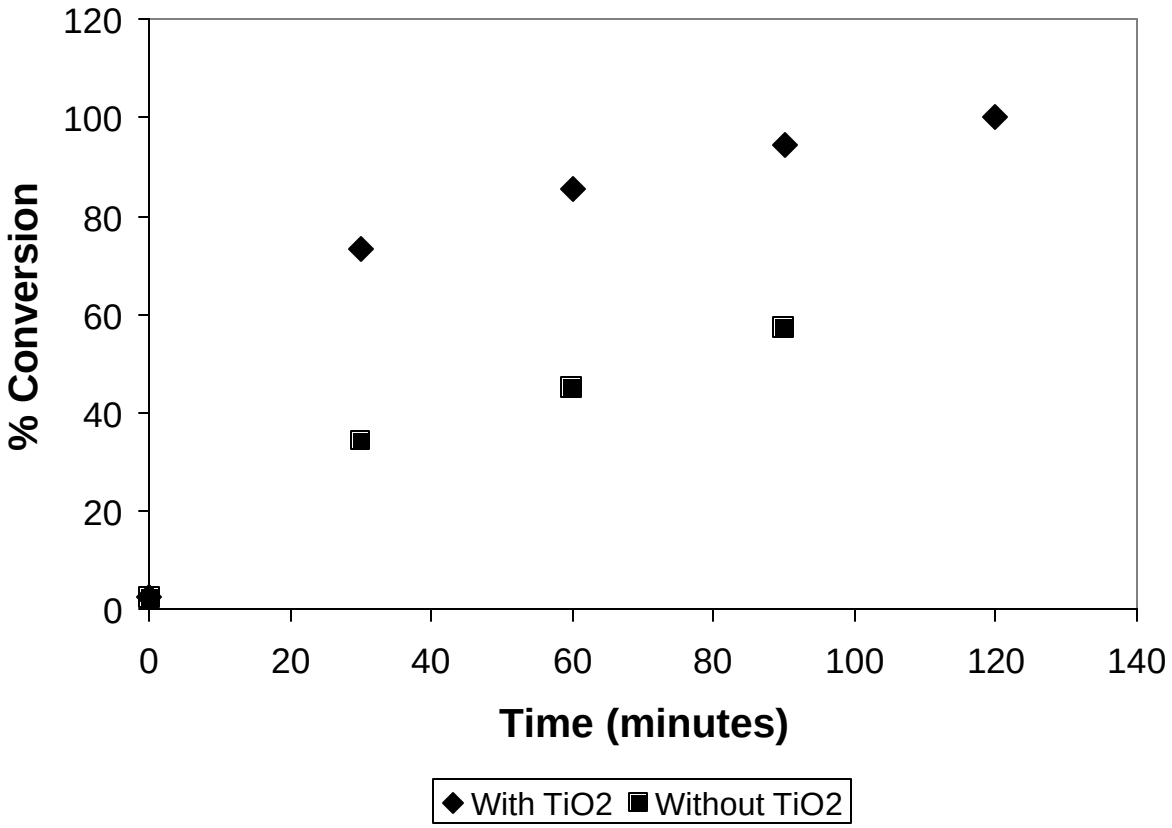

Figure 4.7: Percentage conversion of iodide ions (I^-) tri-iodide ions (I_3^-) versus different irradiation time in the photocatalytic oxidation of potassium iodide in the presence of polypyrrole film with or without TiO_2 NPs.

As clear from Figure 4.6 (a) there is no peak at 352 nm before irradiation, indicating the absence of tri-iodide ion (I_3^-). After two hours of irradiation tri-iodide ions (I_3^-) formed as a result of photo-oxidation of iodide (I-) ions, resulting in an appearance of absorbance at 352

nm. It is quite clear from the figure 4.6 (b), (c) and (d), that more tri-iodide ions (I_3^-) were formed when TiO_2 NPs embedded polypyrrole film had been used as compared to when only polypyrrole film was used. Percentage conversion of I^- ions to I_3^- ions with irradiation time, in the presence and absence of TiO_2 NPs in polypyrrole film is plotted in Figure 4.7. Here the conversion of I to I_3^- in the presence of TiO_2 incorporated PPy film in 2 hr, measured at the absorption maximum of 352 nm (Figure 4.5) was taken as 100%. The plot clearly shows that while the percentage conversion to tri-iodide is only 34.3 % in the presence of a plain polypyrrole film after 30 minutes of irradiation, the value increases to 73.2 % in the presence of TiO_2 NPs embedded in the polypyrole film for the same duration of irradiation. The data also shows that after 2 hours of irradiation while there is about 100 % conversion of I to I_3^- in presence of TiO_2 NPs, the conversion is only 66.7 % in the absence of TiO_2 NPs in the polypyrrole film. The above experiment demonstrates the ability of the TiO_2 NPs embedded polymer film in photo-catalyzing the oxidation of potassium iodide.

We also investigated the catalytic property of TiO_2 NPs embedded thin polypyrrole films on the photo degradation of some typical dyes, such as methyl orange and methylene blue. Similar to the photo catalyzed studies involving iodide ions, for each dye, three solutions of identical concentrations and amounts were taken. In the first beaker polypyrrole film with embedded TiO_2 NPs was immersed, in the second plain polyrrole films was immersed and the third beaker served as the blank.

Figure 4.8 shows the UV-visible spectra of methyl orange irradiated with 365 nm for 90 minutes in absence of the film and in the presence and absence of TiO_2 NPs in the film. It is evident from the figure that in the presence of polypyrrole film containing TiO_2 NPs there was substantial decrease in the absorbance of methyl orange peak at λ_{max} = 462 nm as compared to a polypyrrole film without TiO_2 NPs. Percentage decay with irradiation time plot (Figure 4.9) using absorption at the λ_{max} shows that in presence of TiO_2 NPs embedded polypyrrole film, there was 29.5 % decay after 15 minutes of irradiation as compared only 4.8 % decay in the presence of only polypyrrole film. The percentage decay increased to 46.1% after 90 minutes of UV irradiation for TiO_2 NPs embedded polypyrrole film whereas for the same duration of irradiation the percentage decay in the presence of polypyrrole film was only 17.9 %. The plot clearly shows the effectiveness of the degradation of methyl orange in the presence of polypyrrole film containing TiO_2 NPs as compared to only polypyrrole film.

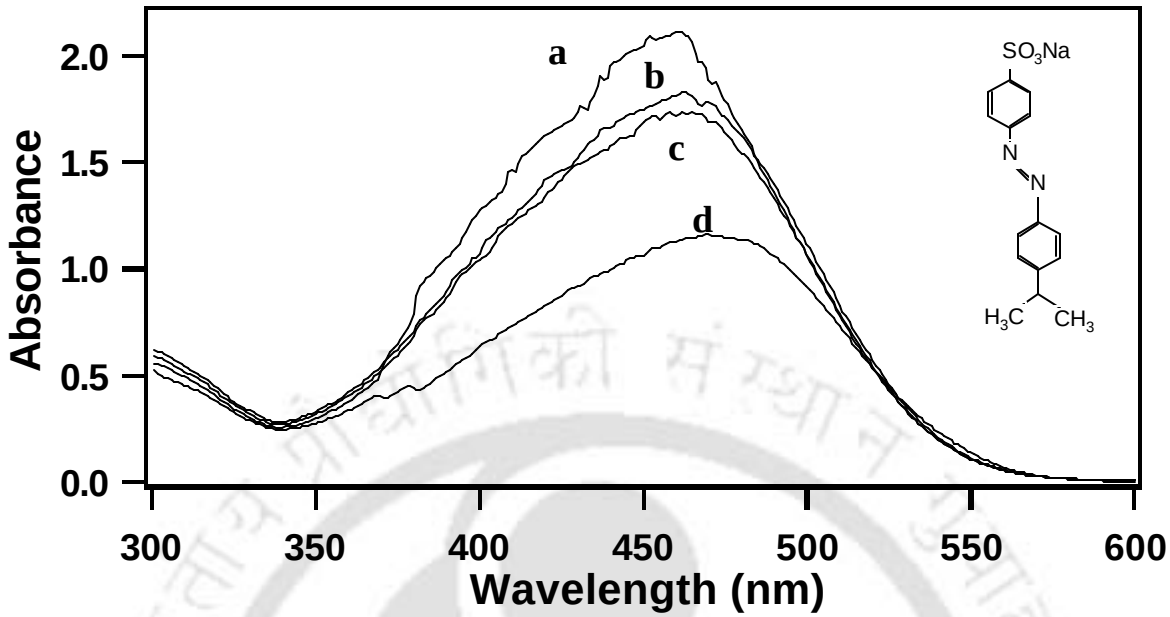

Figure 4.8: UV-visible spectra of methyl orange with UV irradiation for (a) 0 min (b) 90 min (c) 90 min in the presence of polypyrrole film (d) 90 min in the presence of polypyrrole film containing TiO_2 nanoparticles.

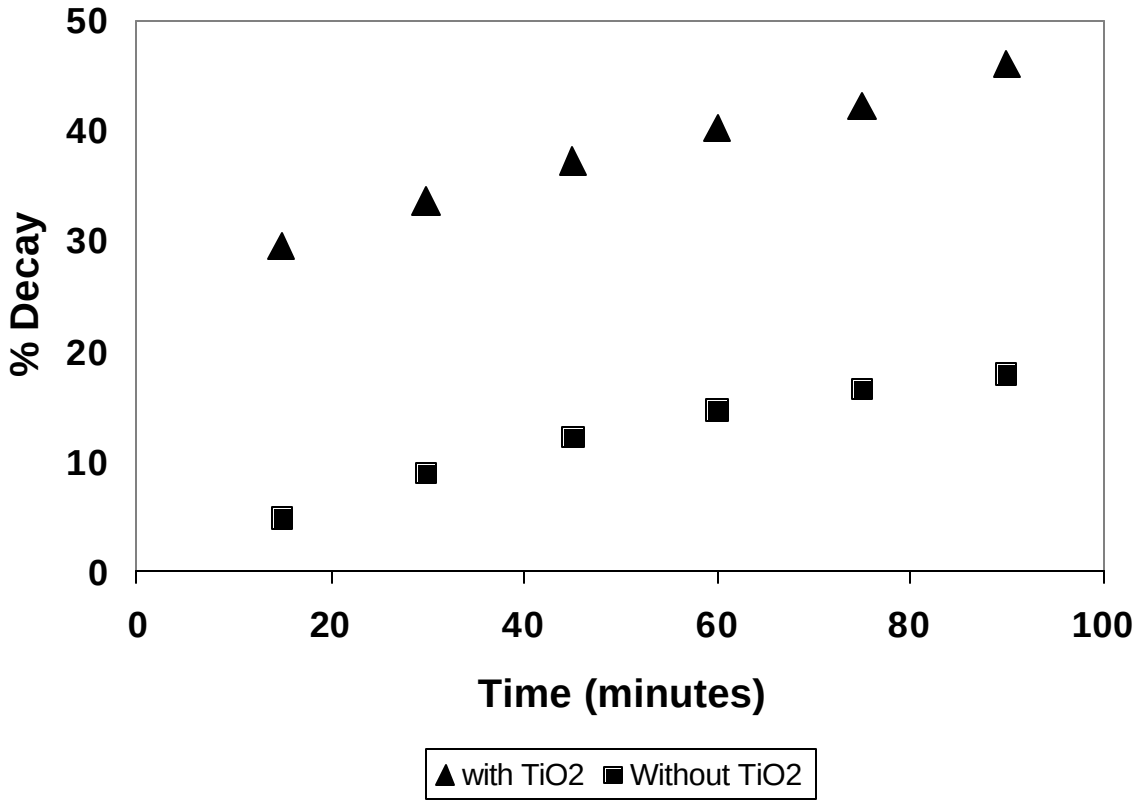

Figure 4.9: Percentage decay versus time with different hours of irradiation in the photocatalytic degradation of methyl orange in the presence and absence of TiO_2 in polypyrrole films.

In a similar fashion, the photodegradation of methylene blue solution by the same three systems mentioned above using a UV light of 365 nm, was monitored by visible spectroscopy and the results are presented in Figure 4.10, where the absorption peak at around 670 nm is due to methylene blue and irradiation time was 60 minutes. Again there is evidence that TiO_2 NPs containing polypyrrole film (Figure 4.10 d) was a more efficient photocatalyst than a simple polypyrrole film (Figure 4.10 c) or by light in the absence of any film (Figure 4.10 b). The degradation of methylene blue is most pronounced in the presence of polypyrrole film containing TiO_2 NPs.

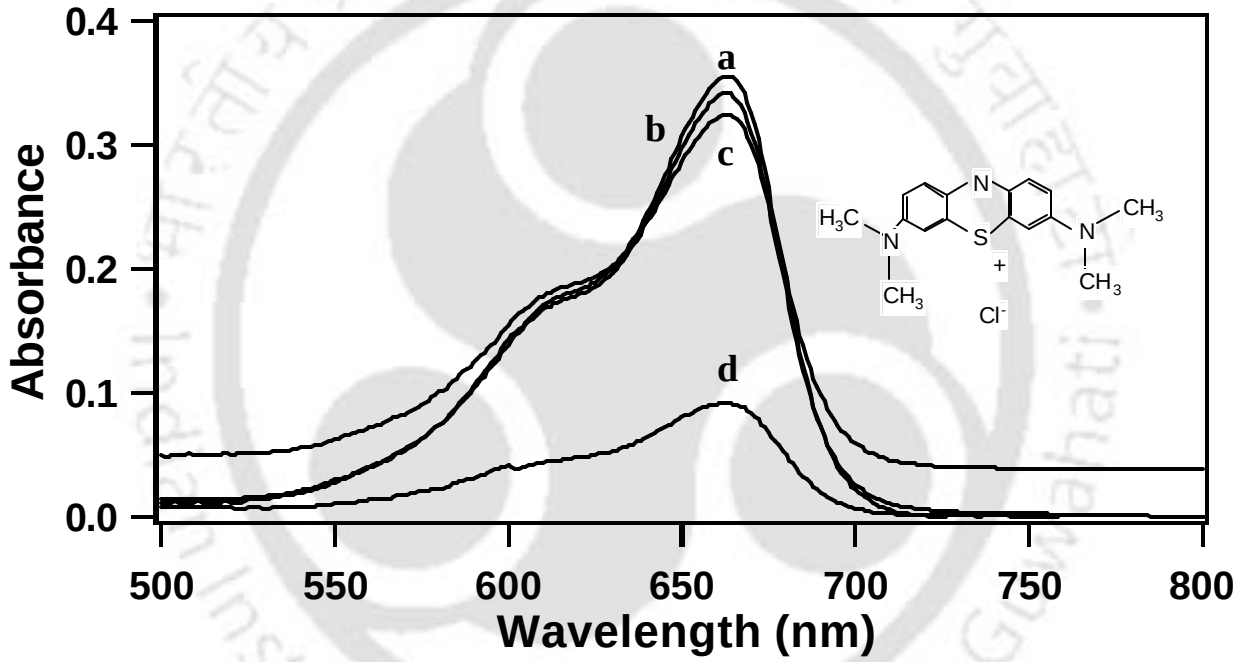

Figure 4.10: UV-visible spectra of methylene blue with UV irradiation for (a) 0 min (b) 60 min (c) 60 min in the presence of polypyrrole film (d) 60 min in the presence of polypyrrole film containing TiO_2 nanoparticles.

In this case too, the percentage decay of methylene blue with irradiation time was plotted (Figure 4.11) using absorbance value at the λ_{max}. For example after a 15 minute irradiation, percentage decay in the presence of PPy film containing TiO_2 NPs is 50% as compared to only 1.4 % in the absence of TiO_2 NPs in the polypyrrole film. The percentage decomposition of methylene blue increased to 74.08% after one hour of UV irradiation

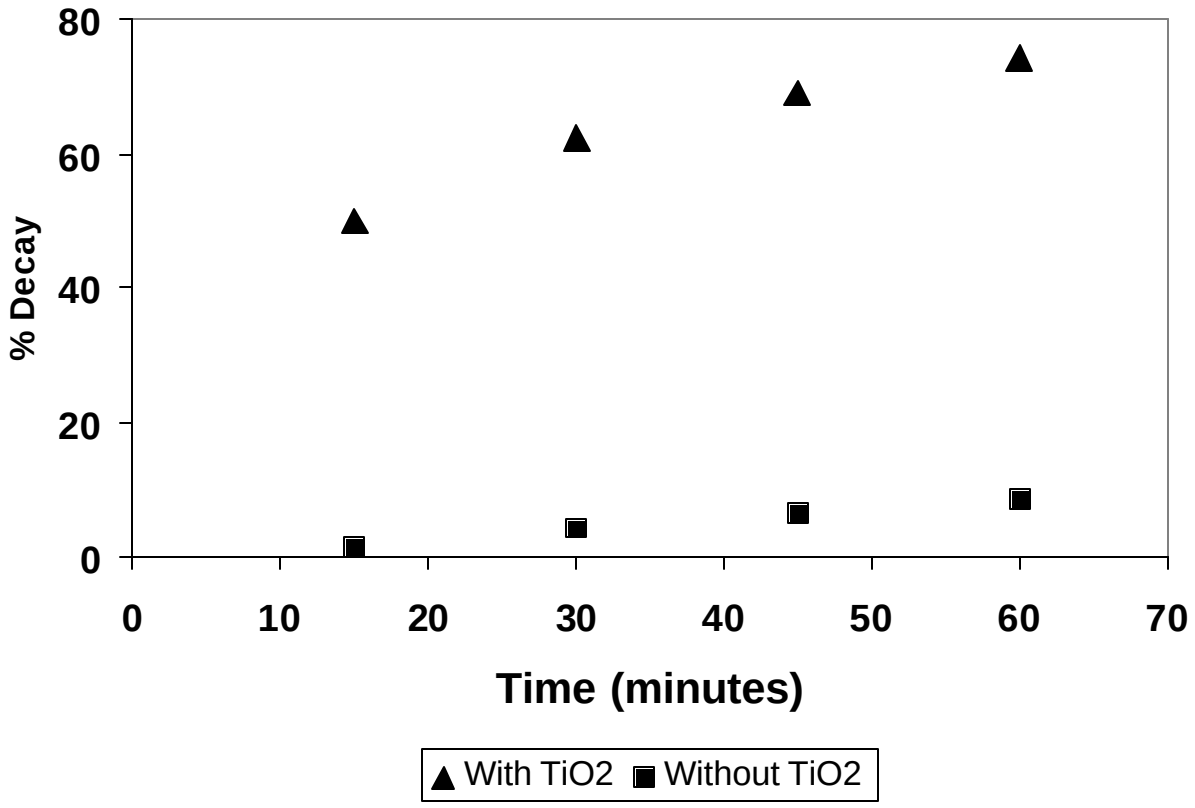

Figure 4.11 Percentage decay versus time with different hours of irradiation in the photocatalytic degradation of methylene Blue

in the presence of polypyrrole film containing TiO_2 NPs, while this was only 8.47 % for the case of polypyrrole film in the absence of TiO_2 NPs. This difference is quite remarkable. It may be mentioned here that the same TiO_2 containing PPy film could be used for several such runs without much change in the catalytic efficiency. We have found that for three consecutive runs the efficiency of degradation of methylene blue was the same.

It is well established [32] that TiO_2 acts as sensitizers for light induced redox process due to its electronic structure, which is characterized by a filled valence band (VB) and an empty conduction band (CB). When a photon with energy of *h?* matches or exceeds the band gap energy of TiO_2 of 3.2 eV, an electron, e^-_{cb}, is promoted from valence band (VB) to conduction band (CB) leaving a hole, $h_{vb}+$, behind. Excited state conduction band electron (e^-_{cb}) and valence band hole ($h_{vb}+$) can either combine and dissipate the input energy as heat,

go to a trapped state or react with suitable electron donor and acceptor on the semiconductor surface.

The trapped state may subsequently be useful to catalyze redox reactions. The valence band holes are known to be powerful oxidants while conduction band electrons are good reductants. Thus TiO_2 NPs present in the film may act as a redox catalyst after absorption of light of appropriate frequency. A general scheme of the primary process may be represented as under.

$$TiO_2 + h? \rightarrow h_{vb}^{+} + e_{cb}^{-}$$

$$h_{vb}^{+} + >TiOH \rightarrow \{>TiOH\bullet\}^{+}$$

$$\{>TiOH\bullet\}^{+} + Red \rightarrow >TiOH + Red\bullet^{+}$$

$$e_{tr}^{-} + OX \rightarrow OX^{\bullet -}$$

where Red is an electron donor (i.e reductant), in our case it is iodide, methyl orange or methylene blue. OX is an electron acceptor (i.e oxidant), in the present system, it will be oxygen. >TiOH represents primary hydrated surface functionality of TiO_2.

Here e_{tr}^{-} represents an electron in a trap state, which may react with any oxidizing species present in the reaction media including the polypyrrole film itself or TiOH (which has to be a slower process in order for the catalysis to be kinetically effective).

4.4 Conclusion

In this chapter we have shown that TiO_2 NPs could be incorporated into thin polypyrrole films by growing the film in the presence of TiO_2 NPs and H_2O_2 along with pyrrole monomer (vapor) present in the reaction medium under acidic condition. The film grew at the air-water interface in addition to bulk polymer formation. We were able to show eidence for the presence of TiO_2 NPs in the film by TEM and XRD methods. In addition, we were also successful in using these films containing TiO_2 NPs to photocatalytically oxidize iodide ions in potassium iodide solution to triiodide. It was further shown that TiO_2 NPs containing thin polypyrrole film could also photocatalyze the decomposition of methyl orange and methylene blue. These films were quite stable to withstand transfer to glass slides, hours of exposure to radiation and the presence of species in the reaction media. At the same time

the advantage of using supported TiO_2 NPs such as ours is that the catalyst can be used repeatedly without any workup that is usually associated with the recovery of a catalyst from the bulk after the reaction is over.

4.5 References

1. Niemeyer, C. M.; Ceyhan, B.; Hazarika, P. *Angew. Chem. Int. Ed.* **2003,** 42, 5766.
2. Kamat, P. V.; Meisel, D. *Curr. Opin. Colloid Interface Sci.* **2002**, 7, 282.
3. Hickey, S. G.; Riley, D. J.; Tull, E. J. *J. Phys. Chem.* **2000**, 104, 7623.
4. Bol, A. A.; Meijerink, A. *J. Lumin*. **2000,** 87, 315.
5. Trindade, T.; O'Brien, P.; Pickett, N. L. *Chem. Mater*. **2001,** 13, 3843.
6. Niemeyer, C. M.; Ceyhan, B.; Gao, S.; Chi, L.; Peschel, S.; Simon, U. *Colloid and Polymer Science.* **2001,** 279, 68.
7. Ago, H.; Ohshima, S.; Uchida, K.; Komatsu, T.; Yumura, M. *Physica B.* **2002**, 323, 306.
8. Hata, K.; Fujihara, H. *Chem. Commun*. **2002,** 2714.
9. Liu, J.; Ong, W.; Kaifer, A. E. Peinador, C. *Langmuir* **2002,** 18, 5981.
10. Corbierre, M. K.; Cameron, N. S.; Suton, M.; Mochrie, S. G. J.; Lurio, L. B.; RÜhm, A.; Lennox, R. B. *J. Am. Chem. Soc* **2001,** 123, 10411.
11. Zhou, Y.; Itoh, H.; Uemura, T.; Naka, K.; Chujo, Y. *Chem. Commun.* **2001,** 613.
12. Iwata, T.; Ishikawa, R.; Ichino, R.; Okido, M. *Surface and Coating Technology*, **2003,** 169-170, 703.
13. Lee, J. H.; Nam, W.; Kang, M.; Han, G. Y.; Yoon, K. J.; Kim, M-S.; Ogino, K.; Miyata, S.; Choung, S-J. *Applied Catalysis A* **2003,** 244, 49.
14. Curri, M. L.; Comparelli, R.; Cozzoli, P. D.; Mascolo, G.; Agostiano, A. *Materials Science & Engineering C.* **2003**, 23, 285.
15. Tokuhisa, H.; Hammond, P. T. *Adv. Funct. Mater*. **2003,** 13, 831.
16. Smestad, G. P.; Grätzel, M. *J. Chem. Edu.* **1998**, 75, 752.

17. Cherepy, N. J.; Smestad, G. P.; Grätzel, M.; Zhang, J. Z. *J. Phys. Chem B.* **1997,** 101, 9342.

18. Meng, Q.-B.; Takahashi, K.; Zhang, X.-T.; Sutanto, I.; Rao, T. N.; Sato, O.; Fujishima, A. *Langmuir* **2003,** 19, 3572.

19. Lenzmann, F.; Krueger, J.; Burnside, S.; Brooks, K.; Grätzel, M.; Gal, D.; Rühle, S.; Cahen, D. *J. Phys. Chem. B.* **2001,** 105, 6347.

20. Nazeeruddin, M. K.; Péchy, P.; Renouard, T.; Zakeeruddin, S. M.; Humphry-Baker, R.; Comte, P.; Liska, P.; Cevey, L.; Costa, E.; Shklover, V.; Spiccia, L.; Deacon, G. B.; Bignozzi, C. A.; Grätzel, M. *J. Am. Chem. Soc.* **2001**, 123, 1613.

21. Pichot, F.; Pitts, J. R.; Gregg, B. A. *Langmuir*, **2000,** 16, 5626.

22. Pelet, S.; Grätzel, M.; Moser, J-E. *J. Phys. Chem. B.* **2003,** 107, 3215.

23. Park, N.-G.; Van de Lagemaat, J.; Frank, A. J. *J. Phys. Chem B.* **2000,** 104, 8989.

24. Huber, R.; Spörlein, S.; Moser, J. E.; Grätzel, M.; Wachtveitl, J. *J. Phys. Chem B.* **2000,** 104, 8995.

25. Lagref, J-J.; Nazeeruddin, M. K.; Grätzel, M. *Synth. Metals* **2003,** 138, 333.

26. Heeger, A. J. *J. Phys. Chem. B.* **2001**, 105, 8475.

27. Kanazawa, K. K.; Diaz, A. F. *J. Chem. Soc. Chem. Commun*. **1979,** 635.

28. Cawdery, N.; Obey, T. M.; Vincent, B. *J. Chem. Soc. Chem. Commun*. **1988,** 1189.

29. Digar, M. L.; Bhattacharyya, S. N.; Mandal, B. M. *J. Chem. Soc. Chem. Commun*. **1992,** 18.

30. Stucky, G. D. *Nature* **2001,** 410, 885.

31. He, H.; Zhu, J.; Tao, N. J.; Nagahara, L. A.; Amlani, I.; Tsui, R. *J. Am. Chem. Soc.* **2001**, 123, 7730.

32. Hoffmann, M. R.; Martin, S. T.; Choi, W.; Bahnemann, D. W. *Chem. Rev.* **1995,** 95, 69.

Chapter 5

Patterning Design in Color at the Sub-micron Scale

5.1 Introduction

The present day gold rush in nanotechnology has witnessed enormous growth in the field and has gone much beyond the original grand vision presented way back in the December of 1959 by Nobel prize laureate Richard Feynman[1-2]. The need for a rapid and concerted development of techniques for fabrication of materials and devices with nanoscale building blocks has led to research activities in an unimaginable scale. The confluence of top-down approaches of engineering and bottom-up approaches using physical, chemical and biological principles has generated hope of making functional nanosctructures a reality in near future. A large number of methods have been developed for fabricating structures with specific application potential in electronics[3], electromechanical systems, information storage and displays, sensors, actuators etc.

5.1.1 Fabrication Techniques

In the efforts of generating structures with nanometer dimension components two principally opposite approaches have come up over the years. One of them is the top-down approach that involves generating patterns on large scale with reduction of its lateral dimensions. The limit of this method depends on control over machinery having control over atoms. The upper limit of resolution has been achieved at the atomic scale with the advent of scanning probe microscopes (SPM). On the other hand, the bottom-up approach starts with atoms and molecules as the building blocks with the help of, among others, synthetic organic and inorganic chemistry, biochemistry, protein and genetic engineering.

Photolithography[4-5] has been playing the key role in fabricating structures using the principle of top-down approach. The method involves the use of a light beam to write with appropriate masking on a substrate coated with photo-resist. The exposed parts of the photo-resist are selectively removed, allowing the replication of the pattern on the substrate. The resolution, R, is subject to the limitations set by optical diffraction according to the Rayleigh equation, which is

$$R=k_1\lambda/NA \qquad \text{--------} \qquad (1)$$

where λ is the wavelength of the illuminating light, NA is the numerical aperture of the lens system, and k_1 is a constant that depends on the photo-resist. The minimum feature size that is practically obtained is equal to the wavelength of the light used even though

the theoretical limit set by optical diffraction is $\lambda/2$. With the growing demand for higher resolution structures, it is becoming increasingly difficult to produce high-resolution structures at economically viable rate. In addition, there are practical limitations in obtaining higher resolution structures with shorter wavelengths of light. These factors have led to intense search for alternative methods of fabrication of structures at low cost. A prominent candidate in this regard is the method of soft lithography, which is the collective name for a set of lithographic techniques in which replication of master is based on physical contact with the substrate. The principle is based on the traditional "post office" stamping but with resolution attainable at the molecular level. Several techniques such as replica molding (REM), microcontact printing (μCP) [6-7], embossing and solvent assisted micromolding have been developed under the banner of soft lithography. All these techniques are efficient methods for pattern transfer. A good contact between the stamp and the surface of the substrate is key to its success. Soft lithographic techniques have the advantage of simplicity and convenience. Also, in these methods the material waste is minimized.

It is important to mention here that several other alternative methods of generation of nanostructures have also been developed using the principle of molecular self-assembly, dip pen lithography (DPN) [8-12], laser assisted direct imprint (LADI) [13] in which single excimer laser pulse melts a thin surface layer of silicon and a mold is embossed into the resulting liquid layer for pattern transfer, electron beam lithography [4] and X – ray lithography [14-18].

5.1.2 Our strategy

The fundamental objective of all the techniques mentioned above has been to manufacture high-resolution structures that are guided by applications such as microreactors, sensors, micro electro mechanical systems (MEMS), nanoelectro mechanical systems (NEMS), microfluidic devices and electronic devices at micro and nano scale[19-28]. None of the methods emphasized the generation of color patterns that has enormous application potential in information storage, sensors and so-called " E-Paper" for display [29-30]. If information can be stored in true color, the processing time for retrieval of information could be shortened considerably. Although ink-jet printing has been used to obtain organic light emitting devices of doped polymers[31], but there have been no reports of making patterns in color at the submicron scale before our work. We

have for the first time in 2001 introduced the concept of submicron scale lithography in color. The present chapter focuses on the development of techniques for sub-micron scale patterns in color and the results of one-color as well as two-color lithography are reported. It is a simple, versatile and inexpensive method of generating submicron - scale colored patterns on various surfaces using the principle of soft lithography. The molds used were the polycarbonate disk and aluminum foil line patterns of an ordinary compact disc (CD) [32]. For patterns of various colors we have used permanent marker pens of various colored inks. The same procedure was used for patterning on glass slides and overhead project (OHP) papers. Similarly, we were successful in making micro arrays of ink positioned at angles determined by the relative angles of positioning of molds twice in sequence. Similar techniques were used for the two-color lithography. In addition, a technique using a combination of soft lithography and fluid flow through microscopic channels were developed for obtaining two color lines at the submicron scale.

5.2 Experimental section

5.2.1 Making single color pattern on different substrate

5.2.1.1 Preparation of Substrates and mold

A compact disk is made up of a polycarbonate disc of about 1.2 mm thick. Spiral tracks are etched on the disc using photolithography or embossing. In the majority of the compact discs a photoresist is spin cast onto the polycarbonate disc for writing data. A thin aluminum layer is then sputtered which acts as a highly reflecting surface. This is followed by spraying a thin acrylic over the aluminum to protect it. A label is then pasted onto the acrylic layer. A cross section of compact disk is shown in Figure 5.1.

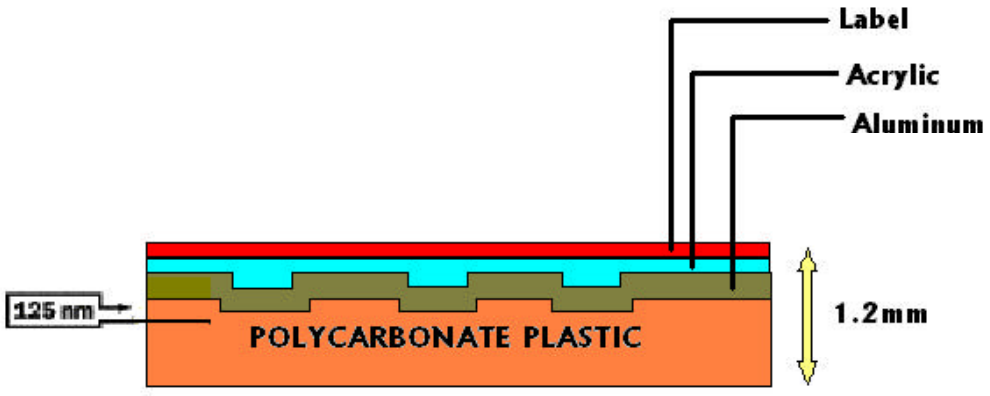

Figure 5.1: Cross section of the commercially available compact disk

Ordinary commercially available compact discs were broken into small pieces of roughly 50 mm x 25 mm sizes. The polycarbonate and aluminum foil (with the label) containing parts were separated with the help of an adhesive tape. The components were washed with ethanol and air-dried. The polycarbonate as well as aluminum foil parts were used as molds. They were checked under optical microscope for uniformity of the microstructures. Typically, each polycarbonate mold consists of parallel lines of 800 nm width separated by 1.6 μm appearing in the forms of "hills" and "valleys" [33]. On the other hand the aluminum foil components also have structures of parallel lines in the form of hills and valleys but of complementary widths. It is known that the depth of a valley from the top of the hill is about 125 nm. The diameter of a typical CD is much larger than the separation between two lines and hence under optical microscope the lines appear parallel with nearly infinite radii of curvatures. This is true for both the polycarbonate and aluminum components. Optical micrographs of patterns found in polycarbonate disc and aluminum foil in a CD are shown in Figure 5.2. It is clear that even after dismantling the CD the original lines remain intact and hence could be used as molds.

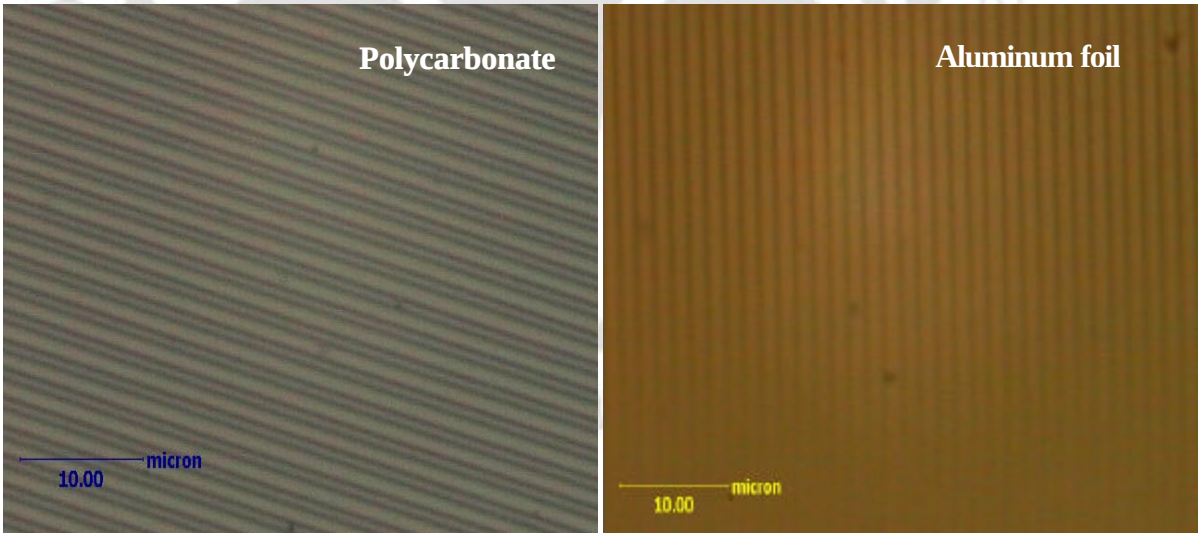

Figure 5.2: Optical micrographs of the polycarbonate disc and aluminum foil of a CD (make Hewlett Packard) that were used as molds in the present experiments. The microscope was a Carl Zeiss Axiotech model.

Microscope glass slides (25 mm x 25 mm) and OHP paper of similar sizes were cleaned with ethanol and dried in the air or by using a tissue paper. They were used as substrates onto which macroscopic lines were drawn using permanent marker pens (Luxor) of different colors.

5.2.1.2 Method

For patterns in single color a macroscopic line mark was made on a glass slide or OHP paper using a permanent marker pen with colored ink. It normally took a little more than a minute for the ink to be dry. However, in order to obtain a pattern the mold was placed on the mark between 10 s and 20 s after the mark was made. Immediately after placing over the mark the mold was either finger pressed or pressed with a home-built screw-press. The setup was kept in pressed position for 30 s.

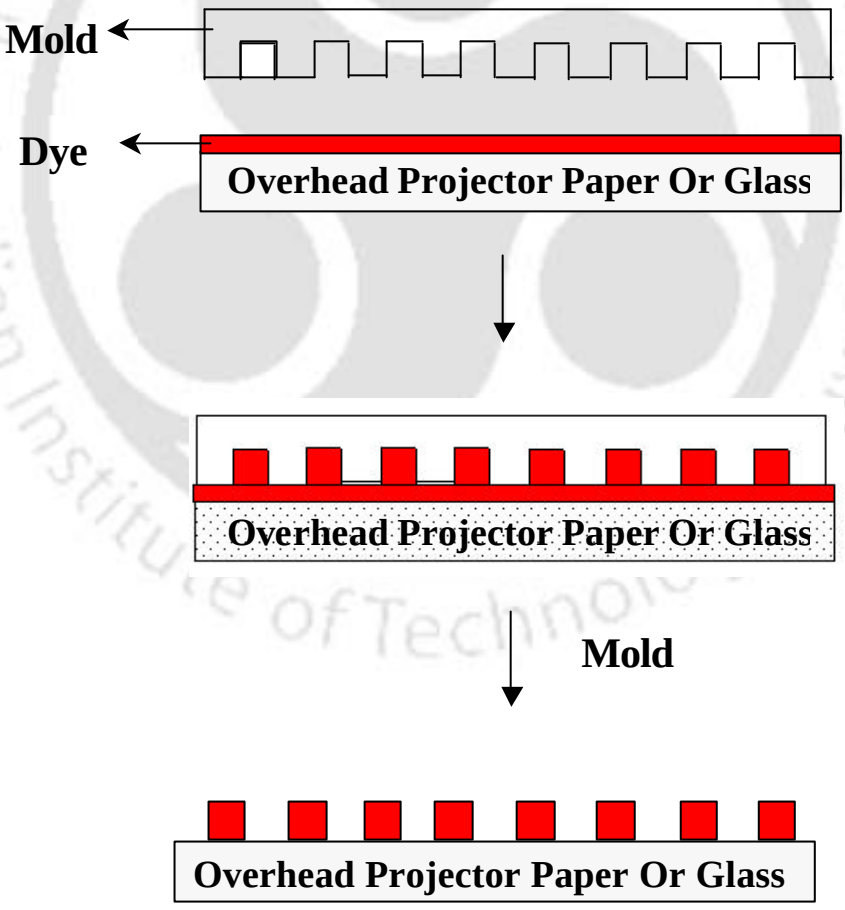

Figure 5.3: A scheme of the present method of imprinting pattern. *(See color plates, page 136)*

We observed smearing of ink if the mold was placed before 60 s. On the other hand no pattern could be observed if the mold was placed after 60 s. For patterns of various colors we have used pen with various colored inks. The schematic diagram of the present method of imprinting patterns is shown in Figure 5.3. The transfer of patterns to the ink was confirmed by observation of the lines under a Carl Zeiss (Axiotech) optical microscope.

In order to obtain cross patterns the following protocol was followed. A colored macroscopic line mark was made on the slide as before. The mold was pressed on the line after 10 s and was kept pressed for 10 s. The mold was removed and immediately placed on the mark but in an angle from the original position and kept pressed for 10 s. We also found that the process worked equally well with the use of a second mold for the second imprint (after the first mold was removed from the line). Typical angle of position of placing the molds in sequence was 90^0 and 60^0. Here also the process worked equally efficiently on both the glass slides and OHP paper.

5.2.2 Making two- colors sub-micron scale patterns on different substrates

5.2.2.1 Substrate and mold

In this case too the substrates used were glass and overhead projector paper. They were cleaned and dried as before. Here also the molds used were polycarbonate and aluminum foil components of a CD. The molds were dismantled and cleaned as before. Permanent marker pen ink of different colors was used as before for making the macroscopic marks. In addition, we have used a water-soluble fluorescent dye (rhodamine B) to obtain lines of red color with the background of a different color. A Carl Zeiss (Axiotech) optical microscope was used in transmission / reflection mode to record the micrographs.

5.2.2.2 Methods

We have used three schemes to obtain two-color lithography at the submicron scale. Two of the schemes use the principle of soft lithography and the third one uses the principle of soft lithography with the aid of fluid flow through the microscopic channels generated by imprinting patterns on the ink. The schemes are described below.

5.2.2.2 A. Scheme1

In this scheme the idea is to have a background color, on top of which lines and gaps of a second color is to be imprinted such that alternate lines of top color and the background color could be seen. In this process, first we have made a macroscopic mark in the form of a line on the substrate using the pen of a particular chosen colour. We allowed the ink to dry for 10 min at room temperature (about 25^0C). We then made another mark on top of this line (first line) with a pen of a different color. In between 20 s and 30 s the mold was pressed above the top mark and keep pressed for 5 min. The mold was then removed. The slide was checked with the optical microscope to observe the quality of structures. The scheme of imprinting by this method is shown in Figure 5.4.

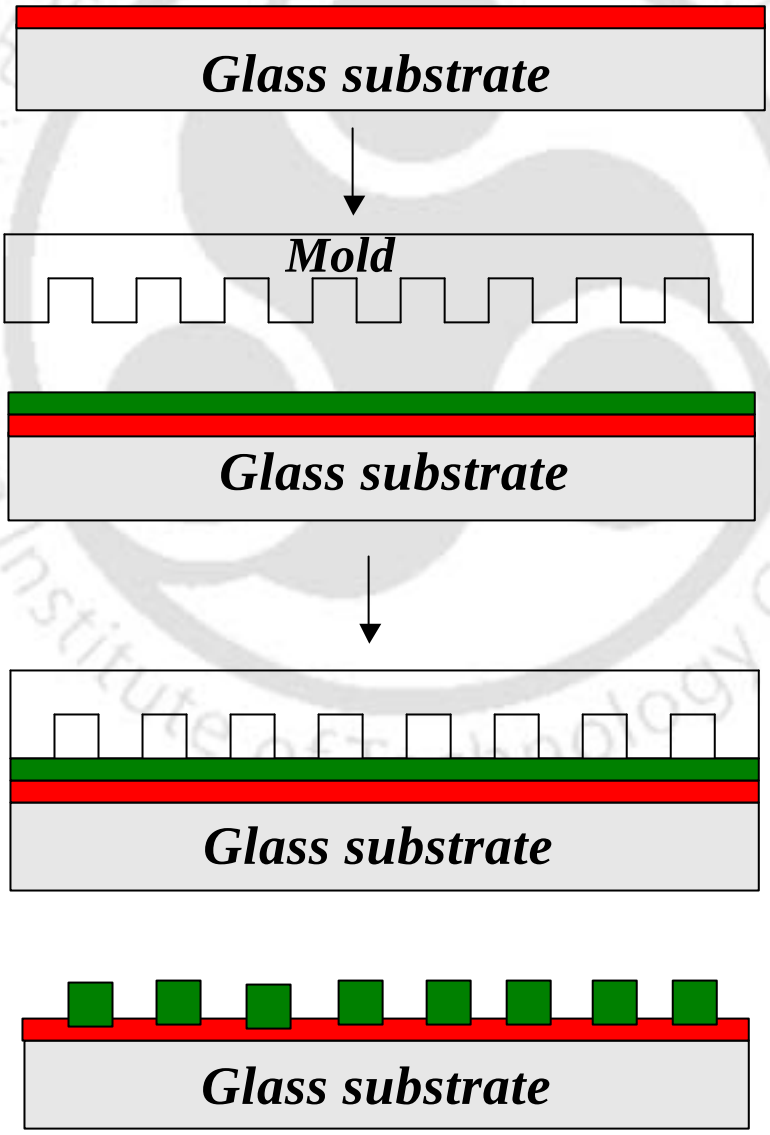

Figure 5.4: Imprinting bi-color pattern using scheme 1. *(See color plates, page 137)*

5.2.2.2 B. Scheme 2

In this scheme we made a macroscopic line of one color on the substrate as in scheme1. After 10 min when the line was dry we inked the mold with a second color. After 20 s of inking the mold was pressed on the first line and kept in that position for 5 min. The mold was then removed following which the slide was checked under optical microscope for quality of alternate parallel lines of different colors. The scheme representing this method is depicted in Figure 5.5.

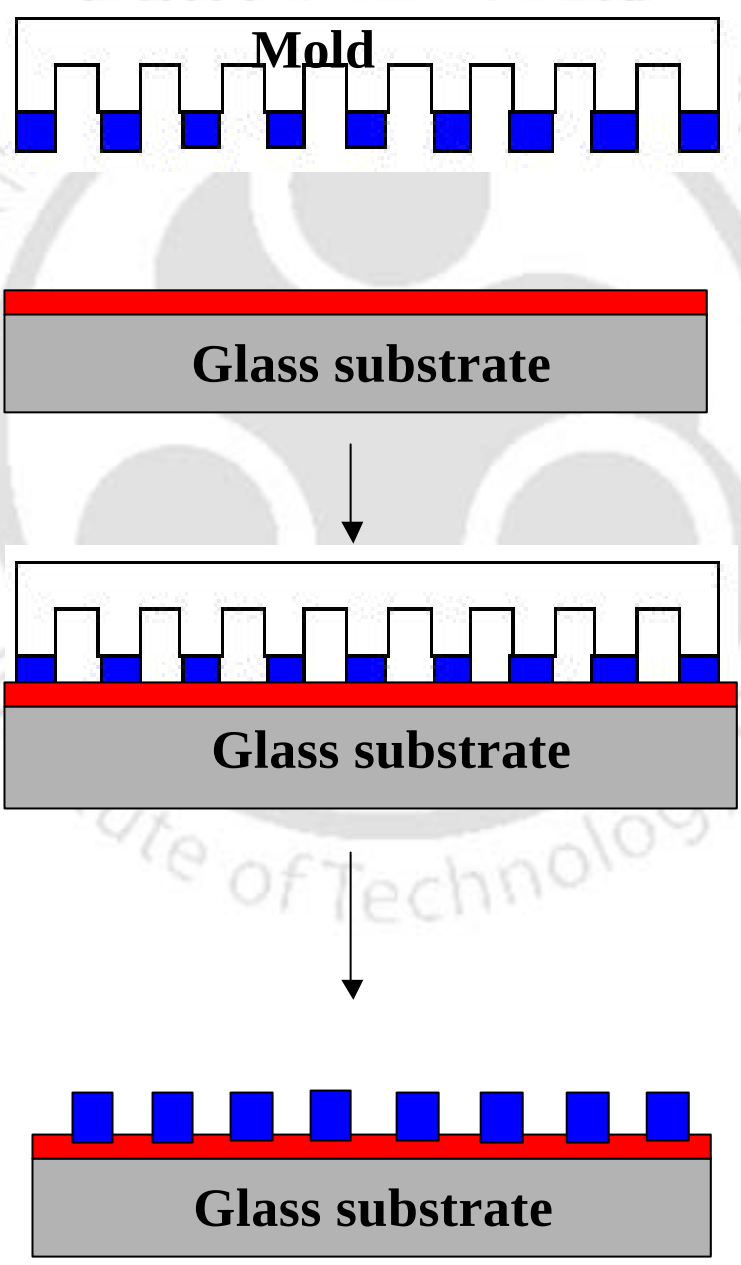

Figure 5.5: Imprinting bi-color pattern using scheme 2. *(See color plates, page 137)*

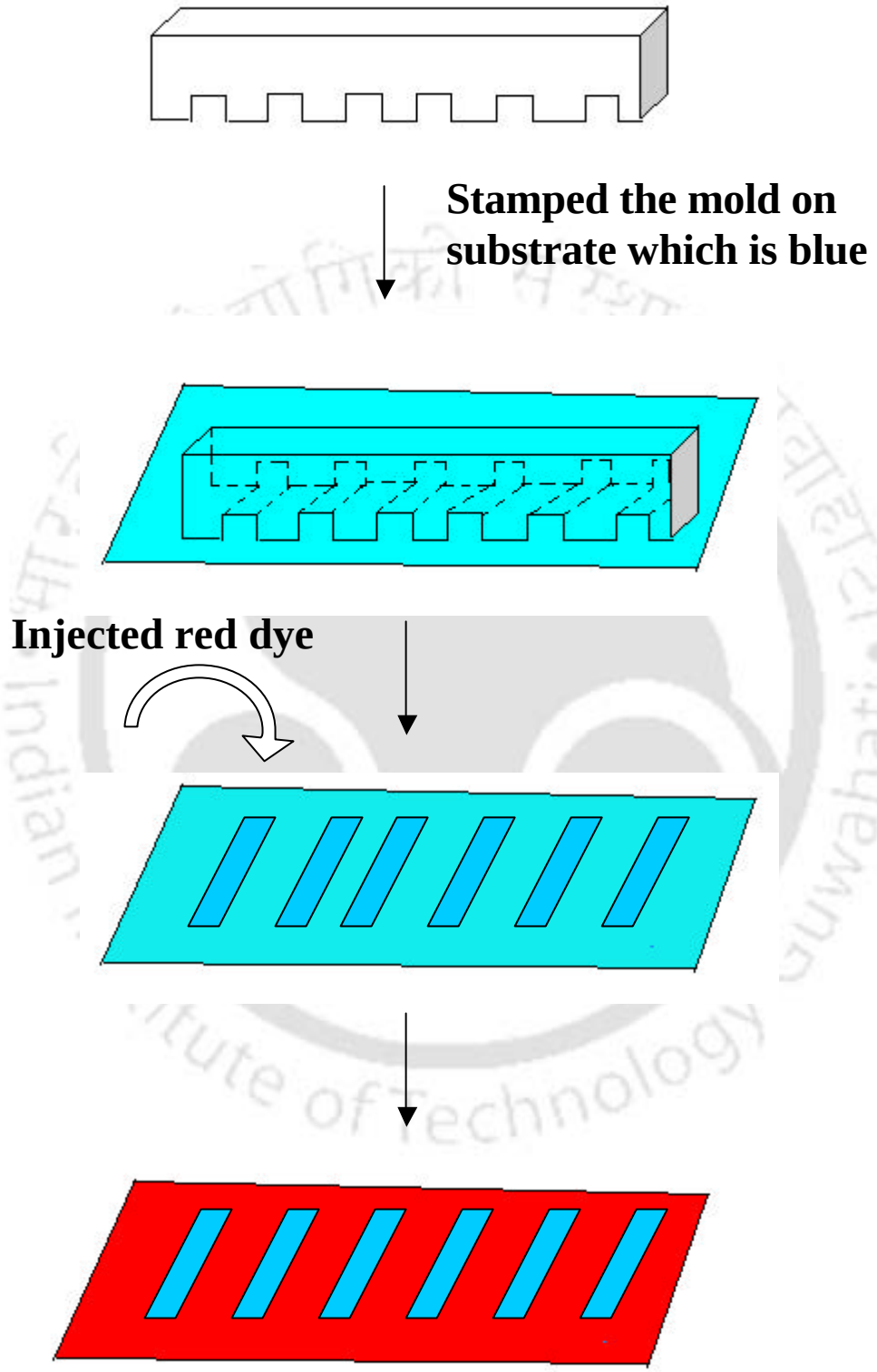

Figure 5.6: Imprinting bi-color pattern using scheme 3. *(See color plates, page 138)*

5.2.2.2 C. Scheme 3

In this scheme we marked the slide with a macroscopic line of one color. After the elapse of 10 s the line was pressed with the mold and then kept in that position for 5 min. After removal of the mold the slide was checked under optical microscope for parallel lines of one color as in single color lithography. We then poured diluted solution of ink of another color (using a syringe) at one end of the slide such that the ink would flow through the channels. With time the ink solution percolated through the channels and filled them. We waited for ½ hr. for the slide to be dry. It was then observed under optical microscope. The diagram depicting this method is shown in Figure 3.4. In addition, we have used a solution of 50mM rhodamine B dye to obtain the marks of the second color by flowing the solution through the channels of the first color.

5.3 Results and discussion

5.3.1 Single color patterns

Figure 5.7, (1), (2) and (3) shows the ordinary lines (insets) drawn using permanent marker pens of blue, green and red colors and optical micrographs of each of them after imprints of patterns from molds. Polycarbonate part of the CD was used to make the imprints. The colors in the micrographs are true colors of the imprints. As clear from the figures is that distinct parallel lines of submicron length scale could be drawn by just pressing the disc onto the ink. The "hills" and "valleys" in the imprints are negative replicas of molds. It may be pointed out here that in the cases mentioned above we did not normally observe smearing out of the ink under pressure. On the other hand if the mold was pressed earlier than the reported time the smearing of ink could be observed and the lines observed were sparse and indistinct. Similar pictures of imprints of lines from Al foil molds are shown in Figure 5.7- (4), (5) and (6). Here also distinct lines characteristics of mold could clearly be observed. In all pictures in Figures 5.7 the depth of lines vary from micrograph to micrograph as the exact pressure when finger pressed also varied with higher pressure generating more distinct lines. There are also defects due to leakage and overflow of inks from the substrate, which could be seen in some of the optical micrograph. This is due to a little early timing (than necessary) of pressing the mold.

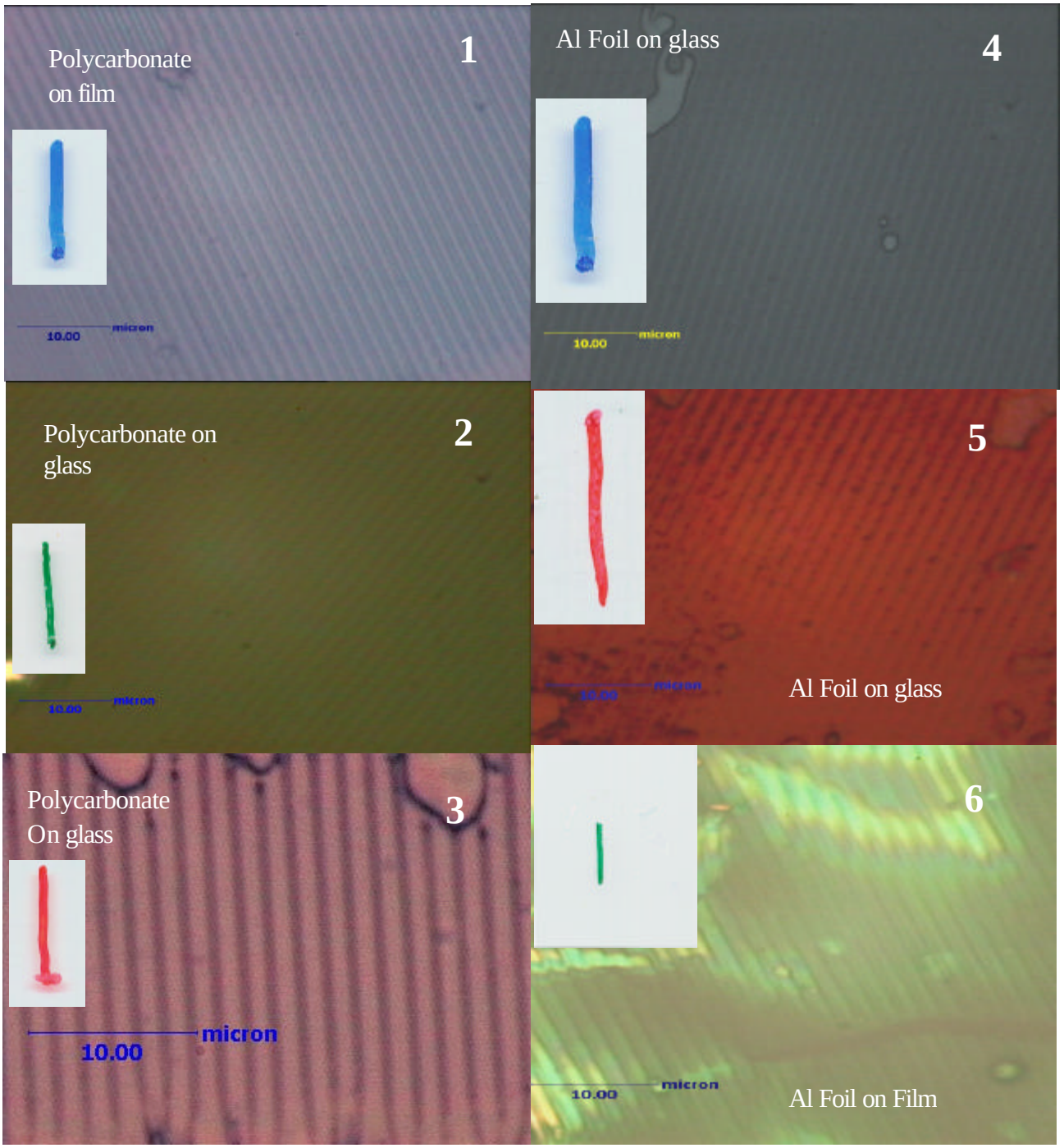

Figure 5.7: Patterns using polycarbonate (**1, 2, 3**) as molds and Al foil (**4, 5, 6**) as mold on OHP film and microscope glass slides. Insets are the pictures of lines, of about 1 mm width, that have the patterns imprinted on them by the molds. The macroscopic pictures were recorded by an EPSON Perfection 610 scanner. *(See color plates, page 139)*

Using similar principle, cross patterns were also generated at sub-micron level on different substrates. Shown in Figure 5.8 are cross - patterns generated on two separate set of lines on glass substrate by a polycarbonate mold. Macroscopic lines are shown in the insets. In each case, at first a single line was drawn by the marker pen on a glass slide. The polycarbonate mold was then pressed onto the line to make parallel microlines as before.

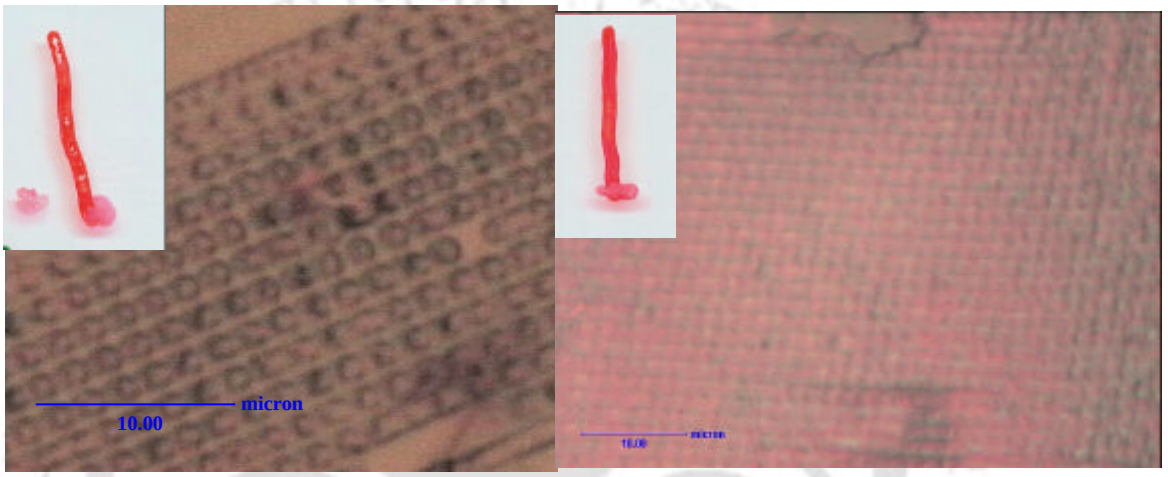

A **B**

Figure 5.8: Cross patterns generated by pressing the molds at two different angles one after the other on previously drawn lines. Insets are the macroscopic lines onto which patterns were imprinted.

The mold was then placed on the line at an angle different from the first position and then finger-pressed. Result was the production of micro arrays of ink positioned at angles determined by the relative angles of positioning of molds. In Figure 5.8, the two sets of arrays were generated by positioning the mold at about 90^{o} (Figure 5.8 A) and 75^{o} (Figure 5.8 B) angles respectively with respect to initial imprints. An approximate area representing the "hills" of these arrays is about 0.64 μm^2. The shortest distance between two hills is 0.8 μm. The variation of clarity of impression here too is a reflection of the variation of pressure exerted while imprinting the design. Of course, there would be effects of non-uniformity of lines as drawn by hand. Hence the exact microstructures would vary from sample to sample and across a sample.

5.3.2 Bi-color pattern

Our next step was the anticipated advancement in this direction in the form of generating bi-color patterns with submicron scale resolution. As discussed in the experimental section the approach here is also based on soft lithography. The optical micrograph figure of bi-color pattern generated by using scheme 1 is shown in Figure 5.9. Here the first color was red and the second mark was done using a green pen.

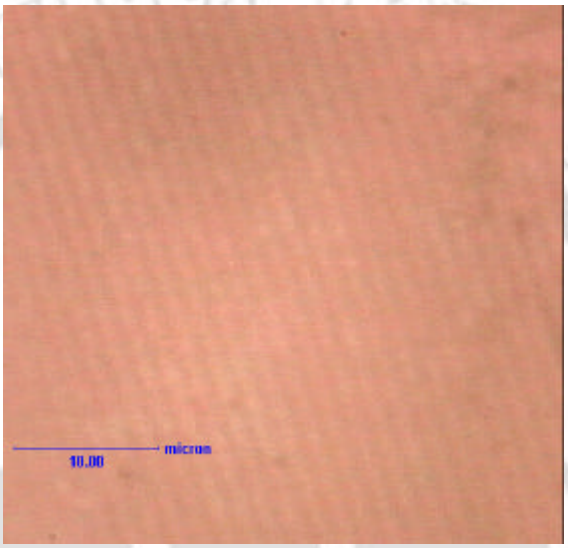

Figure 5.9: Optical micrograph of the bi-color lines obtained using scheme 1: green on red recorded in reflection mode of the microscope. *(See color plates, page 138)*

It is clear from the figure that alternate red and green coloured parallel lines, with widths corresponding to those of the negative replica patterns of the mold, could be imprinted on two-dimensional surfaces. It is also important to mention here that in this scheme the timing of placing the mold after the mark of the second colour is crucial to obtaining the patterns. This is because the method basically involves removing the second colour (green) by pushing it sidewise and then up along the vacant space of the groove of the mold. In addition, the thickness of the second mark is crucial to obtaining reproducible lines.

In the method, involving scheme 2, the mold was inked and the pattern was transferred on top of a mark (previously dried) having a different color. The result

obtained by this method is shown in Figure 5.10. We have Figure 5.10 (A) showing alternate color of blue and red and Figure 5.10 B showing alternate green and red color.

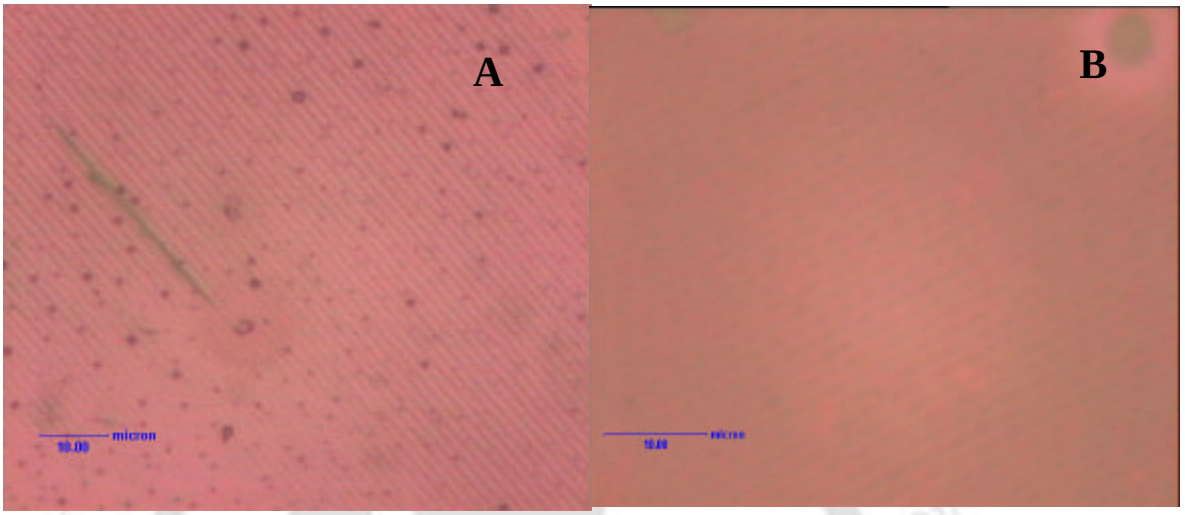

Figure 5.10: Optical micrograph of the bi-colour line obtained using scheme 2; (A) blue on red taken in transmittance mode (B) Green on Red taken in reflection mode. *(See color plates, page 140)*

In order to obtain the line of Figure 5.10 A, the first mark was red and then the mold was inked blue. On the other hand, for Figure 5.10 B the first color was red and the mold was inked green. Here again the lines are clearly indicating the reproducibility of lines using the present method. A careful inking of the mold and timing of the transfer is key to obtaining the reproducibility of the features present in the mold.

Utilizing the method of scheme 3, we have generated line patterns with alternate "hills and valleys" having one color and then filled up the valleys with the second color. Figure 5.11 shows the micrograph of alternate blue and red coloured lines with blue background onto which red colour solution was poured to fill the channels. Here the quality of the imprint is dependent on the appropriate filling of the channels. Overflow of fluid and improper filling of the channels would reduce the clarity of the patterns. The results we have obtained clearly demonstrate the ability to generate bi-colour patterns with submicron resolution. Typically the width of a line is about 0.7 µm while the separation between two such lines is about 0.9 µm, which matches with the mold used. Here the CD molds used were different from the ones used before.

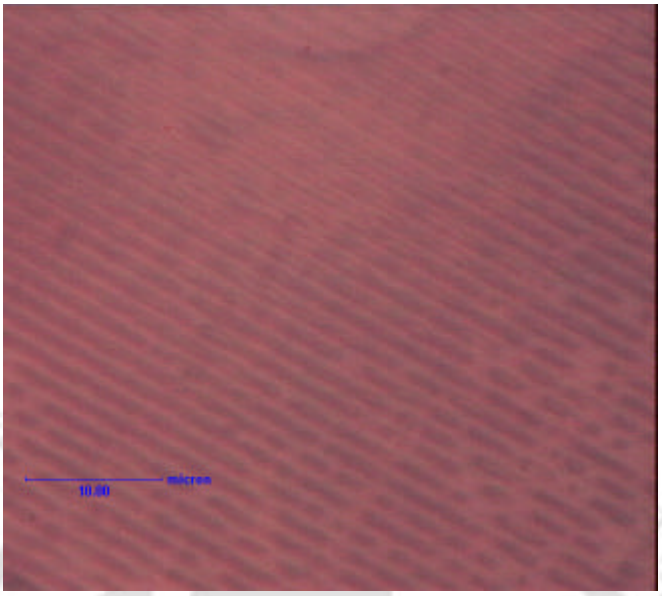

Figure 5.11: Optical micrograph of the bi-colour line obtained using scheme 3, blue line with injected red ink. The micrograph was recorded in reflection mode. *(See color plates, page 140)*

5.4 Conclusion

In this chapter we have demonstrated a method of imprinting lines and arrays of various colors on glass slides and OHP films. Parallel lines with submicron dimensions could be imprinted on such substrates by using polycarbonate and Al foil components of a CD as molds. We have used the commercially available permanent marker pen to write macroscopic lines on the surfaces of OHPs and glass slides and transferred the patterns of the mold onto the lines. Observation under optical microscope exhibited various colored patterns on the film as per the design of the mold. Also, microarrays of ink spots positioned at predetermined angles and spacing determined by the separation of lines in the mold could be generated by pressing the mold on the same parent line in a set of pressing twice in sequence perpendicular to each other. The resolution could further be increased by using mold with lines and patterns of higher resolution. The same principle could be used for imprinting designed arrays of various materials on plastic and glass substrates in accordance with the use. The use of flexible plastic material like OHP paper enhances the possibility of storing designs in foldable substrates.

Our next step was advancement in this direction in the form of generating bi-color patterns with submicron scale resolution using the principle of soft lithography. The

lithography we have developed is printed in the form of parallel lines. The idea is to have features of high-resolution alternate lines in two colours. The same idea in principle can be used to generate patterns of arbitrary shape decided by the nature of patterns on the stamps used to make the imprints. The base material is usually in the form of thin polymer film supported on glass or plastic substrates. In making bi-color pattern, like our earlier method we have typically used parts of the commercially available (CD) as the mold for creating parallel alternate lines of two colors. In addition, we have used coloured fluid flow through the channels to obtain parallel alternate two-colored lines. Conventional optical microscopy was used to observe the colored patterns formed in these ways. One could envision applications with respect to the present development in personal computer (PC) based data retrieval as an ordinary optical microscope could be incorporated as a part of the PC to "read" information of sub-micron scale resolution, stored in color, written on various substrates.

5.5 References

1. Stix, G.; *Scientific American*, Sept **2001**, 32.
2. Roukes, M.; *Scientific American*, Sept **2001**, 48.
3. Compaño, R. *Nanotechnology*, 12, **2001**, 85.
4. Timp, G. (Ed.*): Springer-Verlag New York Inc*, **1999.**
5. Nonogaki, S.; Ueno, T.; Oto, T. *Marcel Dekker Inc, New York* **1998.**
6. Wu, X. C.; Bittner, A. M.; Kern, K. *Langmuir* **2002,** 18, 4984.
7. Arrington, D.; Curry, M.; Street, S. C. *Langmuir* **2002,** 18, 7788.
8. Ivanisevic, A.; Mirkin, C. A. *J. Am. Chem. Soc*. **2001**, 123, 7887.
9. Zhang, H.; Li, Z.; Mirkin, C. A. *Adv. Mater*. **2002**, 14, 1472.
10. Li, Y.; Maynor, B. W.; Liu, J. *J. Am. Chem. Soc*. **2001,** 123, 2105.
11. Zang, H.; Chung, S. W.; Mirkin, C.A. *Nano Lett* **2003**, 3, 43.
12. Lee, K. B.; Park, S. J.; Mirkin, C. A.; Smith, J. C.; Mrksich, M. *Science* **2002**, 295, 1702.

13. Wilder, K.; Adderton, D Bernstein, R.; Elings.; , V.; Quate, C. F. *Appl. Phys. Lett.* **1998**, 73, 2527.

14. Romanato, F.; Businaro, L.; Di Fabrizio, E.; Passaseo, A.; De Vittorio, M.; Cingolani, R.; Patrini, M.; Galli, M.; Bajoni, D.; Andreani, L. C.; Giacometti, F.; Gentili, M.; Peyrade, D.; Chen, Y *Nanotechnology* **2002**, 13, 644.

15. Awad, Y.; Lavallee, E.; Beauvais, J.; Drouin, D.; Yang, P.; Turcotle, D.; Mun, L. K. *J. Vac. Sci. Technol B* **2001**, 20, 3040.

16. Forber, R. A.; Chen, Z. W.; Menon, R.; Grygier, R.; Mrowka, S.; Turcu, I. C. E.; Gaeta, C, J.; Cassidy, K.; Smith, H, I .*J. Vac. Sci. Technol B* **2002**, 20, 2984.

17. Toyota, E.; Washio, M. *J. Vac. Sci. Technol B* **2002**, 20, 2979.

18. Chou, S. Y. Kelmel, C.; Gu, J. *Nature*, **2002,** 417, 835.

19. Haswell, S. J.; Middleton, R. J.; O'Sullivan, B.; Skelton, V.; Watts P.; Styring, P. *Chem. Commun.* **2001**, *5*, 391.

20. De Feyter, S.; Hofkens, J.; Van der Auweraer, M.; Nolte, R. J. M.; Mullen, K.; De Schryver, F. C. *Chem. Commun.* **2001**, *7*, 585.

21. Yang, T.; Jung, S.; Mao, H.; Cremer, P. S. *Anal. Chem.* **2001,** 73, 165.

22. Bernard, A.; Michel, B.; Delamarche, E. *Anal. Chem.* **2001**, 73, 8.

23. Wilson, C. F.; Simpson, G. J.; Chiu, D. T.; Strömberg, A.; Orwer O.; Rodriguez, N.; Zare, R. N. *Anal. Chem.* **2001**, 73, 787.

24. Ramos, L.; Weitz, D. A. *Langmuir* **2001**, *17*, 2275.

25. Lee, J.; Kim, C. J. *J. Microelectromech. Syst*. **2000**, *9*, 171.

26. Liu, R. H.; Stremler, M. A.; Sharp, K. V.; Olsen, M. G.; Santiago, J. G.; Adrian, R. J.; Aref, H.; Beebe, D. J. *J. Microelectromech. Syst* **2000**, *9*, 190.

27. Jacobs, H. O.; Whitesides, G. M. *Science* **2001**, *291*, 1763.

28. Lin, S. Y.; Flemming, J. G.; Hetherington, D. L.; Smith, B. K.; Biswas, R.; Ho, K. M.; Sigalas, M. M.; Zubrzychi, W.; Kurtz, S. R.; Bur, J. *Nature* **1998**, *394*, 251.

29. Comiskey, B.; Albert, J. D.; Yoshizawa, H.; Jacobson, J. *Nature*, **1998**, 394, 253.

30. Dagani, R. *C & EN* **2001**, 79, 40.

31. Hebner, T. R.; Wu, C. C.; Marcy, D.; Lu, M. H.; Sturm, J. C. *Appl. Phys. Lett.* **1998**, *72*, 519.

32. Cavallini, M.; Murgia, M.; Biscarini, F. *Nano Lett.* **2001**, 1, 193.

33. Emmelius, M.; Pawlowski, G.; Vollmann, H. W. *Angew. Chem., Int. Ed. Engl.* **1989**, *28*, 1445.

Chapter 6

Patterning Sub-micron Scale Channel Structures on Glass by Chemical Etching

6.1 Introduction

The industrial and laboratory demands for miniaturization of devices used primarily for chemical assays[1], biological[2-4] and environmental analyses have accelerated the pace of progress made in the field of microfluidics. Technically, microfludics is defined as controlling and manipulating fluids in microscopic channels[5-11]. The advantages of these micro devices lie in the smallness of active-volume with the possibility of fast, efficient and controlled movement of fluids through the channels; be it for mixing, separation of components or carrying out chemical reactions that are otherwise dangerous or expensive to carry out at a larger scale. There are of course other advantages associated with small volumes such as precise and fast reagents introduction, better removal of intermediates and products and better control of factors such as temperature, electric and magnetic fields. As a consequence substantial research in the field has witnessed significant development of newer methods of fabrication of fluidic systems, fabrication of components required for assembling functionally complex fluidic devices and examination of fundamental behavior of fluids in small channels. A special case in point is the fabrication of micro-reactors [12-19]. In a micro-reactor nano-liter and sub-nano-liter quantities of reacting species can be used for test analysis or for obtaining products of chemical reactions. If designed appropriately, a microreactor can ensure localized control over concentration, faster mixing of reactants, appropriate introduction of reactants in a multi-step reaction, separation of reaction products and the possibility of eliminating the unwanted reaction. On the other hand, the decrease in linear dimension allows heat transfer coefficients to exceed those of conventional heat exchangers by an order of magnitude thus favoring efficient control over temperature dependent chemical reactions. The increase of surface to volume ratio, in micro-reactors, also has implications in surface catalyzed reactions.

Glass has been the favorite material of choice for fabrication of miniaturized fluidic devices due to its chemical inertness, electrical, thermal and optical properties. Glass can withstand electric field strengths of several thousands volts per cm. Glass is transparent in some part of UV, all of visible and near infrared region of light facilitating optical detection. For example commonly used Pyrex has thermal conductivity of 1.13 $Wm^{-1}K^{-1}$ and is transparent in the region 360-2350 nm. Because of all these advantages

and ease of molding glass into different shapes it has proven to be a better substrate for microfluidic devices [20-21].

6.1.1 Existing methods

There are quite a number of methods available for fabricating microreactors or microchannel structures such as nano imprint lithography (NIL) [22-23], laser assisted direct imprint (LADI) [24], soft lithography[25-26] making use of microcontact printing[27-28]. However, the commonly used procedure for the fabrication of glass microreactor is as follows[12]. A thin layer of a metal, like Cr, is vapor deposited on the glass plate. The substrate is then spin coated with a photoresist polymer. Appropriate channel structures are then imprinted on the photoresist using UV light (generally) and appropriate mask. The exposed part of the resist is then removed by solvent or other means. This is followed by the removal of Cr wherever photoresist was removed. Now selected parts of the glass surface are exposed. These parts of the surface are then etched by HF or other etchants, such as potassium hydroxide (KOH)[29-30], mixture of hydrogen fluoride and ammonium fluoride. Finally, the photoresist is removed to obtain the desired channel structure on the glass surface. A schematic representation of the whole process is shown in Figure 6.1.

6.1.2 Our approach

As discussed above, the technique mostly used in the fabrication of glass microreactors involves a large number of steps and hence are relatively expensive to produce in industrial scale. In this chapter we report a new method of fabrication of glass microreactors, which could be produced in a short time, with fewer steps and with little investment. The basic idea comes from soft lithography. We have employed the polycarbonate part of a commercially available compact disc (CD) as the mold. The parallel lines in the form of “hills” and “valleys” present in the polycarbonate part were inked with HF. Glass surfaces were etched with the “inked” mold. Parallel lines as negative replicas of the mold could be imprinted on the glass surface. We also could make arrays of non-etched dots on the glass surface at a predetermined angle by stamping the mold twice. Optical microscopic and scanning electron microscopic measurements evidenced the transfer of patterns. The features obtained in this way have submicron dimensions as available in the mold.

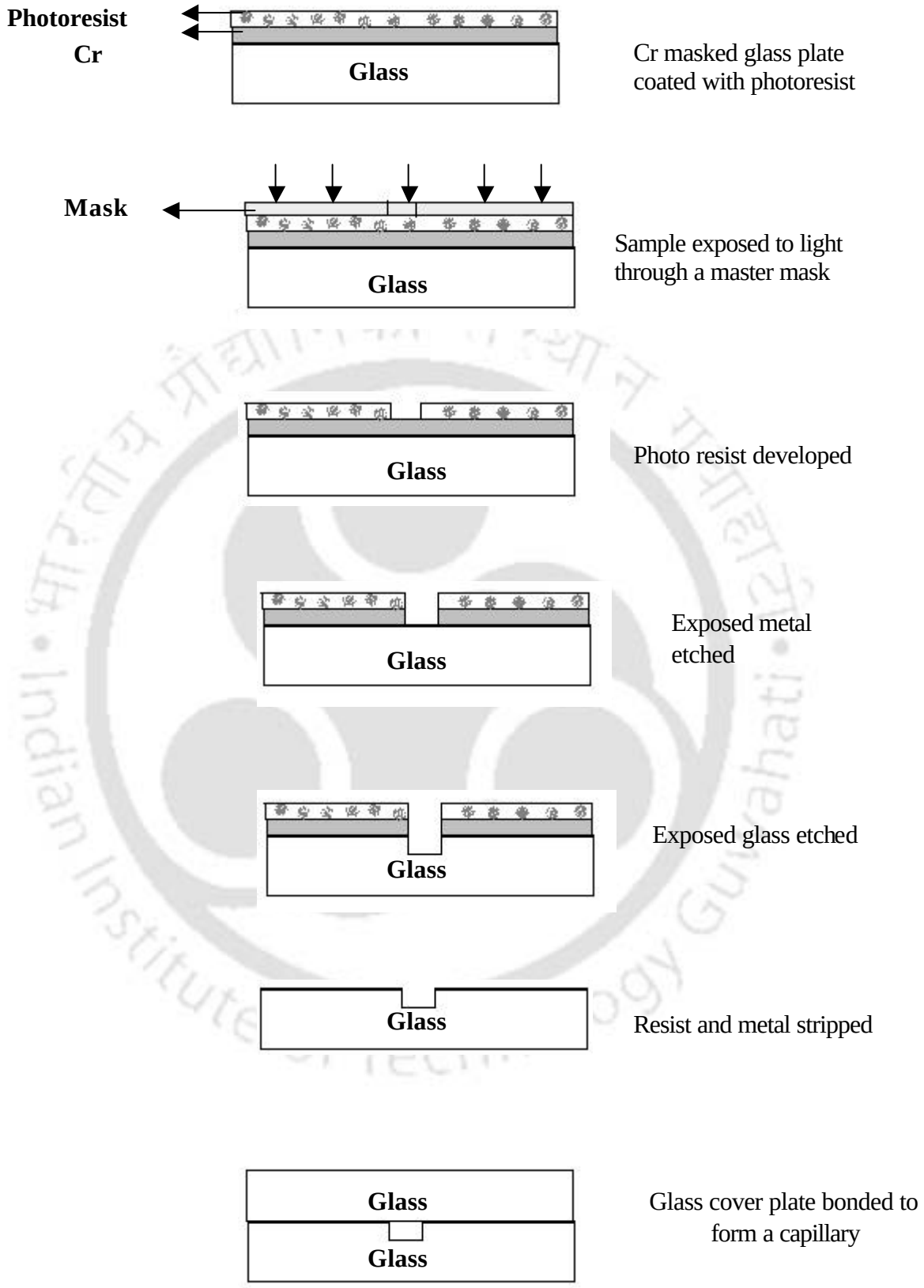

Figure 6.1 Sequence of steps of photolithography and wet chemical etching involved in the popular technique to produce chemical channels on glass.

6.2 Experimental section

6.2.1 Substrate and mold

Commercially available glass slides were cut into 25mm x 25 mm sizes, washed and then dipped into piranha solution (7:3 H_2SO_4 : H_2O_2) for an hour. After removal from the solution, they were cleaned with plenty of water and air-dried before use. Commercially available compact discs were broken into pieces of roughly 25 mm x 25 mm sizes. The polycarbonate parts were carefully recovered and cleaned with EtOH. Aqueous HF was used for etching the slides.

6.2.2 Method

Figure 6.2 shows schematically the present method of etching glass with features at the sub micron scales. Aqueous HF solution (6% v/v) was used as "ink" to wet the top surface of the polycarbonate disc (mold) using a cotton swab. The water used in making the solution was of Millipore grade (resistivity 18.2 M? cm). Parallel lines in the form of "hills" and "valleys" appear on this surface. The disc was then placed onto a previously cleaned glass slide. The whole setup was kept pressed for 5 min using a home - made screw press. The mold was then carefully and quickly lifted and removed. This was to avoid further non-desired etching. The glass slide was cleaned with water and then wiped dry with a tissue paper. The slide was ready for observation under microscope. The pattern obtained was viewed under a Carl Zeiss (Axiotech) optical microscope. The structures obtained were further confirmed by scanning electron microscopy.

In order to obtain two-dimensional arrays of non-etched spots, while the remaining part of the glass surface get etched the following procedure was adopted. At first the mold was inked with the etching solution. The mold was then pressed onto the glass substrate as before. The mold was removed; the glass slide was cleaned with water as before and then wiped dry with a tissue paper. This was followed by inking the same mold or another mold of the same kind with HF solution. The wet mold was then placed on the glass substrate at an angle different from the first position. The whole setup was kept pressed as before for 5 min. The glass slide was recovered and cleaned with water and dried before observations under microscopes.

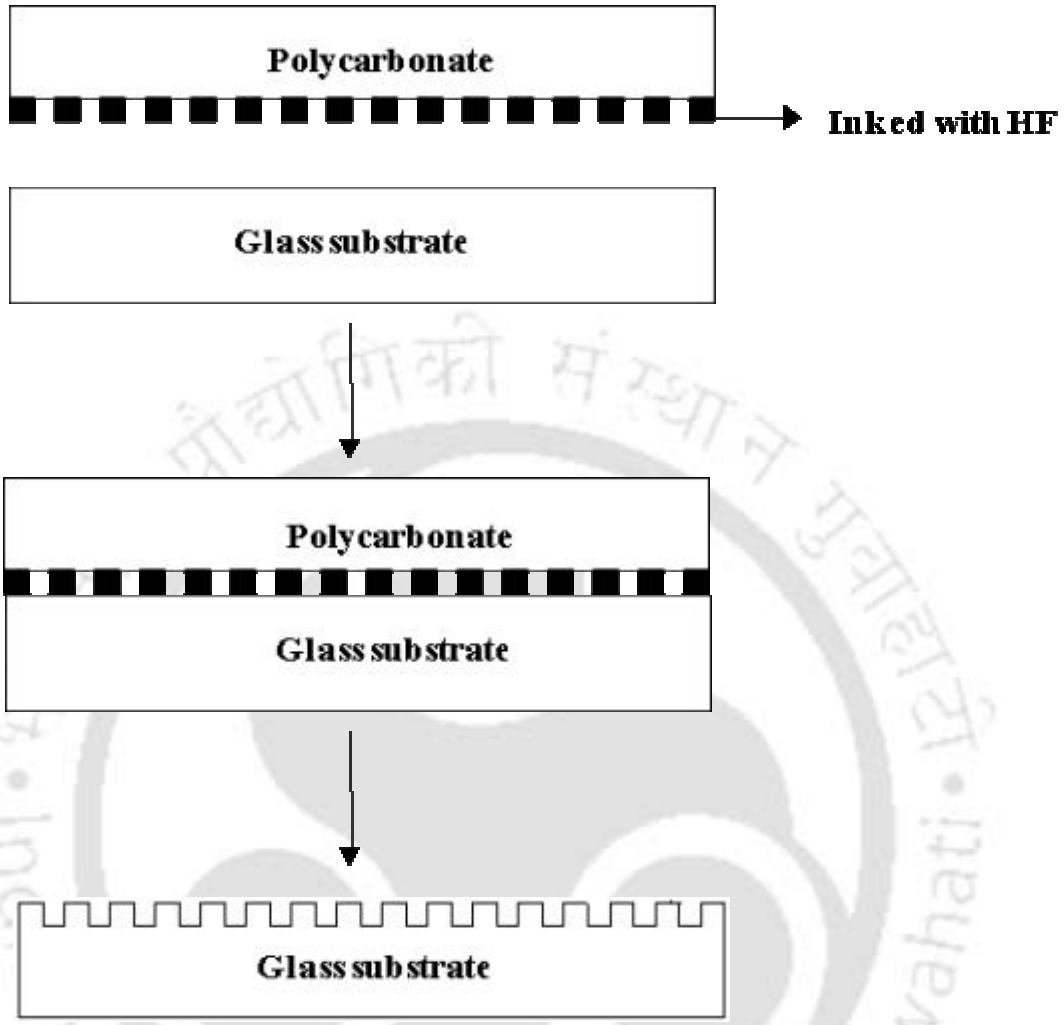

Figure 6.2: Schematic representation of the process of imprinting parallel lines on glass by chemical reaction etching.

6.3 Results and discussions

Glass is easily etched by HF producing gaseous SiH_4 and H_2O.

$$SiO_2\,(s) + 4\,HF\,(aq) \longrightarrow SiH_4\,(g)\uparrow + 2\,H_2O\,(l) \qquad (1)$$

On the other hand polycarbonate does not react with HF. Thus HF ink along with the polycarbonate mold would be an ideal case where the patterns in the polycarbonate mold could be transferred to glass by etching with HF. One could argue that other polymers that

are non-reactive with HF could also be used, which is probably true. We have however stuck to polycarbonate mold because it is commercially available and uniform sub-micron scale parallel line patterns are present in the molds. Figure 6.3 represents a typical optical micrograph of a polycarbonate disk that has been used as the mold in the present work. As clear from the picture, the mold consists of parallel lines ("hills") of about 0.7 μm thick that are separated by about 0.8 μm gaps ("valleys").

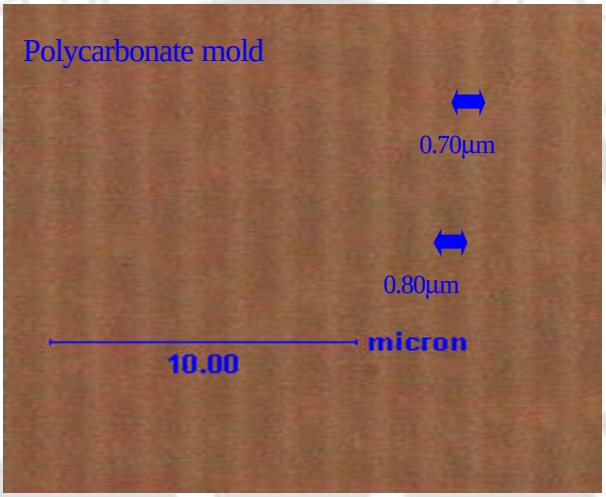

Figure 6.3: Optical micrograph of the polycarbonate piece that was used as a mold for the present method (obtained from a compact disc of SAMSUNG –make)

When the mold was inked with 6% (v/v) aqueous HF solution and pressed onto the glass substrate reproducible parallel line patterns could be transferred to the glass surface. The parallel line patterns were similar to those in the mold. In Figure 6.4 we show optical micrographs of three such slides containing etched parallel lines on the glass surface as imprinted by the present method. As evident from the figures continuous long range parallel alternate dark and light colored lines can be seen running from one end to the other. This shows that the present method could transfer the patterns of the mold onto a glass surface by etching with HF.

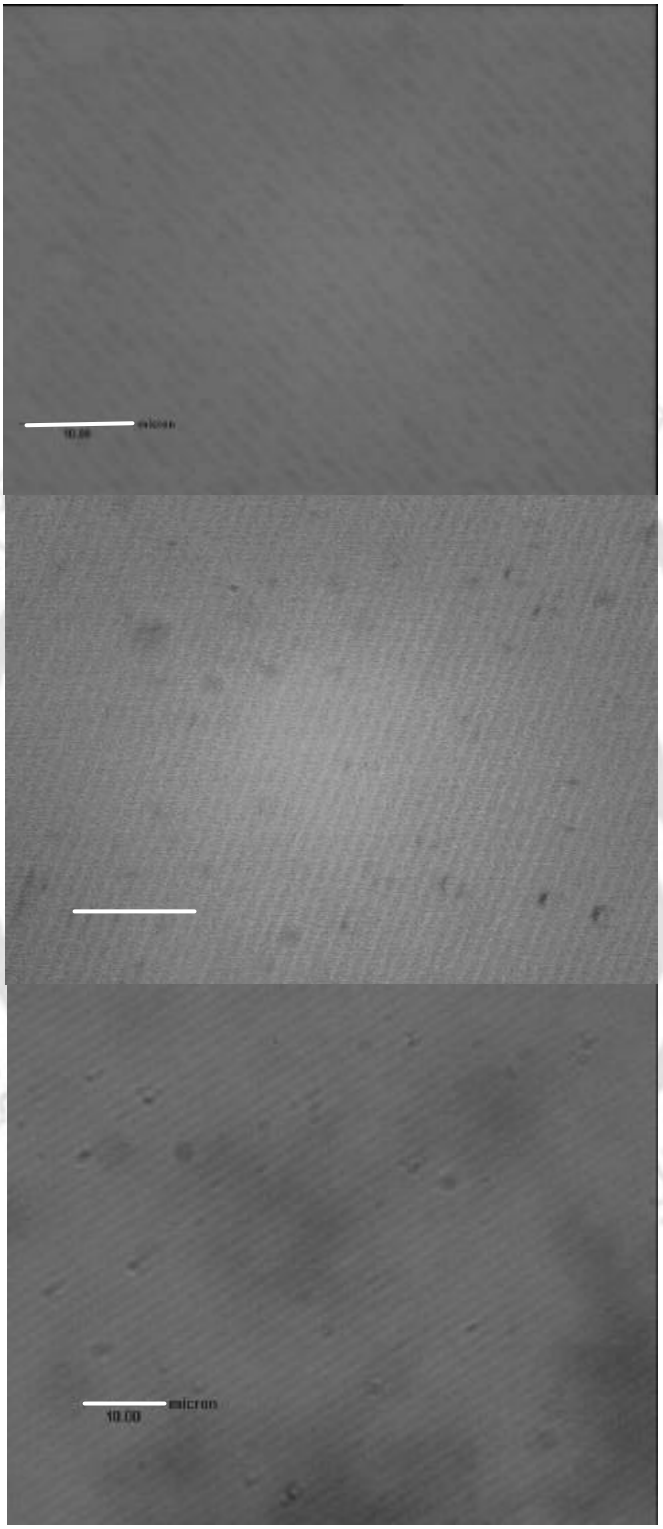

Figure 6.4: Optical micrographs of typically etched glass slides. The slides were etched by HF solution using polycarbonate disk of a CD as the mold. Bar is 10µm.

The width of each light colored line is about 0.7 μm that is nearly equal to that of CD mold, while the width of each dark line is about 0.8 μm and that is nearly equal to the separation of two parallel lines of the CD mold. The imprints of parallel lines via chemical etching using the mold was further confirmed by scanning electron microscopy (SEM). In Figure 6.5 we show the SEM micrographs of two such slides. The dimensions of the lines representing etched channels and non-etched crests match with those of the positive of the mold.

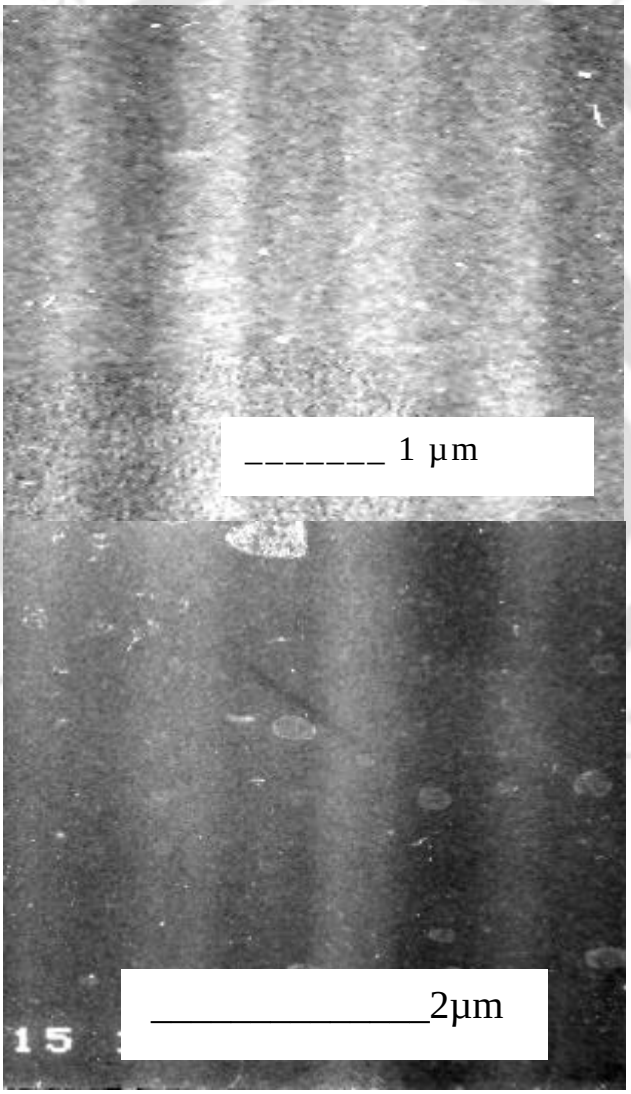

Figure 6.5 Scanning Electron Microscopy (SEM) images of parallel lines obtained by etching glass employing the present method. The micrographs are from two different samples.

Production of micro arrays of spots on glass substrate was also achieved by using the same principle. In Figure 6.6, we show the optical micrograph of a cross pattern generated on a glass surface as a result of stamping twice in sequence using HF – inked mold. In this case, at first parallel line patterns were generated as in Figure 6.4 by stamping the inked mold onto a microscope glass slide. The slide was then washed with water and dried.

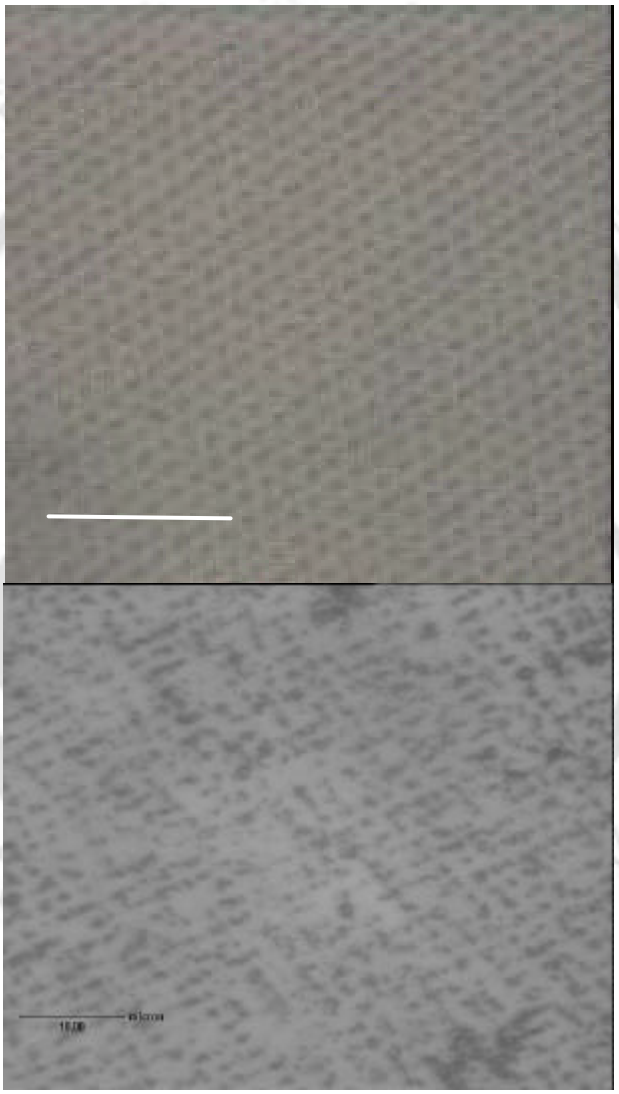

Figure 6.6: Optical micrographs of cross patterns generated by etching the surface twice in sequence at an angle using polycarbonate mold. Bar is 10µm.

This was followed by stamping for a second time at an angle to the previous one. The rest of the procedure was followed as before. Here also distinct features of the stamp–etched surface can be seen in the micrographs. The dark areas represent the non-etched parts of

the slide while the brighter areas are the channels formed due to etching. A typical dark spot here has an area of about 0.64 $(\mu m)^2$ as expected from the dimensions of the mold.

We also wanted to learn how the etching takes place using these nanoscopic patterned polymer discs. But before that let us see how the mold will look like in two dimensions. It will contain "hills" and "valleys" as shown in Figure 6.7. There are two possible mechanisms by which the patterns could be generated. The first is by only the "hills" of the mold upon inking generated these patterns by chemical etching of glass. On the other hand there is a possibility of aqueous HF solution from the swab draining into the channels thus filling them in addition to inking the "hills". Thus the etching process would take place both by the "hills" of the mold and the filled channels. This might seem to inhibit fulfilling our aim of producing nanoscopic lines and instead would produce an etched surface with no features. As this was not the case, the reason for obtaining the channels and cross patters as we did is as follows. Both the "crests" and the filled channels etch the glass plate. Since the channels have much more volume of etching solution than the "crests" could possibly have the regions of glass plates in contact with the filled channels would be etched more than the regions in contact with the "crests" thus producing the patterned channels.

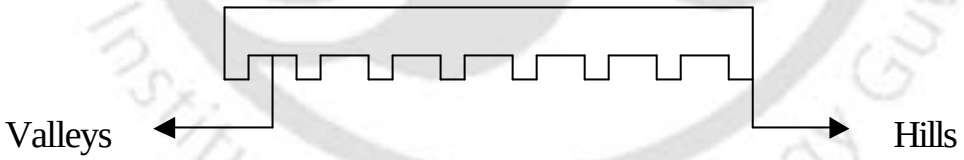

Figure 6.7: Diagram showing polycarbonate part of the compact disk (CD) in two-dimensional plane

To verify this we did the following experiment. We spin coated a glass plate with a thin film of polystyrene. We then cut two widely separated parallel channels on it using a razor blade. We then rubbed a line of the HF "inked" swab against the film in perpendicular to both channels and on the plane of the film. A glass plate was then pressed on this film. In case the HF solution went into the channels it would produce an "H" letter shaped etching on the glass covering the film; otherwise it would produce a

single line with the dimension of the original ink-line. As shown in Figure 6.8 we observed the formation of an "H" shaped mark on the glass plate thus proving that indeed etching of glass took place by HF present in the "crests" and filled channels of the mold.

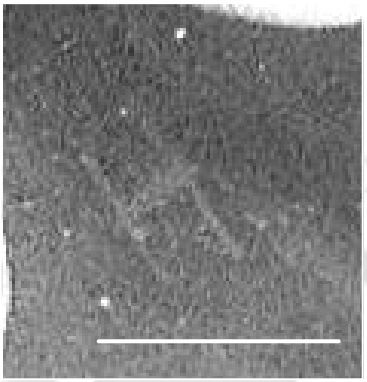

Figure 6.8: Photograph of the macroscopic "H" shaped mark on glass plate due to etching of glass. The bar is 1 cm.

In the experiments described above we have used polycarbonate mold and commercially available microscope glass slides as the substrates for generation of submicron scale patterns by chemical reaction etching. However, as can be seen from Figures 6.4 and Figure 6.6 the pattern transfer has not been perfect for long-range imprints. These are probably due to problems with the mold and substrate rather than the method itself. Polycarbonate is a relatively hard mold offering less flexibility at least with respect to making imprints on non-flat surfaces. On the other hand the glass slides that we have used are not atomically flat. Hence they would be susceptible to defects especially when patterns are being transferred from hard molds. On the other hand previous reports on lithography using a soft mold like polydimethoxy silane (PDMS) have indicated defective pattern transfer due to buckling and bending of the mold[31]. We have shown that under carefully performed pattern transfer defects in the structure could be minimized. From our observations we noticed that best pattern transfer was possible when the pressure applied was 8.5 Kg/cm^2. This condition resulted in good quality pattern transfer shown in Figure 6.4 B, 6.4 C and 6.6 A. Hence it is possible to obtain good quality patterns using the present method.

The next question comes about the way pattern formation take place in the present method. As described above, during the process of inking HF goes inside the channel and

the amount of HF inside the channels ("valleys") would be much more than that on the "hills" of the mold. Thus there is the possibility of the glass surface getting etched everywhere. The silver lining here is that even though the HF in the "hills" of the mold would compete with those in the "valleys", because of the sheer volume in the "valleys", the effective pattern would be due mainly to the "valleys" and hence would serve the purpose of channel formation on the glass surface using the present method.

6.4 Conclusions

In this chapter we have been able to clearly demonstrate the ability to make sub – micron scale two–dimensional stamp–etching of glass surface by simply wetting the mold (polycarbonate membrane of a CD) with the etching solution followed by stamping on the glass substrate. The etched channels appeared as parallel lines as seen in optical and scanning electron microscopy. The etched lines were a reproduction of the positive replica of the mold. We also could make arrays of etched dots of about 0.64 μm^2 area on the surface aligned at a predetermined angle. The present method is advantageous compared to other methods of generating sub-micron scale structural patterns on glass sample. It is a straightforward method and also cost effective. By using the present method one can reduce the number of steps involved thus reducing the cost of production of sub-micron scale channel structures on glass substrates.

6.5 References

1. Becker, H.; Arundell, M.; Harnisch, A.; Hulsenberg, D. *Sens. Actuators B* **2002,** B86(2-3), 271.
2. Wheeler, A. R.; Throndset, W. R.; Whelan, R. J.; Leach, A. M.; Zare, R. N.; Liao, Y. H.; Farrell, K.; Manger, I. D.; Daridon, A. *Anal. Chem.* **2003,** 75, 3581.
3. Vinet, F.; Chaton, P.; Fouillet, Y. *Microelectron. Engineering* **2002,** 61-62, 41.
4. Bernard, A.; Michel, B.; Delamarche, E. *Anal. Chem.* **2001,** 73, 8.
5. Lam, P.; Wynne, K. J.; Wnek, G. E. *Langmuir* **2002**, 18, 948.
6. Boone, T. D.; Fan, Z. H.; Hooper, H. H.; Ricco, A. J.; Tan, H.; Williams, S. *Anal. Chem.* **2002,** 79A.

7. Whitesides, G. M.; Stroock, A. D. *Phys. Today* **2001**, 42.

8. Terry, A.; Oakey, J.; Marr, D. W. M. *Science* **2002,** 296, 1841.

9. Thorson, T.; Maerki, S. J.; Quake, S. R. *Science* **2002,** 298, 580.

10. Kenis, P. J. A.; Ismagiliv, R. F.; Takayama, S.; Whitesides, G. M. *Acc. Chem. Res*. **2000,** 33, 841.

11. Polson, N. A.; Hayes, M. A. *Anal. Chem.* **2001,** 312A.

12. Haswell, S. J.; Middleton, R. J.; O'Sullivan, B.; Skelton, V.; Watts, P.; Styring, P. *Chem. Comm*. **2001**, 391.

13. Dewit, S. H. *Curr. Opin. Chem. Biol.* **1999**, 3, 350.

14. Haswell, S. J.; Watts, P. *Green Chem.* **2003**, 5, 240.

15. Lu, H.; Schmidt, M. A.; Jensen, K. F. *Lab Chip* **2001**, 1, 22.

16. Burns, J. R.; Ramshaw, C. *Chem. Eng. Commun*. **2002,** 189, 1611.

17. Worz, O.; Jackel, K. P.; Richter, T.; Wolf, A. *Chemical Engineering & Technology*. **2001**, 24, 138.

18. de Bellefon, C.; Tanchoux, N.; Caravieilhes, S.; Grenouillet, P.; Hessel, V. *Angew. Chem. Int. Edit.* **2000,** 39, 3442.

19. Chan, E. M.; Mathies, R. A.; Alivisatos, A. P. *Nano Lett* **2003**, 3, 199.

20. Rodriguez, I.; Spicar-Mihalic, P.; Kuyper, C. L.; Fiorini, G. S.; Chiu, D. T. *Anal. Chim. Acta* **2003,** 496, 205.

21. Kikutani, Y.; Hibara, A.; Uchiyama, K.; Hisamoto, H.; Tokeshi, M.; Kitamori, T. *Lab Chip* **2002,** 2, 193.

22. Zhang, W.; Chou, S. Y. *Appl. Phys Lett*. **2001,** 79, 845.

23. Gaboriau, F.; Peignon, M. C.; Barreau, A.; Turban, G.; Cardinaud, Ch. *Microelectron. Engineering* **2000,** 53, 501.

24. Chou, S. Y.; Kelmel, C.; Gu, J. *Nature* **2002,** 417, 835.

25. Unger, M. A.; Chou, H. P.; Thorsen, T.; Scherer, A.; Quake S. R. *Science* **2000,** 288, 113.

26. Yin, Y.; Gates, B.; Xia, Y. *Adv. Mater.* **2000,** 12, 1426.

27. Geissler, M.; Kind, H.; Schmidt-Winkel, P.; Michel, B.; Delamarche, E. *Langmuir* **2003,** 19, 6283.

28. Jun, Y.; Le, D.; Zhu, X.-Y. *Langmuir* **2002,** 18, 3415.

29. Finnie, K. R.; Nuzzo, R. G. *Langmuir* **2001,** 17, 1250.

30. Queeney, K. T.; Fukidome, H.; Chaban, E. E.; Chabal, Y. J. *J. Phys. Chem.* B **2001**, 105, 3903.

31. Xia, Y.; Whitesides, G. M. *Angew. Chem. Int. Ed.* **1998,** 37, 550.

Chapter 7

Spreading and recoil of surfactant containing water drops on glass supported alcohol films.

7.1 Introduction

The phenomena of wetting and dewetting have important technological implications in areas such as microelectronics, coating and painting, spraying of pesticides and herbicides, biological transport, microfluidic devices and oil recovery. For example, surfactants such as trisiloxane alkoxylate[1] are generally mixed with herbicides or pesticides to improve spreading of the fluid in agricultural spray, so as to cover all parts of the leaves quickly and to avoid the formation of drops. One could deposit a monolayer of molecules on a solid surface and change the wettability of the surface by photo-irradiation, where light would ideally catalyze isomerization of the molecules back and forth. In this way, light driven directional motion of a liquid on a solid surface could be achieved [2]. On the other hand the ability to pattern surfaces on a microscope length scale is important in technological application such as fabrication of microelectronic devices, digital storage media, fluidic devices and sensors. An emerging method of making patterned surfaces involves taking advantage of wetting and dewetting properties of liquids on surfaces. Wetting instabilities during the Langmuir-Blodgett film transfer can lead to stripes and channels with alternating wettability [3]. Moreover surfaces with different wettability can be used in fabricating microfluidic devices. These requirements have led to intense phenomenological investigations of the wetting and dewetting properties of liquids on different surfaces. It would be even more advantageous if one could achieve control over wetting and dewetting such that chemical reactions between the reagents present in a thin liquid film and the surface on which the film spreads could be effected in a (controlled) desired manner. In other words by controlling the rate of spreading and recoil the reaction time could be controlled and a gradient in the product formation as a function of residence time of the liquid film could be achieved. We have ventured to proceed in this direction by first studying the spreading and recoil of surfactant containing water drops on various alcohol films supported on glass slides. The findings are described in this chapter.

7.1.1 Previous investigations

Wetting occurs when a liquid drop placed on a surface spreads and the contact angle (the tangential angle that a liquid drop makes with the surface underneath) between the liquid drop and the surface tends to become zero. On the contrary a liquid does not wet the surface when the contact angle is greater than 90° and the liquid tends to ball up and run off the surface. These two behaviors are schematically shown in Figure 7.1.

T > 90 T < 90

Not wetting Wetting

Figure 7.1 A schematic representation of wetting and non-wetting of a surface by a liquid drop. T is the contact angle between the drop and the surface.

There are numerous reports in literature on the wetting and dewetting properties of various liquid films on different substrates. The investigations, however, have focused primarily on studying the wetting and dewetting properties of liquids on solid surfaces and liquids on liquid surfaces.

When a liquid drop is placed on a solid supported surface, a gradient in surface tension leads to spreading, recoil and movement of the drop. There are three ways to generate the gradient in surface tension. They are temperature gradient [4], surfactant concentration gradient [5] or composition gradient. Also, the Marangoni flow known to occur in classical "tear" of wine is driven by surface tension gradient. Chaudhury and Whitesides [6] have been able to move a drop of water uphill against gravity by creating spatial gradient in surface free energy. Wettability gradient across a surface also leads to spreading or movement of liquid across a solid surface[7-8]. On the other hand a liquid drop when placed on an immiscible liquid may either spread to an equilibrium thickness or remain as a lens, as governed by surface tension gradient between the two liquids[9-10]. It has been reported that when a drop of an aqueous surfactant solution is placed on top of a pre-moistened glass surface, the drop spreads with fingering instability whose velocity and fingers depend on the thickness of the film and the concentration of surfactants in the parent solution[11-12]. Afsar-Siddiqui *et al* has investigated the spreading behavior of sparingly soluble[13] and highly soluble[14] aqueous surfactants solution on films of various thickness of water placed on a glass substrate. In the case with sparingly soluble surfactant and at high water film thickness they have observed fingering instability, the onset time of which became shorter with increased surfactant concentration. On the other

hand, when highly soluble surfactant was used the instability had become apparent at a lower surfactant concentration and more pronounced fingers were observed. In both the cases Marangoni effect played a key role in the spreading behavior. In their study of the convective instability of a volatile immiscible liquid placed on water film Dussaud *et al*[15] concluded that evaporative cooling might also be responsible for observation of ½ exponent in the spreading behavior.

Dewetting of a thin liquid film placed on a solid surface is known to be initiated, among others, by rim instability, "spinodal dewetting", coalescence, substrate contamination or by the growth of a directed dewetting front[16-19]. Technological importance in electronic and fluidic devices especially in nanotechnology[20], surface pattering[21-22], understanding of biological phenomena such as low rate of water evaporation from tear film[23], dewetting at soft interfaces[24] has justifiably led to intense experimental and theoretical investigations of wetting and dewetting of thin films on various substrates. It is important to note that an ultra thin film on a solid surface may have structures including preferential orientation of molecules or defects in the form of holes, agglomerations that may as well decide the course of spreading and recoil of a drop when placed on it. This however may not be case for a relatively thicker film, which is expected to be more homogeneous and devoid of the above defects. Further, controlled surface / interface tension gradient could easily be generated by suitable choice of the liquid making the film such that the rate and nature of spreading and or recoil of the drop could be controlled. In this way a potentially vast opportunity of combinations could possibly be created using differential surface tension, viscosity, boiling point, nature of hydrophobic and hydrophilic groups constituting the film molecules.

7.1.2 Our study

Although Dussaud *et al*[15] have investigated the spreading of volatile and non-volatile liquids on water and Afsar-Siddiqui *et al*[13,14] have reported the figuring instability accompanying the spreading of aqueous surfactant solutions on varying thickness of liquid film, as far we know the spreading and recoiling behavior of a highly soluble aqueous surfactant solution on a volatile alcohol film still remains unexplored. In this chapter we report the experimental observations regarding the spreading and recoil of surfactant containing water drops on various alcohol films supported on glass slides. A schematic representation of the basic–experimental setup is shown in Figure 7.2. In all of the experiments a drop of water containing a certain concentration of a surfactant is placed on

an alcohol film supported by a glass slide. The observations are made with respect to the spreading and recoil of the drop and the fate of the alcohol film.

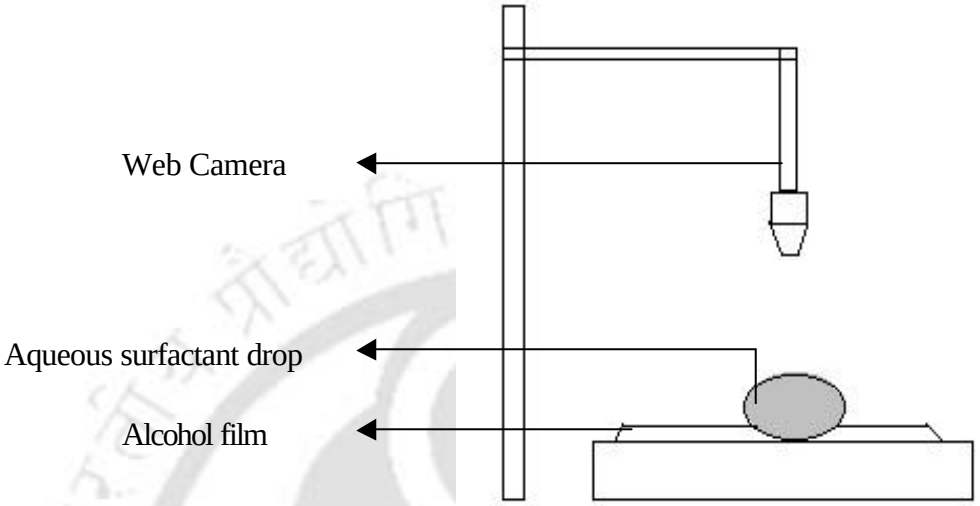

Figure 7.2: A schematic representation of the basic idea of the experiment. The experimental set up comprises of aqueous surfactant drop placed on alcohol film; both supported by the glass slide. The Web camera was placed vertically above the drop.

The choices made in our experimental conditions offer four unique advantages. They are as follows.

(a) The molecular defects, in terms of size of clusters, holes etc. possibly present in an ultrathin film of water or such species on a solid surface would be absent in a relatively thick film of alcohol. Thus the spreading behavior would primarily be governed by the film properties rather than defects in the film.

(b) The surfactant concentration in the drop could easily be varied by starting with different initial concentrations. Thus a control could possibly be achieved with respect to surface tension of the drop and interfacial tension between the drop and the film. The surfactant is highly soluble both in water and the alcohol. Also, water and alcohol mix well. Thus the surfactant concentration in the drop may affect the interfacial mixing of the drop and the film.

(c) The alcohols chosen have different boiling point and thus rate of evaporation of the film would be different. As the evaporation would lead to cooling, the rate of cooling would also be different depending upon the choice of alcohol. Thus a

varied temperature gradient could possibly be created between the drop and the film. This would have important consequences on the spreading behavior of the drop.

(d) There would be a surfactant concentration gradient between the center of the drop and the periphery where it meets the film. Thus Marangoni effect driven flow might also add to the behavior of spreading of the drop.

Herein we report the results of investigation of spreading and recoil of sodium dodecyl sulfate (SDS) containing aqueous drops on glass supported liquid films of methanol (CH_3OH), ethanol (C_2H_5OH) and iso-propanol (i-PrOH). We found that in all the cases the spreading and recoil occurred without fingering instability. We observed that the drop spreads the fastest on CH_3OH, followed by C_2H_5OH and the slowest on i-PrOH. On the other hand the drop recoiled the slowest on CH_3OH and the fastest on i-PrOH while it recoiled with intermediate time on C_2H_5OH. In addition, concentration of surfactant in the drop played a prominent role in the spreading and recoil time of the drop with higher surfactant concentration making the drop spread and recoil faster. Moreover the time dependent velocity profiles were Gaussian in nature, while the radius dependent velocity profile showed oscillatory behavior. Finally, using FTIR spectroscopic evidence we show that the drop had mixed with alcohol during spreading and recoil.

7.2 Experimental section

Methanol (HPLC grade, Merck), ethanol (Bengal Chemical & Pharmaceuticals Ltd) and iso-propanol (Analytical Reagent Grade, Merck) were used as purchased. Sodium dodecyl sulfate was purchased from Sigma-Aldrich Chemical Company and was used as received. Microscope slides were from Blue Star, India. For better viewing of spread and recoil of the surfactant-laden aqueous drop on alcohol film, rhodamine B dye (1.5mM, Aldrich) was used. Millipore ultrapure water (resistivity 18.2 MΩ cm) was used in all of this work.

The microscope glass slides were cut into small pieces with dimension of about 25 X 25mm. The glass slides were then cleaned in piranha solution (7:3 = H_2SO_4: H_2O_2). 45µL of either of CH_3OH, C_2H_5OH or i-PrOH was poured on glass micro slides to form a film over it. For each study, 3 µL of aqueous solutions of sodium dodecyl sulfate (SDS) of different concentration mixed with rhodamine B was dropped on the alcohol film using

a micropipette (Finnpipette from Labsystem, volume 20-200 µL and 2-20 µL). The spreading and recoil of the aqueous drop on alcohol film was monitored using a Creative Web Camera (model PD1001).

A schematic view of the set up is shown in Figure 7.2. The camera was placed vertically above the drop (about 4 cm from the glass plate) and was connected to a personal computer (PC). The recording was made at 30 frames per second. It was started right after the addition of alcohol to the slide and before the addition of the drop on the film so that the fate of the drop right from the moment it was placed could be monitored. A graph paper was placed below the glass slide for measurements requiring quantitative data such as rate of spreading and change of diameter.

7.3 Results and Discussion

We have investigated the spreading and recoil of aqueous surfactant drops on glass supported liquid films of CH_3OH, C_2H_5OH and i-PrOH. The alcohols we have used are highly miscible in water and hence a liquid drop of water on a liquid film of alcohol could not be stabilized for investigation without a support of a solid surface. We used glass slides as the solid surface supporting both the liquids where the spreading of one against the other could be easily studied. The alcohols differ in the number of alkyl head groups connected to the OH group and also on their boiling points. However, they have very similar surface tension values (Table 7.1).

Table 7.1 The boiling points and surface tension values of alcohols used in our study

S. NO	ALCOHOLS	BOILING POINT (°C)	SURFACE TENSION
01	Methanol	64.7	22.61
02	Ethanol	78	22.75
03	Iso-propanol	82.4	26.0

Hence significant differences that might occur in spreading of the drop against the films will probably be due to differences in the rate of mixing of alcohol with water at the interface, the differences due to the head groups and differences in the boiling points of the alcohols. The last factor affects the rate of evaporation of the alcohol film.

With the help of a micropipette, 45 µL either of CH_3OH, C_2H_5OH or i-PrOH individually was poured onto a 25 mm X 25 mm microscope slide. The alcohol spread

completely on the glass slide so as to make a 72 μm thick film. A film with thickness lower than 72μm, for i-PrOH, evaporates before observation could be completed. So the thickness of all alcohol films was kept uniform at 72 μm, unless otherwise stated. As the aqueous surfactant solution is colorless, we have used a rhodamine B dye (1.5mM) in the drop for enhanced viewing of spreading and recoil with the camera. The extinction coefficient of rhodamine B is high and as a result a small amount of dye was enough to give good coloration of the solution without affecting surface tension or other properties of the surfactant laden aqueous drop. The recording was started just before the addition of the drop on the film so that we could record the fate of the drop right from the moment it had been placed. However, here we show selected pictures of the drop from right after it was placed. In addition to studying the spreading of a surfactant containing water drop on various alcohols, we have varied the concentration of SDS in the drop and studied its effect on the rate of spreading and recoil on a specific film of alcohol. From these studies we have calculated the mean diameter at various points of time during spreading and recoil and report the same.

7.3.1 Spreading and recoiling phenomenon

The time dependent evolution of the surfactant-laden water drop on alcohol films exhibited interesting behavior. As an example, we show photographs of selected time frames of a drop of aqueous SDS on i-PrOH in Figure 7.3. As can be seen in the photographs the diameter of the drop did not increase much in the beginning (first 25 s). There was a sudden increase in the diameter starting at 45 s with a maximum value occurring at 82 s, when the diameter reached to a value of about 20 mm. The recoil began almost immediately and the rate of decrease in the diameter, on return, was much faster than the rate of increase as it spread. Finally, the drop had returned to nearly its original diameter. The exact nature of spreading varied from drop to drop depending on the initial waves created on the alcohol film due to the impact of the drop. However, the general spreading as well as recoil behavior was similar to the above. A remarkable feature that we would like to point out here is that while the drop had spread against the alcohol film there was no observable fingering instability as had been observed in the case of spreading of aqueous surfactant drops against thin water film[10-13,25]. However, towards the end when the drop had spread to its near maximum diameter there were fingers observable at the periphery of the film. This could be due to the absence of alcohol film, which probably

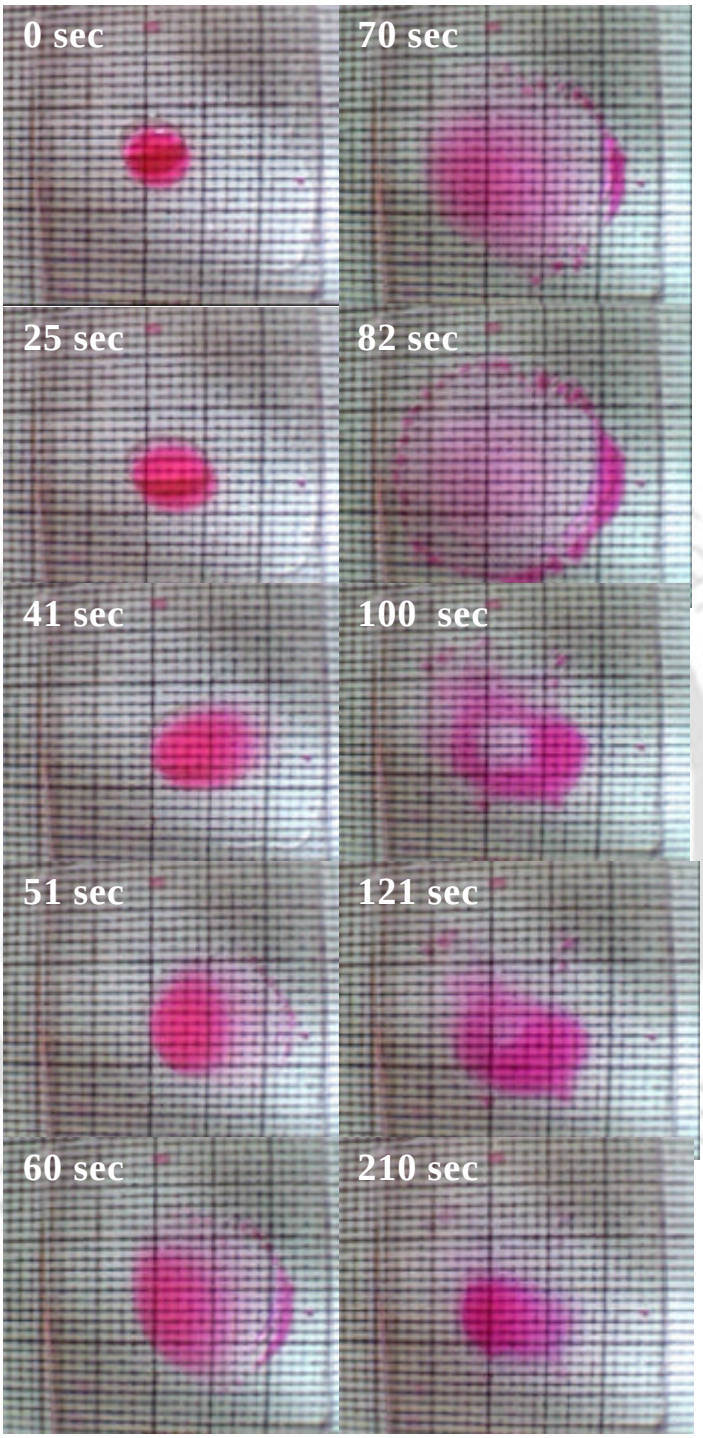

Figure 7.3. WEB camera shots of time dependent spread and recoil of an aqueous surfactant drop over i-PrOH film. The concentration of SDS in the drop was 32 mM. These are selected pictures representing the fate of the drop. The background squares are from an ordinary graph paper placed underneath the glass plate. *(See color plates, page 141)*

had dried (or mixed with the drop) by the time the drop expanded to its near maximum diameter, and hence the drop spread with regular fingering instability.It is worth mentioning here that we found a surfactant drop on a virgin glass slide had spread with the maximum final diameter of only one fourth of that attained by the surfactant drop placed on glass supported on alcohol film. Also, no observable recoil was found in the former case.

7.3.2 Effect of the nature of alcohols on spreading and recoil

Studies with CH_3OH, C_2H_5OH and i-PrOH films suggest that the profiles of spreading and return of the drop were similar whereas the time taken to reach its maximum diameter as well as recoil was different for different alcohol films. In a typical experiment the time taken to reach maximum diameter was 42 s for CH_3OH, 61s for C_2H_5OH and 82 s for i-PrOH. The results typically obtained are plotted in a dimensionless scale (D/Do – 1) versus time and are shown in Figure 7.4.

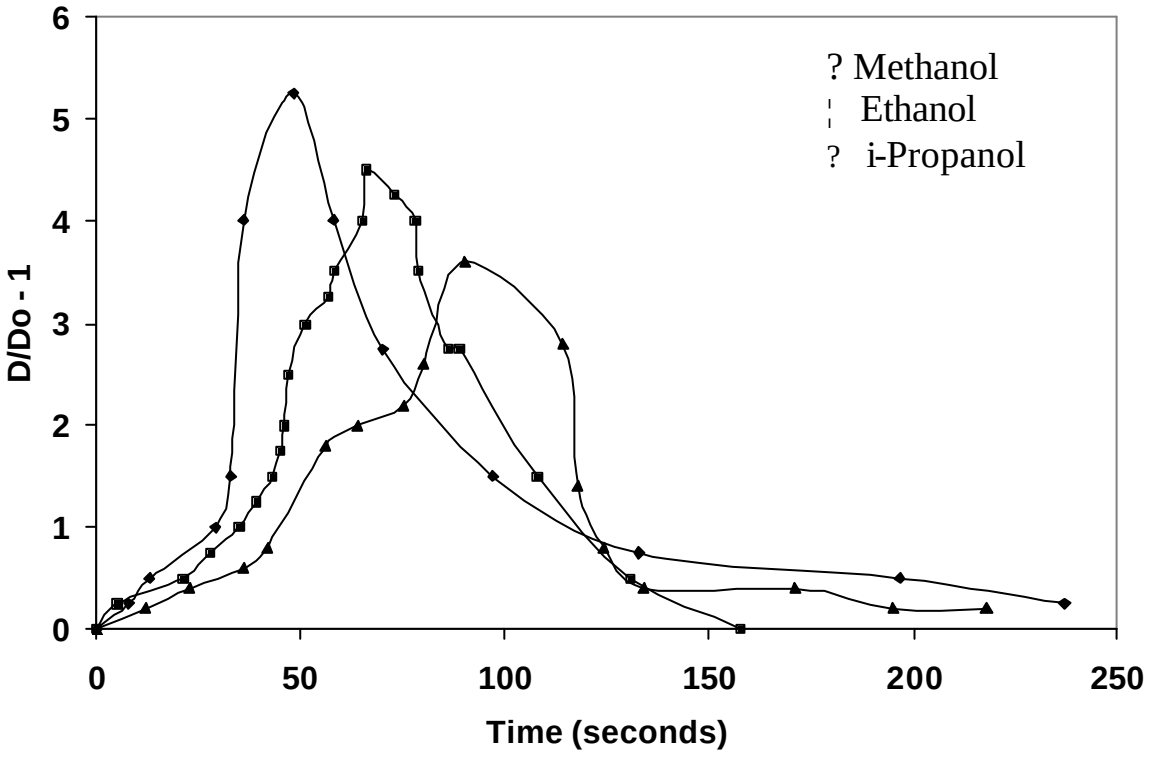

Figure 7.4: Time depended plot of D/Do –1 for different alcohol systems.

As evident from the figure, the spreading behavior of the drops, such as slow initial rise in the diameter and then sudden increase followed by fast return to nearly original diameter were characteristics of all the alcohol films studied. On the other hand, its also clear from the figure that the time for reaching the maximum diameter on CH_3OH was much shorter than that on C_2H_5OH, which was less than that on i-PrOH. It may further be noted that the behavior of the return time was different for different alcohol film. For example, the drop on CH_3OH took the longest time (88 s) to return which was a little longer than on C_2H_5OH (84 s), while the drop on i-PrOH took the shortest time (74 s) of the three to return back to the final diameter.

7.3.3 Effect of surfactant concentration on spreading and recoil

An important part of these studies was the observations of the effect of various surfactant concentrations on the rate of change of diameter of a drop placed on an alcohol film. In Figure 7.5 we show the results obtained from a collection of shots when the concentrations of SDS in the drop was kept at 4mM, 8mM, 16mM and 32mM and the film was made of C_2H_5OH. These concentrations correspond to about ½, 1, 2 and 4 times the critical micellar concentrations (CMC) respectively of SDS in pure water.

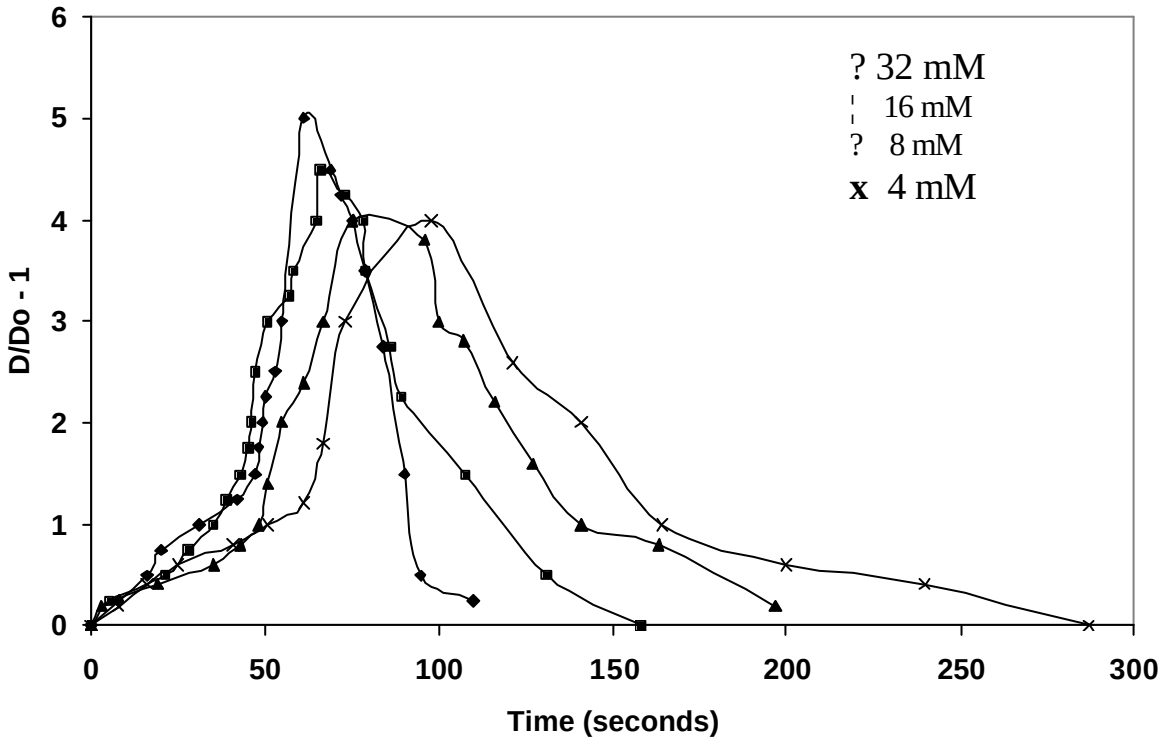

Figure 7.5: Time depended plot of D/Do –1 with different surfactant concentration.

In these cases also we have plotted the behavior in a dimensionless scale (D/Do –1) versus time at different surfactant concentrations. As can be seen from the figure, the drop with 32mM SDS concentration took the shortest time to rise and return followed by 16mM concentration drop and then 8 mM and then 4 mM. Thus our observations suggest that increasing the concentration of the surfactant hastens the spreading and recoil of the drop. The spreading rate on the alcohol films increases with surfactant concentration as usually observed in simple systems[22].

7.3.4 Effect of thickness of film on spreading

The effect of thickness of the alcohol film on the spreading was also studied. A particular value of thickness of the alcohol film was obtained by pouring appropriate amount of alcohol on the glass slide. The thickness was calculated by dividing the volume of the alcohol by the area of the slide. The results obtained with films of C_2H_5OH are tabulated in Table 7.2. The surfactant concentration used was kept at 32mM. As clear from the table with increase in the thickness of the alcohol film, the time taken for the drop to spread to reach to its maximum diameter increased. It is interesting to note that when the thickness varied between 48 and 72 μm, the time taken for maximum spread varied little. However, increase in the thickness up to 80 μm and beyond slowed down the spreading of the drop significantly. For example, it took 120 s for the drop to spread to its maximum diameter when the film thickness was 88 μm, whereas the time taken for the drop to spread over a 80 μm thick film was 90 s. Such large difference was not observed at lower thickness of the film.

Table 7.2: Time of maximum spread with various thickness of alcohol film

S. No	System	Thickness (μm)	Time taken for spreading to maximum diameter (s)
01	Ethanol	48	56
02	Ethanol	56	58
03	Ethanol	64	60
04	Ethanol	72	61
05	Ethanol	80	90
06	Ethanol	88	120

7.3.5 Velocity distribution

The time dependent velocity distribution of spreading and recoil of drops with various surfactant concentrations is shown in Figure 7.6. Each plot was fitted to a single Gaussian function. As evident from the graphs, the spreading of the drop, on each alcohol film, did not start immediately after placing the drop on the film. However, once the spreading started the velocity profiles were Gaussian with the maximum velocity on CH_3OH reached the earliest and then C_2H_5OH followed by i-PrOH. For example, the drop with 16 mM SDS reached maximum velocity on CH_3OH at 35 s, at 49 s on C_2H_5OH and at about 85 s while spreading on i-PrOH. On the other hand the recoil velocity peaks occurred at 56 s, 86 s and 117 s respectively. The recoil of the drop on each alcohol film started right after the complete spread. The value of the maximum velocity (spreading and recoil) for all the systems was in the range of 0.3-1.5 mm/s. In general, for each alcohol the time of reaching velocity maximum occurred earlier with increasing concentration of surfactant in the drop. For example, maximum of spread velocity of the drop on CH_3OH occurred at 43s, 36s and 33s when the concentration of SDS in the drop was 8mM, 16mM and 32mM respectively. Thus higher the concentration of the surfactant faster was the attainment of the maximum spreading velocity. The recoil behaviors under the above conditions were similar. We also calculated the velocity profiles with increasing radius of the drop as it spread and decreasing radius as it recoiled on different alcohol films. The plots are given in Figure 7.7. The plots show oscillatory behavior of velocity with the radius of the drop, which indicates the existence of an interface phenomenon. There are three oscillation peaks for both spreading and recoil on CH_3OH and two oscillatory peaks for spreading on EtOH and i-PrOH. These oscillations could be explained by possible establishment of an equilibrium surfactant concentration at the interface between the drop and alcohol film. At the interface, surfactant molecules will desorb from the aqueous phase and adsorb into the alcohol film during the process of spreading. If the spreading velocity is higher than the rate of mixing of the surfactant in the bulk alcohol film, a temporary equilibrium surfactant concentration will be created at the alcohol film interface thus opposing the spreading i.e. reducing the spreading velocity[13]. Once the surfactant molecules mix with the bulk film this local equilibrium will be lost and the drop again will resume spreading with higher velocity. Observations of oscillations in velocity during recoil also indicates the existence of interfacial phenomenon but of a different kind. When the drop recoils back from its maximum diameter the rate of reduction of diameter might be faster than the rate of mixing and hence there would be time required for reaching

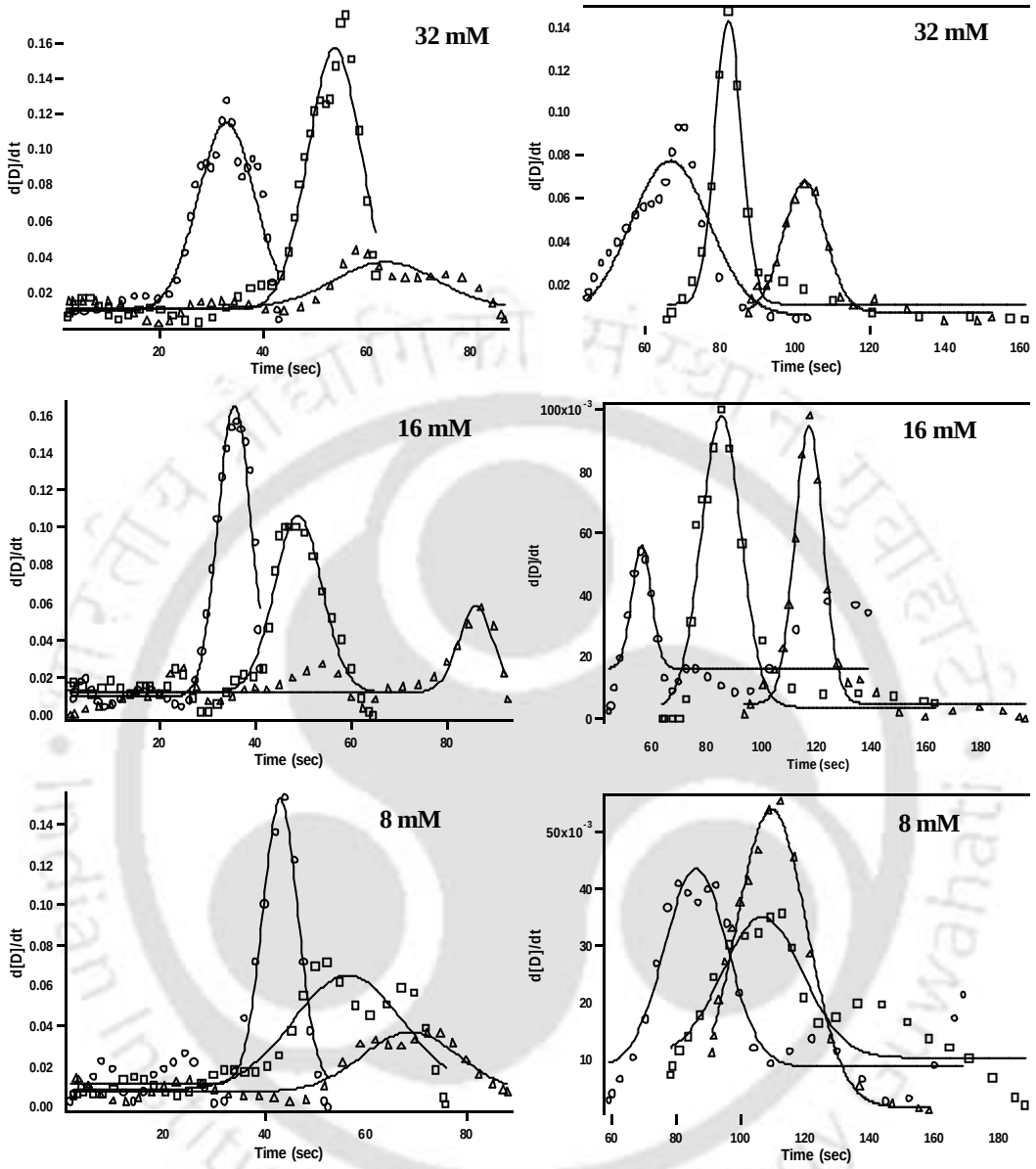

Figure 7.6: Velocity versus Time plots of spreading as well as recoil of aqueous surfactant solution on different alcohol films: (o) methanol, ( ) ethanol and (?) i-propanol. The data points were fitted using a Gaussian function.

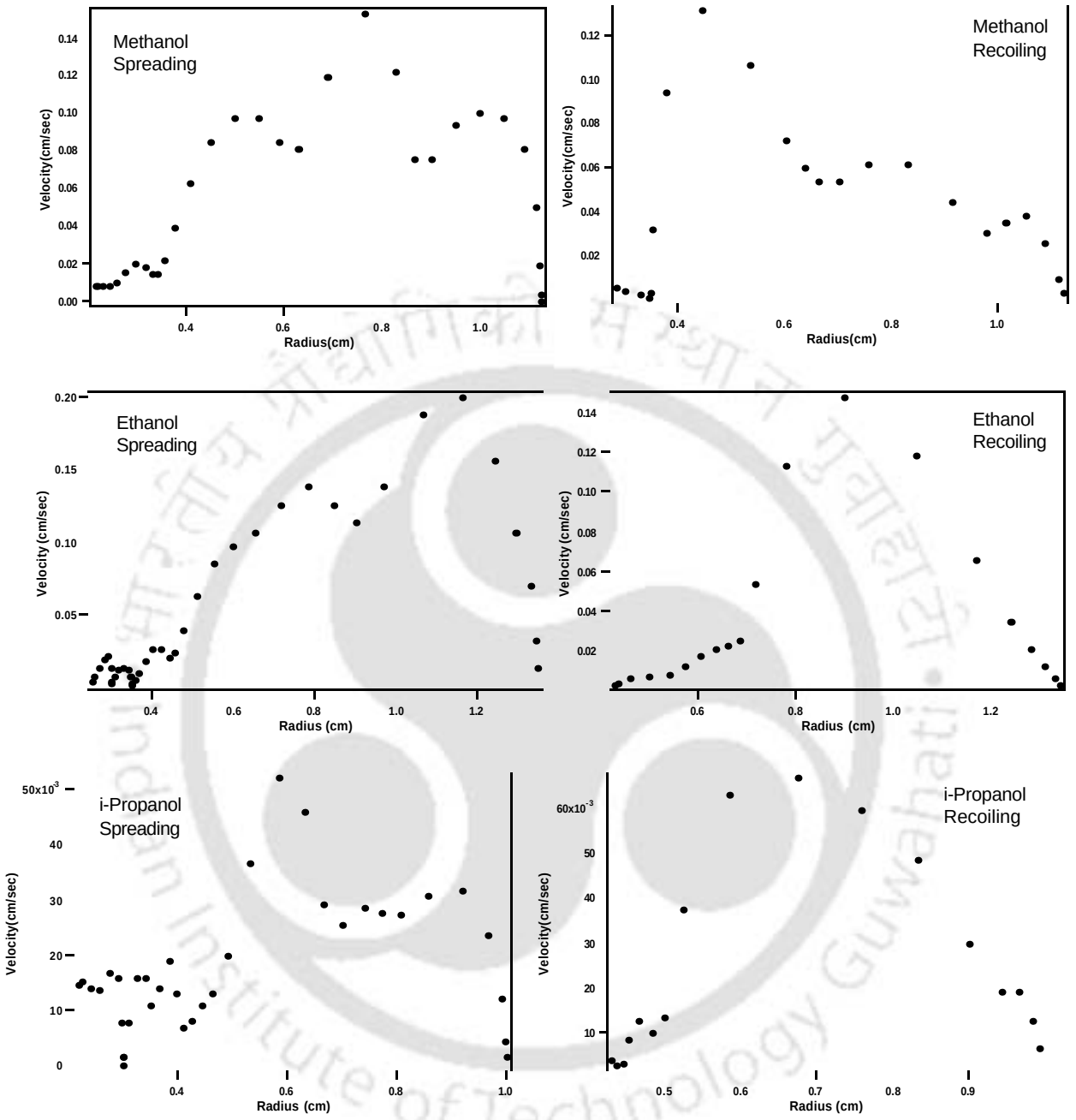

Figure 7.7: Velocity versus Radius plots of spreading and recoil of aqueous surfactant drops on different alcohol films. The surfactant concentration was 32mM.

equilibrium. In addition, if there is a difference in the shrinking velocity at the periphery (faster) and that near the center of the film/drop (slower) there would be opposition to shrinkage until equilibrium is reached and thus the observed oscillations in velocity profile. In addition, the alcohol as well as water would preferentially evaporate from the periphery and thus would be responsible for difference in surfactant concentration between the edge of the film/drop and near the center. Thus oscillations would be observed until equilibrium is reached.

7.3.6 Composition of a dewetted drop

We wanted to probe whether there was mixing of alcohol in the drop while it spread. To study this we had used CD_3OD as the alcohol film instead of CH_3OH, since the C-D stretching vibrational frequencies of the alcohol are clearly distinguishable from those of C-H stretching vibrations of the surfactant and O-D stretching frequency is different from that of O-H of H_2O. This is not possible if CH_3OH is used instead. We recorded FTIR spectra of the drop surfactant solution, of CD_3OD and that of the drop after it had spread against a 72 μm thick film of CD_3OD and recoiled back. The spectra are shown in Figure 7.8. As clear from the figure, the observation of C-D stretch in the region of 2160-2300 cm^{-1} and O-D stretch at 2500 cm^{-1} in Figure 7.7 C (i.e. of the drop after recoil) establishes that there was mixing of CD_3OD with the surfactant drop during its spreading and recoil

We also wanted to investigate whether the drop of an aqueous surfactant solution mixed quickly with the alcohol film such that the alcohol no longer remains pure and is mixed with water and surfactant immediately after the drop was placed. To answer this question we did the following experiment. On the alcohol film a drop containing a mixture of alcohol and aqueous surfactant solution taken from a stock solution with the ratio of 3μL of surfactant solution and 45 μL of alcohol was placed. In this case the drop spread in 6 s compared to more than 60 s needed for complete spreading of a surfactant only solution drop on alcohol film. This means that even though there is a possibility of mixing between the drop and the film, rapid mixing may not be the major factor at least at the initial stages of spreading of a surfactant-laden aqueous drop on an alcohol film.

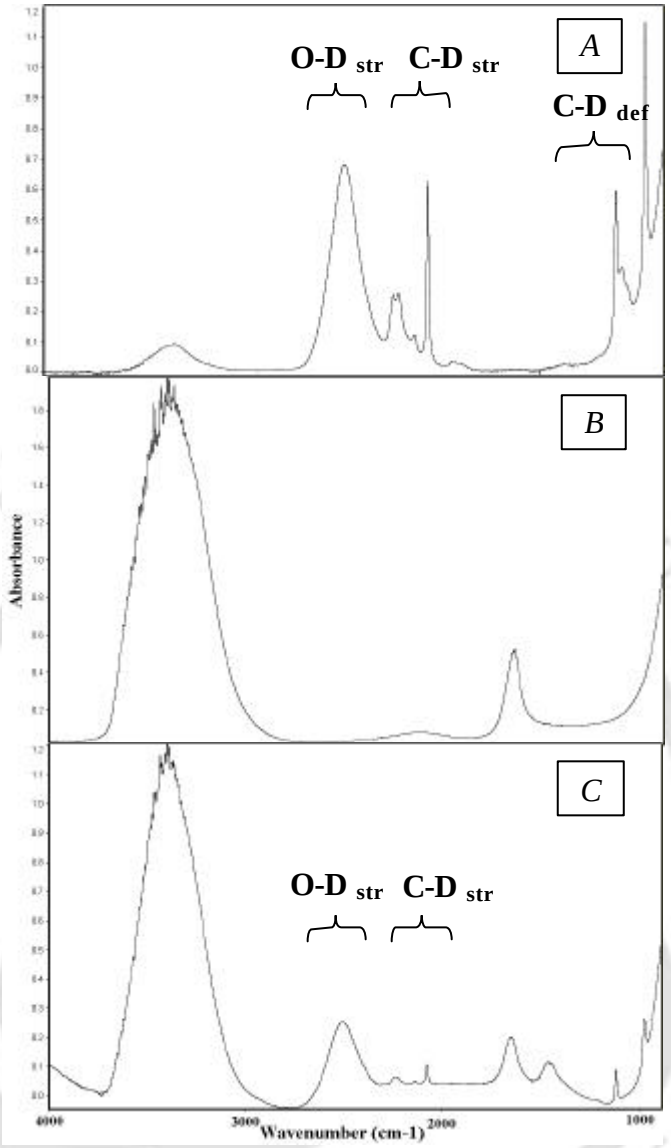

Figure 7.8. FTIR spectra of (A) CD_3OD, (B) 8.1mM SDS solution and (C) the liquid that was left after the drop had recoiled back.

7.3.7 What is really happening?

There are four factors that probably control the spreading of an aqueous surfactant drop on the alcohol film as we have observed. The first is the negative spreading parameter based on the difference in surface / interface tension if we consider the spreading of drop on alcohol film. This means the surfactant in the drop reduces the surface tension of water to a lower value but still higher than that of alcohol. For example, by using Wilhelmy plate method, we have found that at 30^0C the surface tension values of all surfactant solutions (above critital micellar concentration) used in our experiments

differed little and were nearly equal to 30.0 mN/m. If we consider the surface tension of alcohol to be about 22 mN/m, the spreading parameter, S in equation 1,

$$S = \gamma_a - \gamma_d - \gamma_{ad} \quad (1)$$

where γ_d, γ_a are the surface tension of the drop solution and alcohol respectively and γ_{ad} interfacial tension between the two liquids

even without taking interfacial tension into consideration becomes negative. Moreover, the interfacial tension parameter between the drop and alcohol reduces the spreading parameter even further. Thus the overall spreading parameter is negative, which disfavors spreading of the drop on the film. However, with increasing surfactant concentration the surface tension of the drop goes down (albeit little) which means that spreading parameter became less negative and progressively reduces the opposing parameter. It has been observed earlier that an aqueous surfactant drop with lower surface tension spreads on a glass supported thin film of water having higher surface tension[10]. However, that situation is exactly opposite to our system. The second factor controlling the spreading is Marangoni effect due to the gradient in surfactant concentrations at the center of the drop compared to that at its edge that induces widening of the drop. The third is the interfacial mixing of water and alcohol that helps in spreading of the drop. The fourth is the evaporative cooling of the alcohol film that creates a temperature gradient with the drop having higher temperature than the film thereby creating a temperature gradient induced widening of the drop. CH_3OH has lower boiling point (64.7^oC) and higher latent heat of vaporization (983 kJ/Kg) than C_2H_5OH (boiling point 78^oC and latent heat 854 kJ/kg) while i-PrOH has the highest boiling point (82.4^oC) and lowest latent heat value of 665 kJ/kg (Table 7.3). Thus cooling rate due to evaporation may be the highest with CH_3OH and the lowest with i-PrOH, which means that the drop would spread the fastest on CH_3OH and slowest on i-PrOH. This is what we have observed in our experiments. The importance of third and the fourth factors in our observations is further corroborated by the following observations. When we had put a drop of pure water on an alcohol film the drop also spread against the alcohol film even though the surface tension of alcohol (22 dynes/cm) is much less than that of water (72 dynes / cm). Typically it took about 75 s for the drop to spread against C_2H_5OH, which is longer than observed for the case of surfactant-laden drop, and much longer than 6 s observed for alcohol pre-mixed surfactant solution (section 7.3.6). We have not shown this behavior, as a figure, as the recoil

behavior was different from those observed with surfactant-laden drop on alcohol and also there is no simple way to control the spreading and recoil time of the drop, which was one of the principal objectives of our work. In addition, when the reverse experiment was performed, i.e. a drop of alcohol on an aqueous surfactant solution film, the drop did not spread. In other words, the part of the glass slide containing alcohol drop would probably have less temperature than the water film therefore making opposite temperature gradient which disfavors spreading. On the other hand the alcohol drop and the film (of surfactant solution) mixed slowly to finally obtain a thin film of the mixture, probably as a result of interfacial mixing. The different rate of evaporation that results in cooling of the glass slide may also be the reason for different time dependent velocity profiles of the drop on three different alcohol with reaching the maximum velocity at the earliest on CH_3OH and the latest on i-PrOH. However, the surfactant dependent difference in velocity profiles indicate that different rate of mixing also plays an important role with

Table 7.3: Latent Heat of vaporization of alcohols used in the experiments

S. No	Alcohol	KJ/kg
01	Methanol	983.13
02	Ethanol	854.0
03	Iso-Propanol	665.0

higher surfactant concentration favoring faster mixing resulting in attainment of earlier maximum velocity. The broad nature of Gaussian distribution of radius dependent velocity profiles indicates that as the drop spreads to larger radius the effect due to evaporative cooling becomes increasingly smaller and also as the mixing between alcohol and drop progressively increases the effect becomes less distinct.

The next question comes is whether the alcohol mixes with the drop as the drop spread or surfactant-laden drop pushes the alcohol film and at the same time induces unidirectional mixing of water (with surfactant) to alcohol film. The answer to this question came from the FTIR spectroscopic observation, which indicates that as the drop progressively expanded the alcohol from the film had mixed with the drop. That is what we observed in the form of presence of C-D and O-D peaks in the spectrum of liquid collected after the recoil (Figure 7.7). Also, we have not observed any liquid dropping out

of the slide as the drop spread indicating that alcohol film progressively became more contaminated with water and surfactant.

7.3.7 Why does the drop recoil?

The mixture of alcohol, water and surfactant does not wet the glass slide and hence the liquid drop after spreading to its maximum diameter recoils back to nearly original diameter and the difference that we observe is due to gravitational effect where the drop spreads by its own weight. The dewetting is probably controlled by the spreading parameter between glass surface and aqueous surfactant solution mixed with alcohol. The variation that we observe is possibly due to the content of alcohol and surfactant concentration in the recoiling film, which results in different spreading parameter values for different concentration of surfactant and alcohol in different films.

7.4 References

1. Nikolov, A. D.; Wasan, D. T.; Chengara, A.; Koczo, K.; Policello, G. A.; Kolossvary, I. *Adv. Colloid Interface Sci.* **2002,** 96, 325.
2. Ichimura, K.; Oh, S. K.; Nakagawa, M. *Science* **2000,** 288, 1624.
3. Glelche, M.; Chi, L. F.; Fuchs, H. *Nature* **2000,** 403, 173.
4. Cazabat, A. M.; Heslot, F.; Troian, S. M.; Carles, P. *Nature* **1990,** 346, 824.
5. Brochard, F. *Langmuir* **1989,** 5, 432.
6. Chaudhury, M. K.; Whitesides, G. M. *Science* **1992,** 256, 1539.
7. Ichimura, K.; Oh, S. K.; Nakagawa M. *Science* **2000,** 288, 1624.
8. Daniel, S.; Chaudhury, M. K.; Chen, J. C. *Science* **2001,** 291, 633.
9. Adamson, A. W.; Gast, A. P. *In Physical Chemistry of Surfaces 6th Ed.;* John Wiley & Sons, Inc, New York, **1997.**
10. Wyart, F. B., Martin, P.; Redon, C. *Langmuir* **1993,** 9, 3682.
11. Troian, S. M.; Wu X. L.; Safran, S. A. *Phys. Rev. Lett*. **1989,** 62, 1496.
12. Troian S. M., Herbolzheimer, E.; Safran S. A. *Phys. Rev. Lett*. **1990,** 65, 333.
13. Afsar-Siddiqui, A. B.; Luckham, P. F.; Matar, O. K. *Langmuir* **2003,** 19, 696.

14. Afsar-Siddiqui, A. B.; Luckham, P. F.; Matar, O. K. *Langmuir* **2003,** 19, 703.

15. Dussaud, A. D.; Troian, S. M.; Harris, S. R. *Phys. Fluids* **1998,** 10, 1588.

16. Yerushalmi-Rozen, R.; Kerle, T.; Klein, J. *Science* **1999,** 285, 1254.

17. Reiter, G.; Sharma, A. *Phys. Rev. Lett.* **2001,** 87, 166103-1.

18. Troian, S. M. *Phys. Rev. Lett* **1993,** 71, 1399.

19. Karapanagiotis, I.; Evans D. F.; Gerberich, W. W. *Langmuir* **2001,** 17, 3266.

20. Nguyen, V. X.; Stebe, K. J. *Phys. Rev. Lett.* **2002,** 88, 164501-1.

21. Higgins, A. M.; Jones, R. A. L. *Nature* **2000**, 404, 476.

22. Gu, Z. Z.; Fujishima, A.; Sato, O. *Angew. Chem. Int. Ed.* **2002,** 41, 2067.

23. Shahidzadeh, N.; Bonn, D., Meunier, J.; Mavon, A. *Phys. Rev. E* **2001,** 64, 021911.

24. Martin, A.; Buguin, A.; Brochard-Wyart, F. *Langmuir* **2001,** 17, 6553.

25. Stoebe, T.; Lin, Z.; Hill, R. M.; Ward, M. D.; Davis, H. T. *Langmuir* **1997,** 13, 7270.

Chapter 8

A simple UV-visible spectroscopic probe for observing collapse of Langmuir-Blodgett monolayers at air-water interface

8.1 Introduction

In recent years, with the progress made in the area of material science, considerable amount of interests have been generated for the research and development in the field of, what may be termed as, "materials engineering". The primary aim of such research has been the attainment of capability of assembling individual molecules into highly ordered architectures. Principles of molecular self-assembly[1-2], chemical vapor deposition[3-5], electrochemical deposition[6], surface modified chemical deposition[7], photochemically induced pattern formation[8-9], photolithography[10] and soft-lithography[11] based pattern generation are some of the methods that have been developed for achieving directed higher order molecular architecture. On the other hand, an enormous amount of work has been done in the development of techniques based on the Langmuir-Blodgett (LB) films[12]. The LB film transfer technique provides the capability to construct devices with ordered molecular assemblies having applications in molecular electronics, biological and permeable membranes, mechanical filters, piezoelectric devices and in biological sensors.

Engineering materials with molecular level precision requires understanding of the properties of the building materials at various stages involved in the process of manufacturing. In LB films, amphiphilic molecules are the building block. A monolayer of these molecules typically float at the air-water interface with hydrophilic head groups immersed in water while the hydrophobic tails protrude out to the air. This molecular film at the air-water interface is known as a Langmuir film. Usually the collective property of the molecules in a Langmuir film are studied by measuring the average surface pressure, π:

$$p = s_0 - s$$

where σ_0 is the surface tension of pure water and σ is the surface tension of water in the presence of the amphiphilic molecules. A plot of surface pressure as a function of the average area of water surface available to each molecule (Å) at a constant temperature is known as the surface pressure-area adsorption isotherm (π -A isotherm)[13]. A knowledge of pressure-area isotherm is important in understanding the average collective property, such as the stability of the monolayer at air-water interface, the reorientation of molecules in the 2-D system, phase transitions and conformational transformations of the Langmuir film. A schematic π -A isotherm is shown in Figure 8.1. The experiment is usually

performed by moving a barrier, at a constant rate, to reduce the available surface area per molecule. The behavior of the molecules and the phase transitions in 2-dimension are akin to those in the 3-dimension. As the barrier is moved to reduce the surface area per molecule the monolayer goes from 'gas' phase to 'liquid' phase through a well-defined transition, followed by phase transition to 'solid' phase. The reduction in area beyond the equilibrium spreading pressure (ESP) drives the monolayer into a metastable state from which it relaxes by the nucleation and growth of three-dimensional (3D) structures. This two-dimensional to three-dimensional relaxation phenomenon is referred to as collapse. During collapse a decrease in pressure is observed. The surface pressure at which collapse of a monolayer occurs is characteristic of the film but is also influenced by the temperature, the pH of the sub-phase, past history of the film and the speed of the barrier movement. It is believed that during collapse, molecular layers ride and/or slide on top of each other leading to disordered multilayers accompanied by sudden decrease in surface pressure.

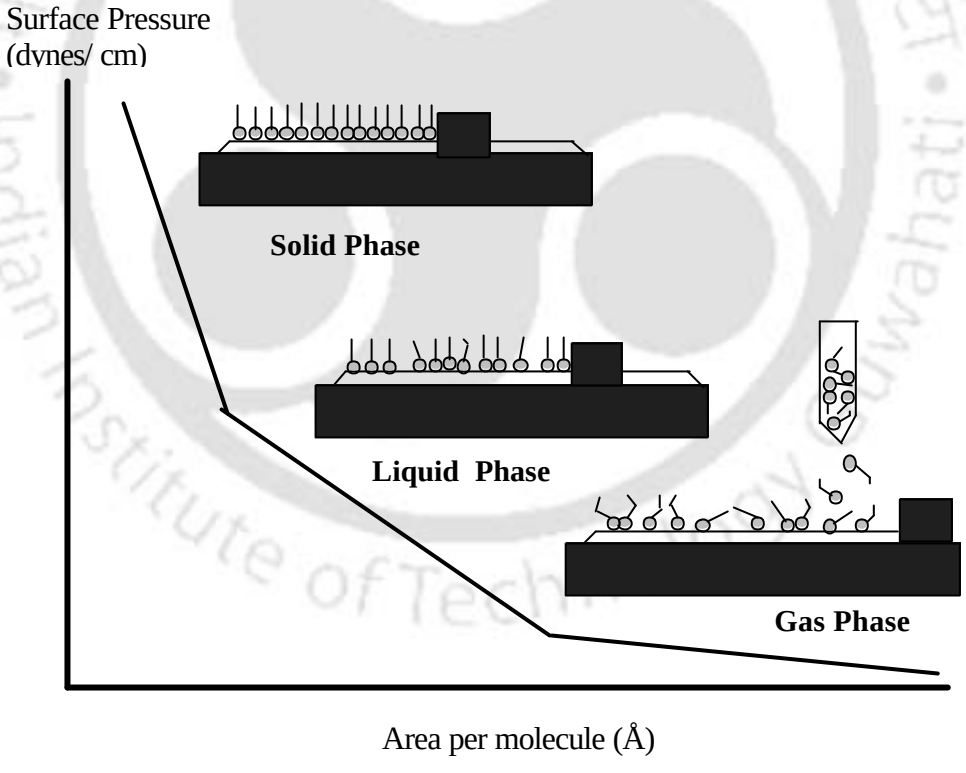

Figure 8.1: A schematic of a typical Pressure–Area isotherm**.** Also depicted are the position of the barrier and the orientation of the amphiphilic molecules at the interface. In gas phase the molecules are randomly oriented. In liquid phase molecules are more ordered than gaseous phase. In solid phase the molecules are closely packed and uniformly oriented.

A large number of methods ranging from light scattering to spectroscopy and microscopy are currently available to study the properties of a monolayer. In-situ surface X-ray diffraction[14-15] and in-situ synchrotron X-ray diffraction[16] studies of self-assembled monolayer (SAM) have been performed. The viscoelastic behavior of an amphiphilic polymer was studied by surface light scattering analysis [17]. Resonance light scattering (RLS) [18-20] is useful in this regard especially with enhanced backscattering of light from thin film[21]. In addition, liquid / liquid interface has been studied by the RLS method [22]. Brewster angle microscopy (BAM) [23] is a powerful tool in probing the detail of a monolayer at air-water interface. A number of systems have been studied using BAM including phospholipids [24], mixed Langmuir monolayers[25-27] and growth of mesostructured silica thin film at air-water interface[28]. Scanning electrochemical microscopy (SECM) [29-30] and scanning electron microscopy (SEM) [31] have also been used observe reaction of amphiphilic molecules at the air-water interface. Other microscopic techniques that have been used to study the properties of monolayer include fluorescence microscopy [32] and fluorescence near-field scanning optical microscopy (FL-NSOM) [33].

Spectroscopic techniques have an advantage over microscopy, as spectroscopic probes are versatile, sensitive and specific. They are also non-destructive and can easily fit to the experimental geometry for *in situ* studies. Additionally, both time dependent and time independent phenomenon occurring at an interface can be studied using various spectroscopic probes. Two spectroscopic probes that are often used are fluorescence[34-35] and UV-visible. The quenching of fluorescence is a major disadvantage in fluorescence spectroscopy at the interface. Simple *in situ* UV-visible probe of interfacial phenomenon can be potentially useful and versatile in areas such as combinatorial surface chemistry[36], assembly of inorganic thin films[37], synthesis and self-assembly of nanoparticles at an interface[38] and generation of two-dimensional colloidal crystals[39]. Knowledge of monolayer collapse condition is vital to obtaining tailor made ordered and defect free monolayers or multilayers films. Further a better and more convenient probe of monolayer collapse would help understand the workings of complex natural surfactant systems such as lung surfactants. This method could in principle be extended to study phenomena occurring at the liquid – liquid interface. We report here a new and simple method of observing two-dimensional phase changes and collapse of Langmuir films using the optical fiber reflection-absorption probe of an UV-visible diode array spectrophotometer. The principle is based on the contribution of scattering in the

extinction coefficient of the medium. When light passes though a turbid and absorbing medium, the sum of absorbance A(ν) and scattering S(ν) is equal to its extinction E(ν) = ε(ν)cl, where ε(ν) is the extinction coefficient, c is the concentration of the species absorbing and scattering and l is the path length in the medium [40].

$$\mathbf{A(}\nu\mathbf{) + S(}\nu\mathbf{) = E(}\nu\mathbf{)}$$

In this chapter we report the observation of collapse of monolayers of stearic acid and 1,2 dipalmitoyl- sn-Glycero 3-[phospho-rac-(1-glycerol)] (DPPG), at the air-water interface. In our approach we have simultaneously observed the conventional pressure area isotherm of a monolayer using a LB film balance and the UV-visible light scattering characteristics of LB films as a function of surface pressure. While the pressure area isotherms indicated various phases and their transition as the surface pressure of the monolayer was increased, the light scattering studies indicated the states of surface molecular layer that had a structure characteristic of collapse. Our observations are that when only stearic acid was used a sharp change in scattering amplitude could be observed at the collapse, just beyond the solid phase. In the study with DPPG lipid, significant changes in the scattering amplitude could be observed at gas – liquid transition as well as prior to the liquid – solid transition. These extinction spectra are typically sharp and they indicate the states of the molecular layer that are not otherwise observable in the conventional pressure area isotherm. Also, our method indicates the presence of collapse like structure at the gas – liquid phase transition that is otherwise not observable in the pressure – area isotherm.

8.2 Experimental Section

A schematic of the experimental setup is shown in Figure 8.2. An Apex - Scientific LB-2000 (Kolkata, India) Langmuir Film Balance equipped with a filter paper Wilhelmy plate, a Teflon trough and a single movable Teflon barrier was used to record the pressure – area isotherm. The output of a Sartorius balance connected to the Wilhelmy plate was taken as proportional to surface pressure and the normalized barrier position was taken to be the surface area in the measurement of a pressure - area isotherm at constant temperature, while the fiber optic reflection - absorption probe of Ocean Optics diode array UV-visible spectrophotometer (model no. SAD-500), placed vertically at the

interface was used to measure the scattering amplitude as a function of surface area occupied by a molecule.

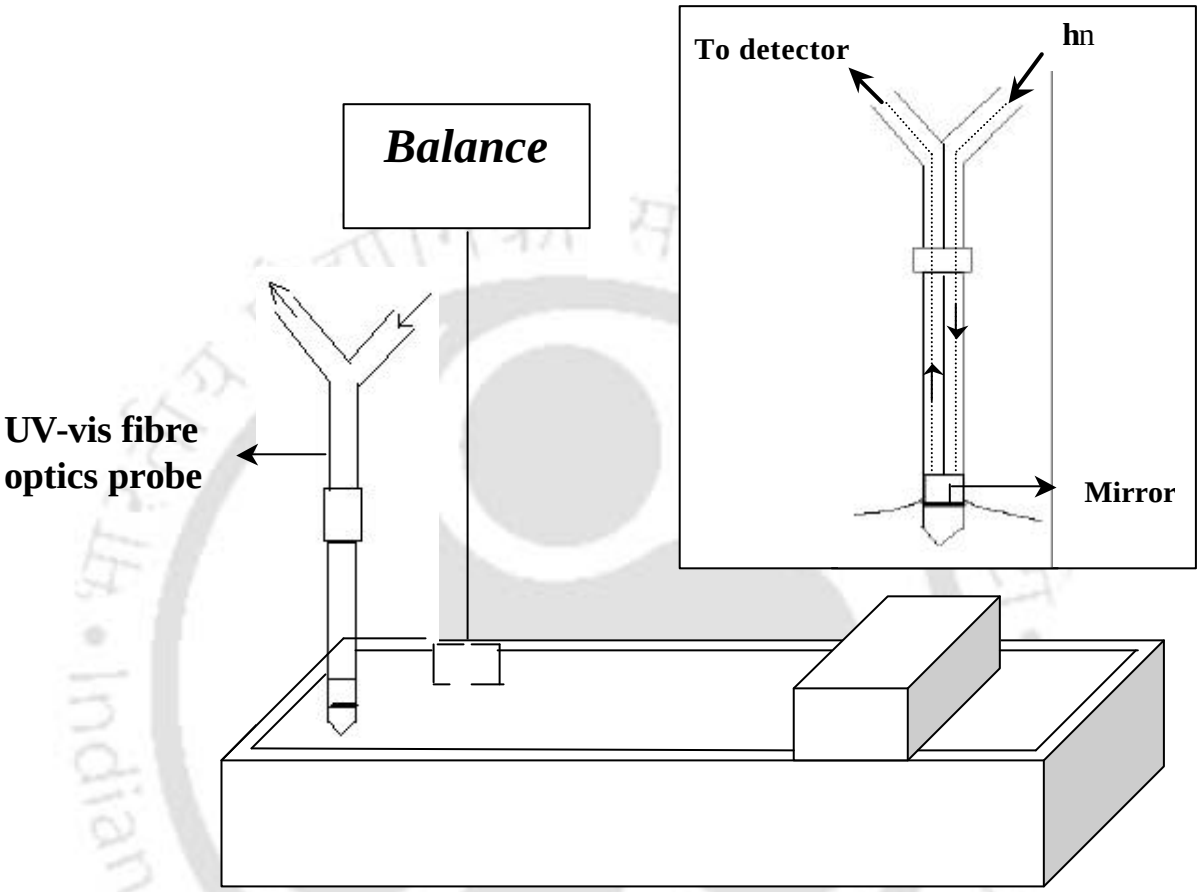

Figure 8.2: A schematic of the experimental setup. The magnified sketch of the optical fiber UV-vis probe used is shown in inset.

The key component of the optical fiber probe used in our experiment is expanded for a better view in the inset of Figure 8.2. In a typical experiment the tip of the probe was placed below the air-water interface such that the mirror had completely immersed in water and was within 1 mm of the interface. Generally a diode-array spectrophotometer uses an array of detectors and a "reverse" optics configuration, that is, the dispersion device comes after the sample, which is useful in minimizing stray light from the surroundings.

The Teflon barrier speed was set at 10 mm / min and was kept constant for all experiments. Stearic acid was purchased from Aldrich Chemical Co. and DPPG lipid was

from Avanti Polar Lipids Inc. The chemicals were used as received. Samples were prepared in $CHCl_3$ HPLC grade (MERK) and added to the trough using a micropipette. Millipore filtered water (resistivity18.2 MΩ cm) or Elix - water (Millipore) was used in the trough. In general time dependent changes in extinction were measured at 5 arbitrary wavelengths (285, 326, 342, 427 and 690 nm) with the spectrophotometer set in the absorption mode. However, other than in Figure 8.3 we show only one of the five spectra recorded at different wavelengths of light, as the spectra were nearly identical except for the exact values of the extinction. The pressure area isotherms and extinction traces were recorded simultaneously by moving the barrier at a speed of 10 mm / min.

8.3 Result and discussion

In a LB film balance as the surface area available per molecule is gradually decreased, the measured pressure of the two-dimensional monolayer of molecular assembly increases, indicating the presence of a phase, its behavior and phase transitions in two dimensions. These appear as regions of different slopes in a plot of surface pressure versus area available to each molecule. As expected, the pressure is the lowest at the maximum available area, which is generally the two-dimensional analog of gas phase behavior. As the area is decreased a change in slope occurs indicating a phase transition to liquid phase, which is generally more ordered than the gas phase. Again a phase transition occurs at higher pressures, which is indicated by change in the slope. Further decrease in the available area leads to the sudden decrease in the surface pressure indicating the loss of the monolayer. A common substance generally used for a case study at the air-water interface is stearic acid. As shown in the Figure 8.3, the pressure-area isotherm of stearic acid (serrated line) used in our experiment passes through all of the above mentioned phases. On the other hand, the optical extinction as a function of available area per molecule of stearic acid exhibited a completely different behavior. As shown in Figure 8.3 (normal lines), there was no observable extinction of light due to reduction of available area all through the gas, liquid and beyond the transition to the solid phase. However, well into the solid phase and just prior to the collapse of the monolayer, a sharp increase followed by immediate and sudden decrease in extinction could be observed. The extinction of light was roughly the same when measured at different wavelengths of light, for example at 285, 326, 342, 427 and 690 nm.

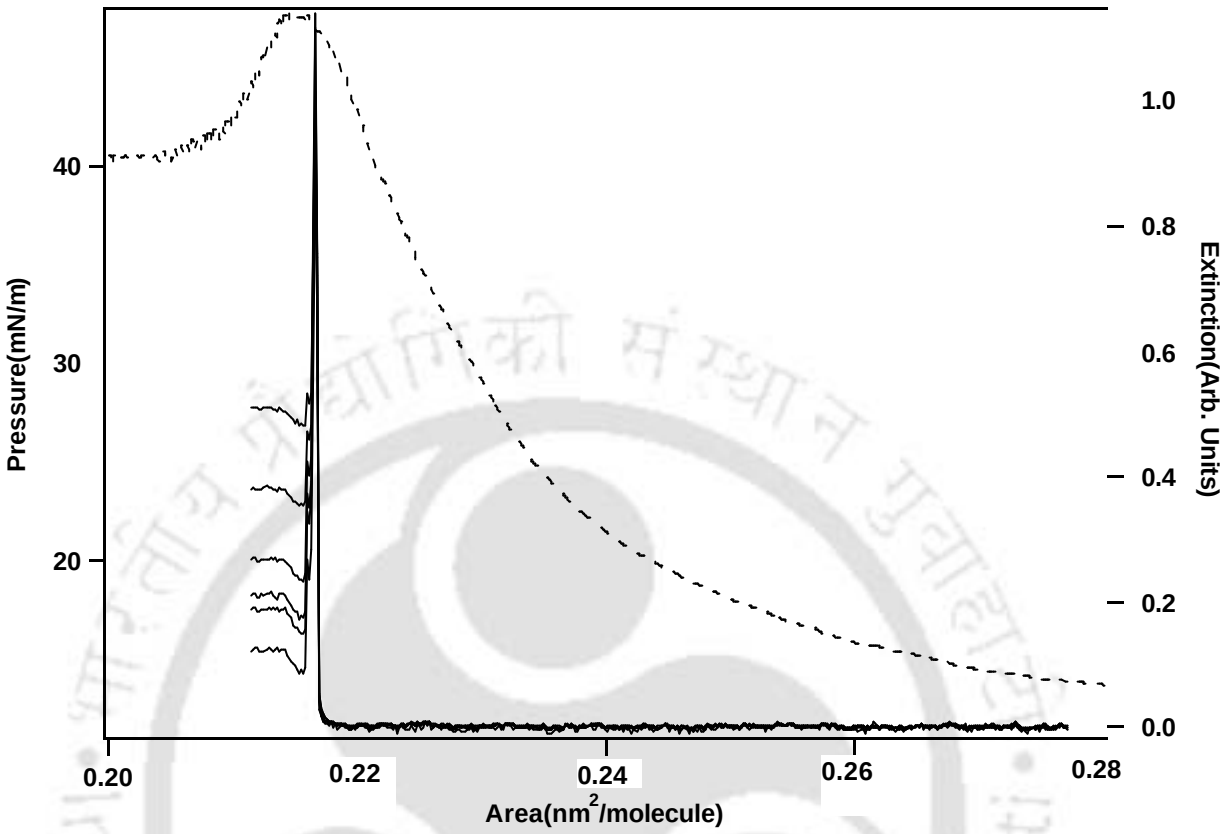

Figure 8.3: Pressure-area isotherm by the Wilhelmy plate method (------) and UV-vis optical fiber probe extinction spectra (——) recorded simultaneously for stearic acid at five different wavelengths.

As can be seen in Figure 8.3 there is significant difference in background extinction observed after collapse for observations at different wavelengths. However, there were proportional differences in extinction values at near collapse. In other words, the difference in extinction between the peak and baseline after collapse was the same for all wavelengths. It is important to note here that in conventional LB film balance definite information about two-dimensional phases and their transitions and finally collapse of a monolayer could be obtained. On the other hand the case study with stearic acid indicates that information about phases and transitions from one phase to the other could not be observed for a monolayer film, at the interface, by following the extinction of light. However, there is an important difference in observations between the two methods. In LB film balance measurements the observation indicates that collapse of the monolayer is a relatively slower process. There is no indication of additional structure formation during

the process of collapse from the solid state. The optical extinction measurement, on the other hand, indicates the presence of a special feature just before the collapse. There are several mechanisms that have been proposed to explain the collapse of a monolayer. A monolayer may undergo buckling before it finally collapses. Multiple layer formation followed by migration of layers into the subphase may lead to the collapse of the monolayer. In addition, structure formation (spherical or other assemblies) followed by dissolution in the subphase may lead to the collapse of a monolayer. Electron microscopic investigations have shown the formation of stable ridges in a collapsing monolayer. Such a formation is schematically shown in Figure 8.4.

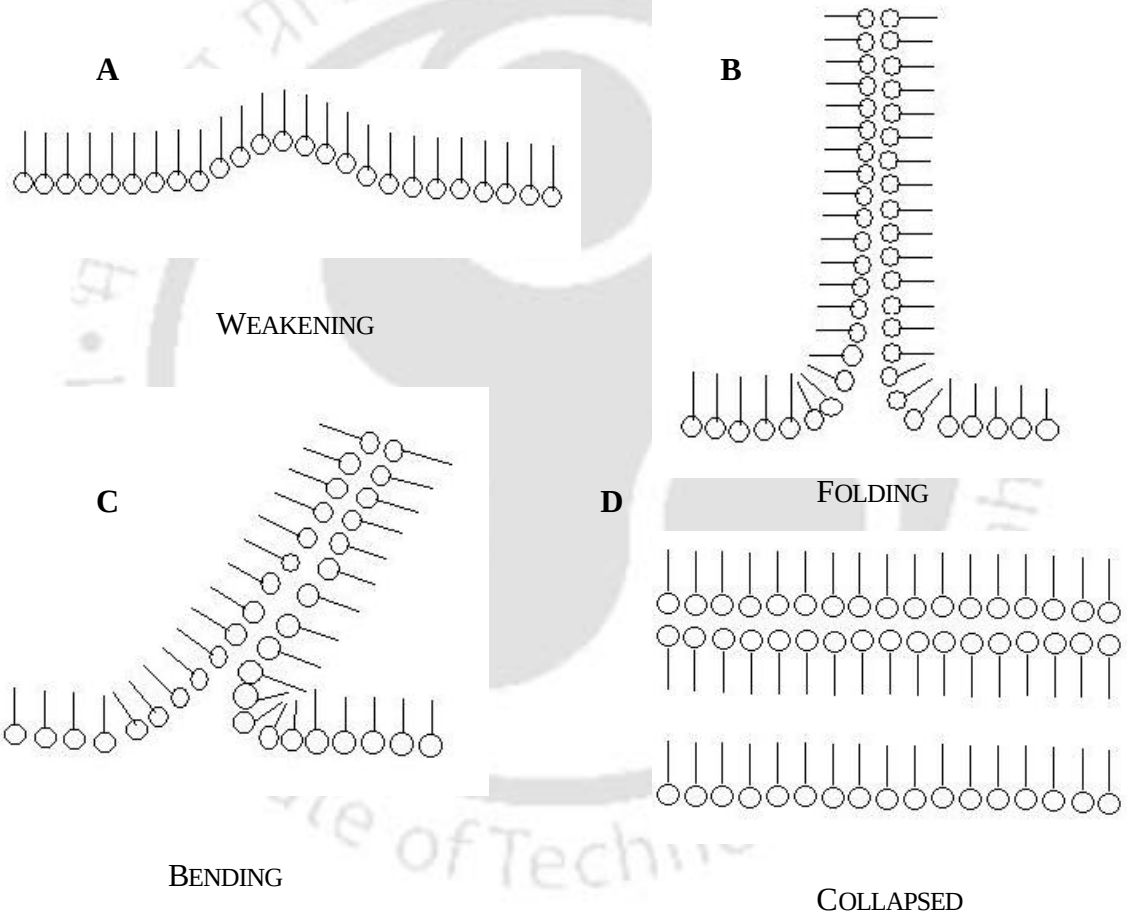

Figure 8.4: Schematics of mechanisms of monolayer collapse.

The conventional method of measuring pressure-area isotherm does not indicate any special structure formation between the transition to the solid phase and collapse of the monolayer. However, our observation suggests that after liquid to solid phase transition, when available surface area per molecule is further decreased, there is the formation of a structure that is responsible for the extinction of light, and the structure may

possibly be different from a regular solid phase structure. This is evidenced by a sharp rise and fall of the extinction of light compared to slow evolution of pressure when area available per molecule was decreased after the liquid to solid phase transition. The extinction is possibly due to enhanced scattering of light because of the formation of ridges. At the collapse of the monolayer, the surface probably looses parts of these structures by dissolution in the subphase (in the form of structures like micelles) or multiple layer formation and hence the extinction goes down.

We were further interested to probe whether the structure responsible for the extinction of light before the collapse of the monolayer was transient or a stable one. To pursue this we moved the LB barrier to reduce the area occupied per molecule up until the extinction was significantly high (area occupied per molecule was about 0.18 $Å^2$). Pressure-area isotherm was simultaneously recorded by the film balance.

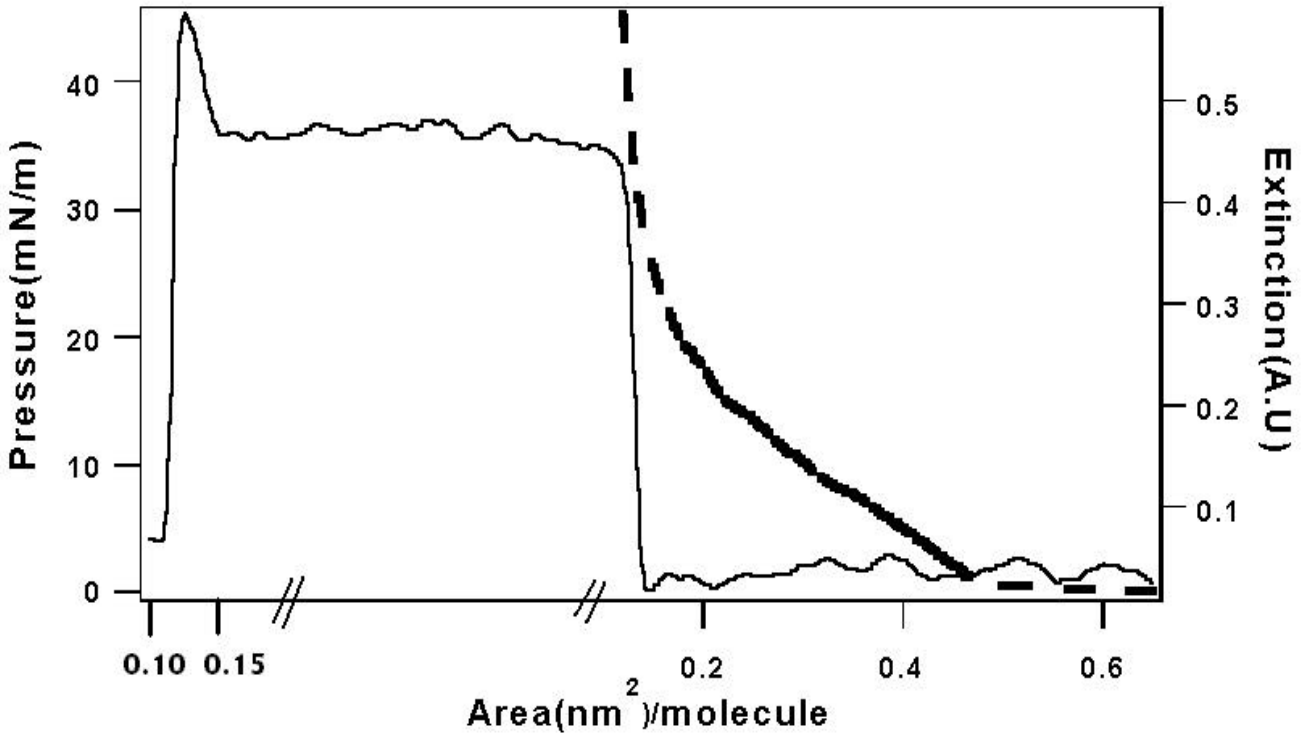

Figure 8.5: Simultaneously measured pressure – area isotherm (------) and UV – visible extinction trace (——) of stearic acid with the barrier stopped at 0.18 nm^2 / molecule for 25 minutes and then restarted for observing the subsequent collapse. The extinction trace was recorded at 427 nm.

We then stopped the barrier at this point and continued monitoring the extinction coefficient as a function of time. We did not observe any significant change in the extinction coefficient for twenty-five minutes. The barrier was moved further to reduce

the area. An increase in extinction was observed followed by sudden decrease in the coefficient just like the regular one observed while moving the barrier continuously till the collapse. The results are shown in Figure 8.5 measured at the wavelength of 427 nm. Thus our observation shows that the structure of the monolayer formed after liquid to solid phase transition and that is responsible for sudden rise in extinction of light is stable for a long time at constant pressure. This structure vanishes due to further decrease of available area. It may be mentioned here that our observation is similar to that of Reis [41] where he reported the formation of stable ridges in fatty acid monolayer at the air-water interface. Similar observations were reported by Ybert et. al. [42] with respect to the formation of stable "folds" in fatty acid monolayers. Finally, the wavelength independent extinction of light also supports the idea of formation of ridge-like structures that would lead to scattering of light independent of wavelength.

We were further interested to carry out similar experiments with lipids, the systems that have been intensely investigated owing to their applications in biomimetic systems as well as electronic devices. Also, previous experiments have shown the occurrence of phase separation in mixtures of lipids and lipid bilayers. We noticed that with our experimental setup we could not observe gas-liquid and liquid-solid phase transitions in the same run. This is because of wide separation between the available area per molecule required for gas-liquid phase transition and that for liquid-solid phase transition. To circumvent this problem we performed two experiments. The first one was performed by initially pouring 200 µL of 0.75mg/mL of the lipid solution while the second one was performed by initially pouring 125 µL of 0.75mg/mL on the interface. We observed liquid-solid phase transition as well as collapse in the first case while we observed gas-liquid phase transition in the second experiment, although we were past the phase transition but not the collapse of the monolayer. The results are shown in Figure 8.6. and Figure 8.7 respectively. The extinction of light by DPPG, however, is a little different from that due to stearic acid. For example, as clear from Figure 8.6, the extinction of light starts right at the liquid-solid phase transition (with area occupied per molecule is about 0.22 $Å^2$) and the extinction spectrum is broad compared to that of stearic acid. This means that for the case of the lipid, the ridges or the structure responsible for the extinction of light starts appearing at the transition rather than after the transition. The structures are quite stable for a wider range of compression compared to that of the acid.

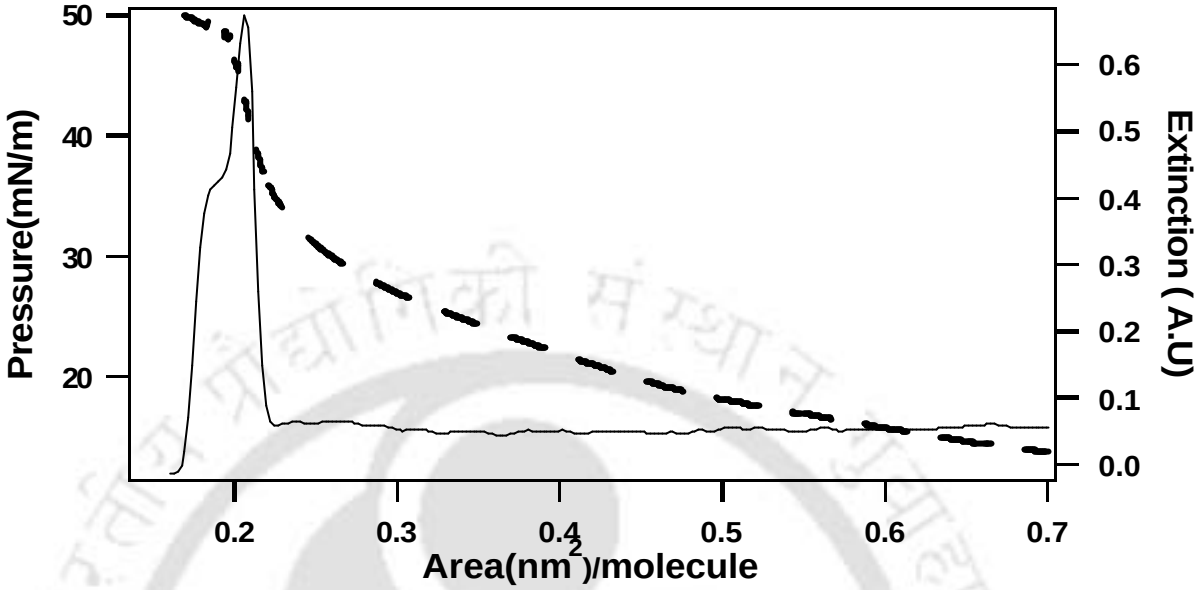

Figure 8.6: Simultaneously measured pressure area isotherms (-----) and UV – vis extinction traces (———) of monolayers of DPPG lipid at high initial lipid concentration The extinction traces were recorded at 690 nm.

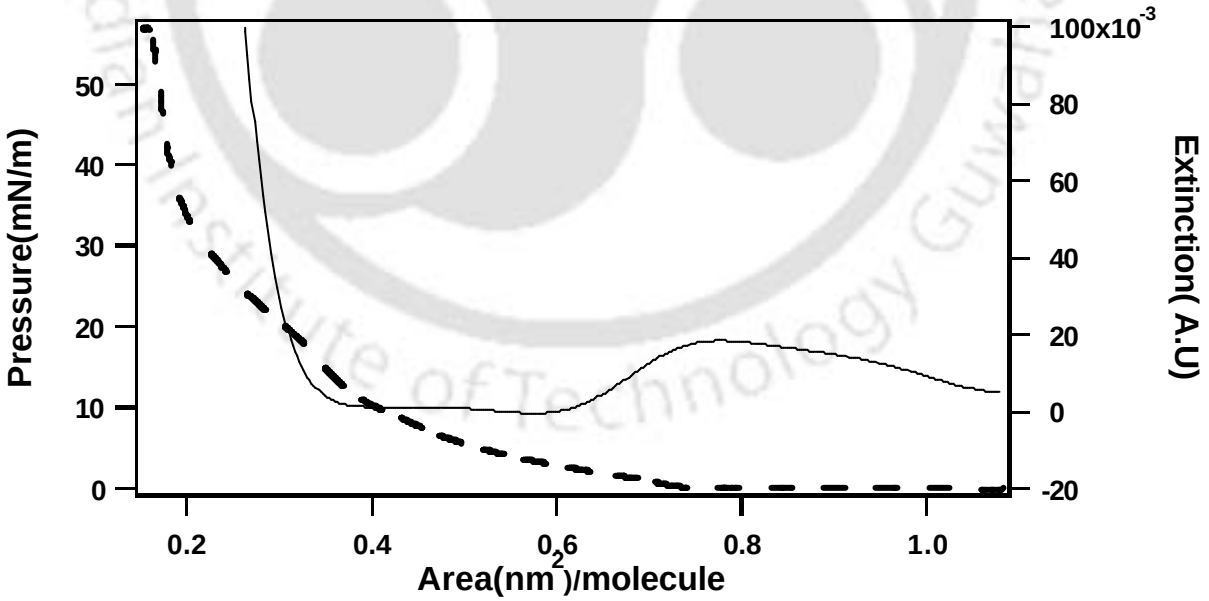

Figure 8.7: Simultaneously measured pressure area isotherms (-----) and UV – vis extinction traces (———) of monolayers of DPPG lipid at low initial lipid concentration. The extinction traces here too were recorded at 690 nm.

It is even more interesting to note that we also observed a broader extinction of light (Figure 8.7) during compression in the gas phase as well as at the gas-liquid phase transition occurring in the range of 1.1 to 0.6 $Å^2$ per molecule. Thus our observation indicates the presence of ridges or similar structures even at the gas and liquid phases and at their transition point. This however could not be ascertained from the mere observation of pressure-area isotherm in the LB film balance. In addition, Figure 8.7 also indicates that when lower initial concentration of the lipid was used there was extinction of light even at the surface pressure below the liquid to solid phase transition. For example, the extinction of light started occurring at an available area of 0.36 Å per molecule whereas the phase transition occurred at an area of 0.21 Å. On the other hand with the higher starting lipid concentration the phase transition occurred simultaneously with extinction of light (structure formation) at an area per molecule of 0.22 Å. These observations indicate that structures responsible for the extinction of light are formed at various points of phases and their transitions. The broadness of the nature of the extinction spectra indicates that the structures are stable over a wide range of surface pressures.

8.4 Conclusion

In this chapter we have reported the development of a simple UV-visible optical fiber probe method that can be used to observe extinction of light due to structure formation like ridges, domains and folds mainly during the transition from solid phase to collapse of a two-dimensional Langmuir monolayer. In stearic acid the observation suggests the formation of stable ridges or folds that are stable for a long time under constant surface pressure but however exists within a narrow range of surface pressure (that is surface area occupied per molecule). Our observations with DPPG lipid suggests that structures formed in the lipid that are responsible for the extinction of light are quite stable over a larger range of pressures. In addition, our observations indicate the presence of similar structures in the gas phase up until the phase transition to the liquid phase. Further, the pressure – area isotherm indicates phase transitions at nearly the same area available per molecule for both higher as well as lower initial lipid concentration. On the other hand the extinction spectra indicate structure formation at various points in all phases as well as during the phase transitions.

Observation of time invariant extinction (higher than the baseline) at constant pressure before collapse indicates that the monolayer before collapse has an equilibrium

structure. In other words structures that are responsible for the enhancement in scattering of light are equilibrium structures at a constant pressure. It may be noted here that a normal pressure – area isotherm of a Langmuir monolayer does not indicate the details of structures present at various phases and phase transitions. Various sophisticated and expensive microscopic techniques can indicate the exact nature of the film constituting the monolayer at various surface pressures. On the other hand we have demonstrated that a simple optical fiber probe is sufficient to indicate the presence of structures responsible for enhanced light scattering at various phases and during phase transitions. In addition, the present technique could be useful in understanding the nature of the monolayer in cases where in situ microscopy cannot be performed. It is possible to extend this simple technique to studying the structures at liquid-liquid interfaces by placing the probe at the appropriate region, where microscopic imaging may prove more challenging.

8.5 References

1. Hu, J.; Zhang, J.; Liu, F.; Kittredge, K.; Whitesell, J. K.; Fox, M. A. *J. Am. Chem. Soc.* **2001,** 123, 1464.
2. Shimazu, K.; Kawaguchi, T.; Isomura, T. *J. Am. Chem. Soc.* **2003,** 124, 652.
3. Jeon, N. L.; Nuzzo, R.G.; Xia, Y.; Mrksich, M.; Whitesides, G. M. *Langmuir* **1995,** 11, 3024.
4. Fan, S.; Chapline, M. G.; Franklin, N. R.; Tombler, T. W.; Cassell, A. M.; Dai, H. *Science.* **1999,** 283, 512.
5. Cohen, Y.; Hatton, B.; Miguez, H.; Coombs, N.; Fournier-Bidoz, S.; Grey, J. K.; Beaulac, R.; Reber, C.; Ozin, G. A. *Adv. Matter.* **2003,** 15, 572.
6. Wu, L-Q.; Yi, H.; Li, S.; Rubloff, G. W.; Bentley, W. E.; Ghodssi, R.; Payne, G. F. *Langmuir* **2003,** 19, 519.
7. Meldrum, F. C.; Flath, J.; Knoll, W. *Langmuir* **1997,** 13, 2033.
8. Avey, A.A.; Hill, R. H. *J. Am. Chem. Soc* **1996**, 118, 237.
9. Ikeda, S.; Akamatsu, K.; Nawafune, H. *Journal of Materials Chemistry* **2001**, 11, 2919.

10. Wallraff, G. M.; Hinsberg, W. D. *Chem Rev*. **1999,** 99, 1801.

11. Xia, Y.; Whitesides, G. M. *Angew. Chem. Int. Ed.* **1998,** 37, 550.

12. Roberts, G. *Langmuir-Blodgett Films ,Plenum Press, New York,* **1990.**

13. Ulman, A. *An introduction to Ultrathin Organic Films from Langmuir-Blodgett to Self Assembly,* Academic Press, Inc. San Diego, **1991.**

14. Durbin, M. K.; Malik, A.; Richter, A. G.; Huang, K. G.; Dutta, P. *Langmuir,* **1997**, 13, 6547.

15. Schreiber, F.; Gerstenberg, M. C.; Dosch, H.; Scoles, G. *Langmuir* **2003,** 19, 10004.

16. Ball, M. J.; Lucas, C. A.; Markovic, N. M.; Stamenkovic, V.; Ross, P. N. *Surf. Sci.* **2002,** 518, 201.

17. Esker, A. R.; Zhang, L-H.; Sauer, B. B.; Lee, W.; Yu, H. *Colloid Surf. A* **2000,** 171, 131.

18. Pasternack, R. F.; Collings, P. J. *Science,* **1995,** 269, 935.

19. Pasternack, R. F.; Bustamante, C.; Collings, P. J.; Giannetto, A.; Gibbs, E. J. *J. Am. Chem. Soc*. **1993,** 115, 5393.

20. Collings, P. J.; Gibbs, E. J.; Starr, T. E.; Vafek, O.; Yee, C.; Pomerance, L. A.; Pasternack, R. F. *J. Phys. Chem B.* **1999,** 103, 8474.

21. Leskova, T. A.; Chaikina, E. I.; Navarrete, G.; Martinez-Niconoff, G. *Phys. Rev. B* **1999,** 59, 11062.

22. Pang, X. B.; Huang, C. Z.; Li, Y. F.; Lu, W. *Bull. Chem. Soc. Jpn.*, **2003,** 76, 1941.

23. Minones, J.Jr.; Carrera, C.; Dynarowicz-Latka, P.; Minones, J.; Conde, O.; Seoane, R.; Rodriguez Patino, J. M. *Langmuir,* **2001,** 17, 1477.

24. Kubo, I.; Adachi, S.; Maeda, H.; Seki, A. *Thin Solid Film* **2001,** 393, 80.

25. Vila-Romeu, N.; Nieto-Suarez, M.; Dynarowicz-Latka, P.; Prieto, I. *J. Phys. Chem B* **2002,** 106, 9820.

26. Teer, E.; Knobler, C. M.; Braslau, A.; Daillant, J.; Blot, C.; Luzet, D.; Goldmann, M.; Fontiane, P. *J. Chem. Phys.* **2000,** 113, 2846.

27. Munoz, M.; Deschenaux, R.; Coleman, A. W. *Journal of Physical Organic Chemistry,* **1999,** 12, 364.

28. Edler, K. J.; Roser, S. J.; Mann, S. *Chem. Commun.* **2000,** 773.

29. Zhang, J; Slevin, C. J.; Morton, C; Scott, P; Walton, D. J.; Unwin, P. R. *J. Phys. Chem B* **2001,** 105, 11120.

30. Zhang, J; Unwin, P. R *Langmuir* **2002**, 18, 1218.

31. Meine, K.; Vollhardt, D.; Weidemann, G. *Langmuir* **1998,** 14, 1815.

32. Volinsky, R.; Gaboriaud, F.; Berman, A.; Jelinek, R. *J. Phys. Chem B.* **2002**, 106, 9231.

33. Cordero, S. R.; Weston, K. D.; Buratto, S. K. *Thin Solid Films.***2000,** 360, 139.

34. Yamazaki, I.; Tamai, N.; Yamazaki, T. *J. Phys. Chem.* **1987,** 91, 3572.

35. Dutta, A. K.; Salesse, C. *Langmuir,* **1997,** 13, 5401.

36. Huo, Q.; Sui, G.; Kele, P.; Leblanc, R. M. *Angew. Chem. Int. Ed.* **2002**, 39, 1854.

37. Akshay, I. A.; Trau, M.; Manne, S.; Honma, I.; Yao, N.; Zhou, L.; Gneter, P.; eisenberger, P. M.; Gruner, S. M. *Science* **1996,** 273, 892.

38. Li, M.; Schnablegger, H.; Mann, S. *Nature* **1999,** 402, 393.

39. Ramos, L.; Lubensky, T. C.; Dan, N.; Nelson, P.; Weitz, D. A. *Science* **1999**, 286, 2325.

40. Micali, N.; Mallamace, F.; Castriciano, M.; Romeo, A.; Scolaro, L. M. *Anal. Chem***. 2001**, 73, 4958.

41. Ries Jr. *Nature* **1979,** 281, 287.

42. Ybert, C.; Lu, W.; Möller, G.; Knobler, C. M. *J. Phys. Chem. B.* **2002,** 106, 2004.

Color Plates

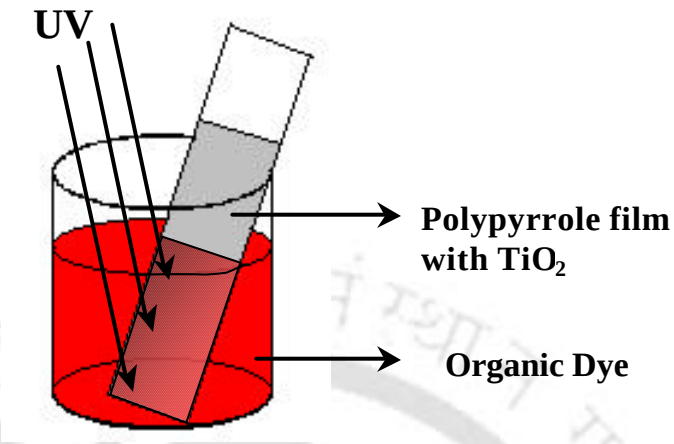

Figure 4.1: The general strategy adopted in studying the photocatalyst properties of the polypyrrole film embedded with TiO_2 NPs. *(Page 56)*

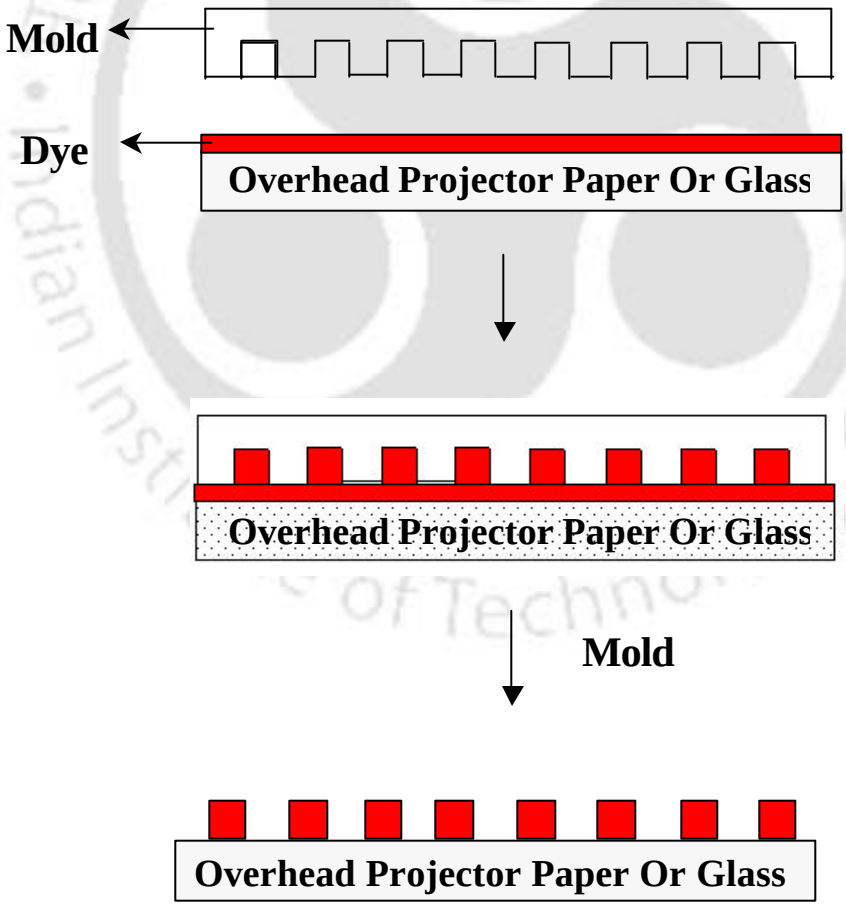

Figure 5.3: A scheme of the present method of imprinting pattern. *(Page 73)*

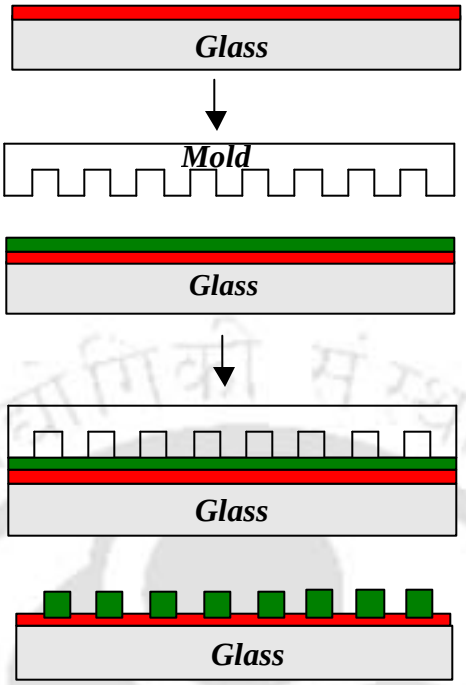

Figure 5.4: Imprinting bi-color pattern using scheme 1. *(Page 75)*

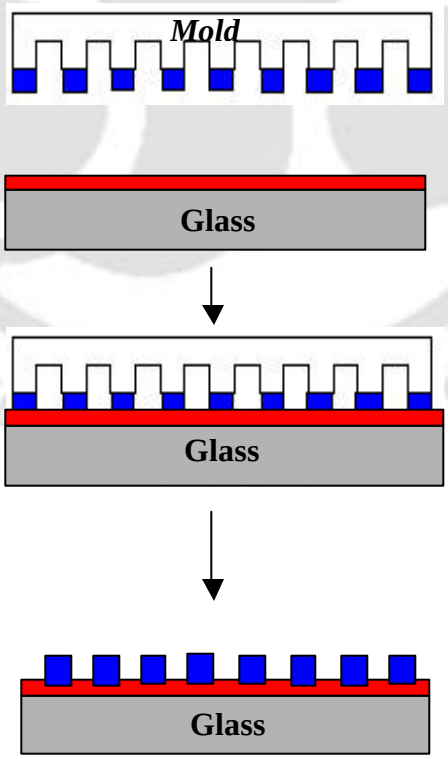

Figure 5.5: Imprinting bi-color pattern using scheme 2. *(Page 76)*

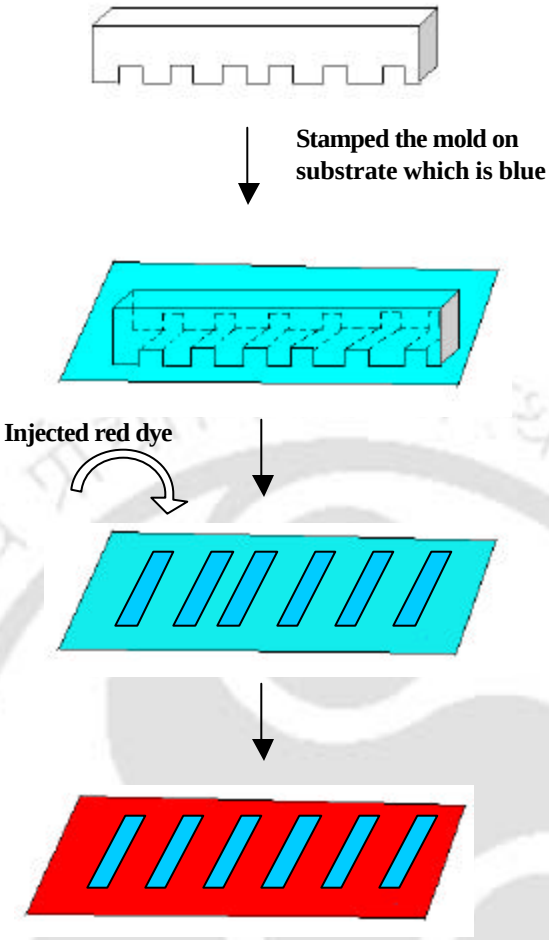

Figure 5.6: Imprinting bi-color pattern using scheme 3. *(Page 77)*

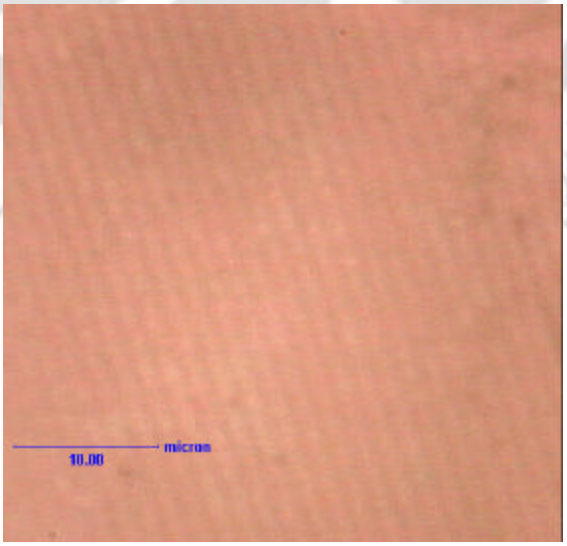

Figure 5.9: Optical micrograph of the bi-color lines obtained using scheme 1: green on red recorded in reflection mode of the microscope. *(Page 81)*

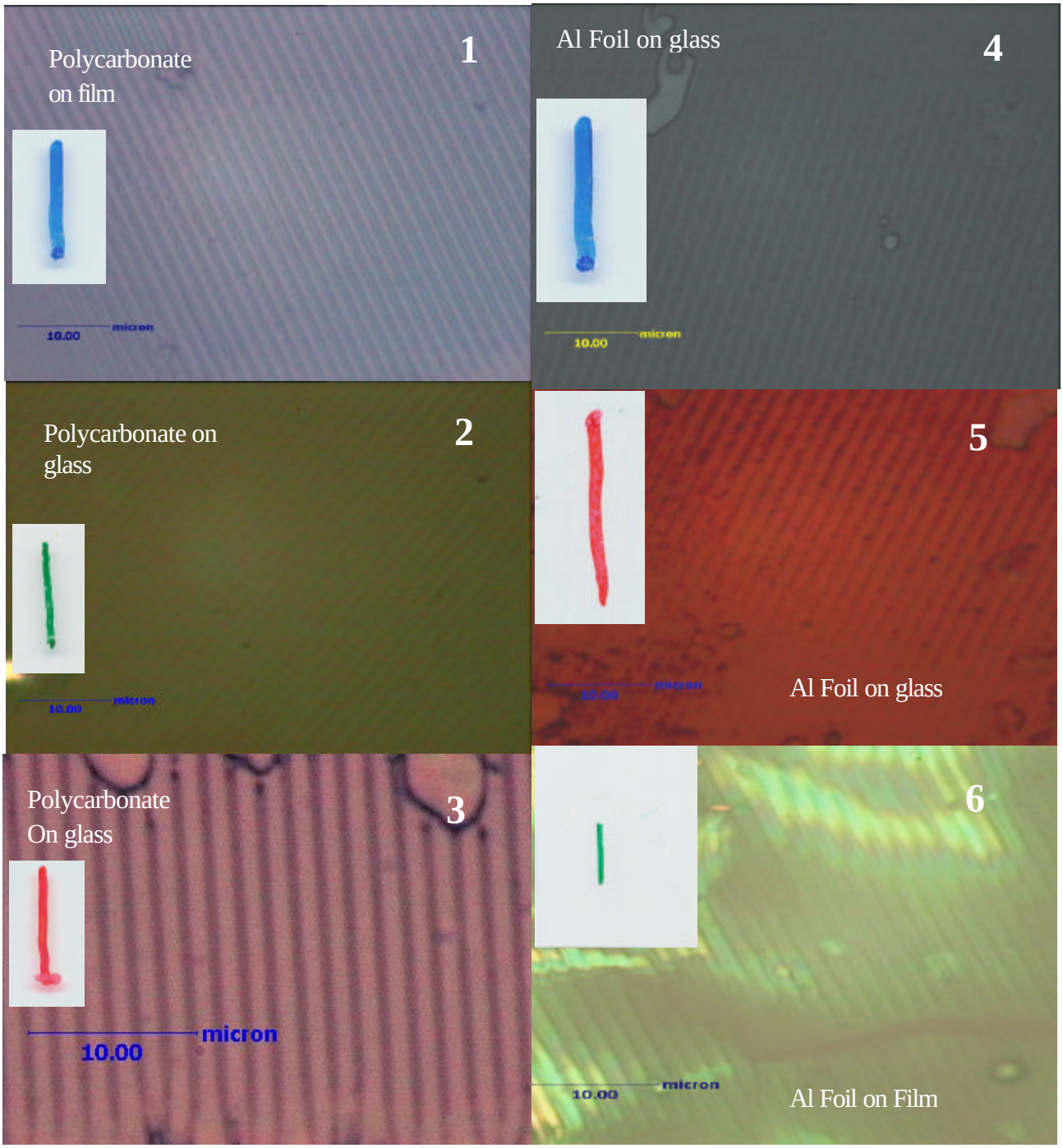

Figure 5.7: Patterns using polycarbonate (**1, 2, 3**) as molds and Al foil (**4, 5, 6**) as mold on OHP film and microscope glass slides. Insets are the pictures of lines, of about 1 mm width, that have the patterns imprinted on them by the molds. The macroscopic pictures were recorded by an EPSON Perfection 610 scanner. *(Page 79)*

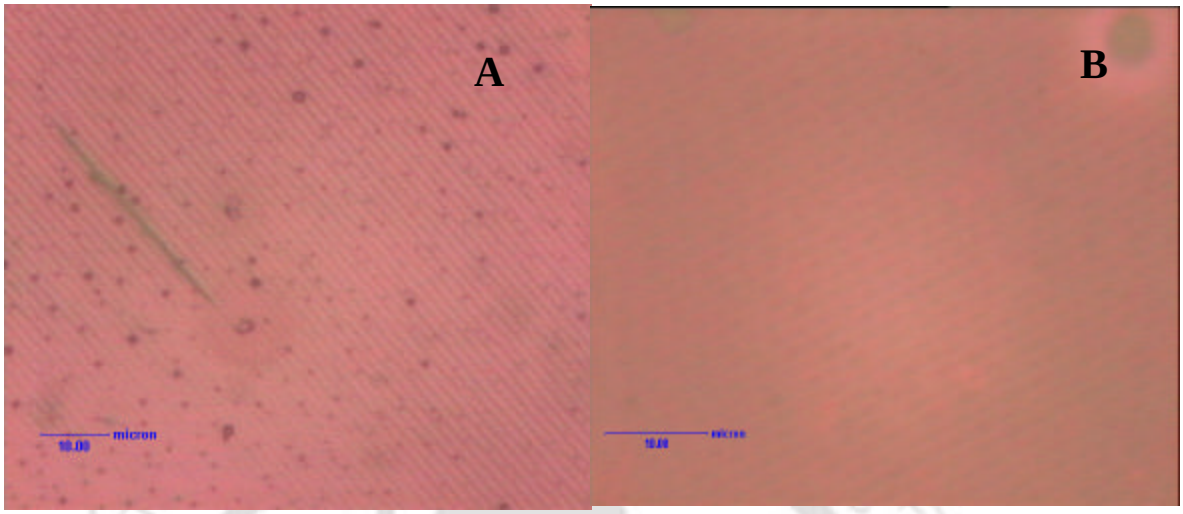

Figure 5.10: Optical micrograph of the bi-colour line obtained using scheme 2; (A) blue on red taken in transmittance mode (B) Green on Red taken in reflection mode. *(Page 82)*

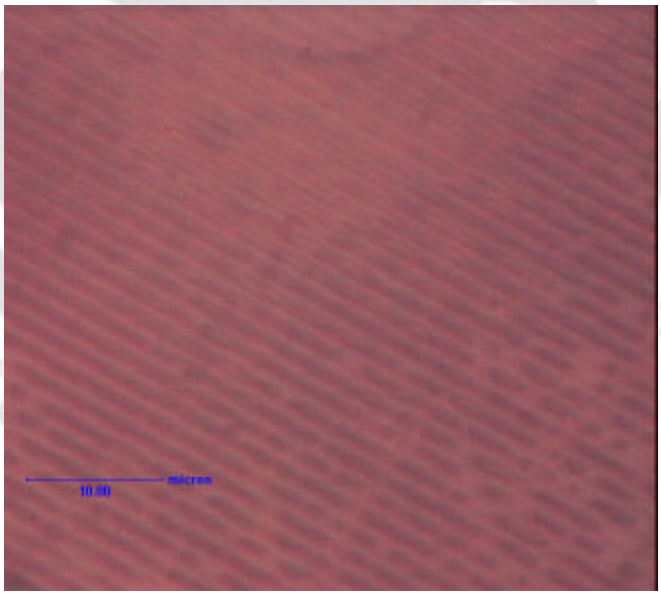

Figure 5.11: Optical micrograph of the bi-colour line obtained using scheme 3, blue line with injected red ink. The micrograph was recorded in reflection mode. *(Page 83)*

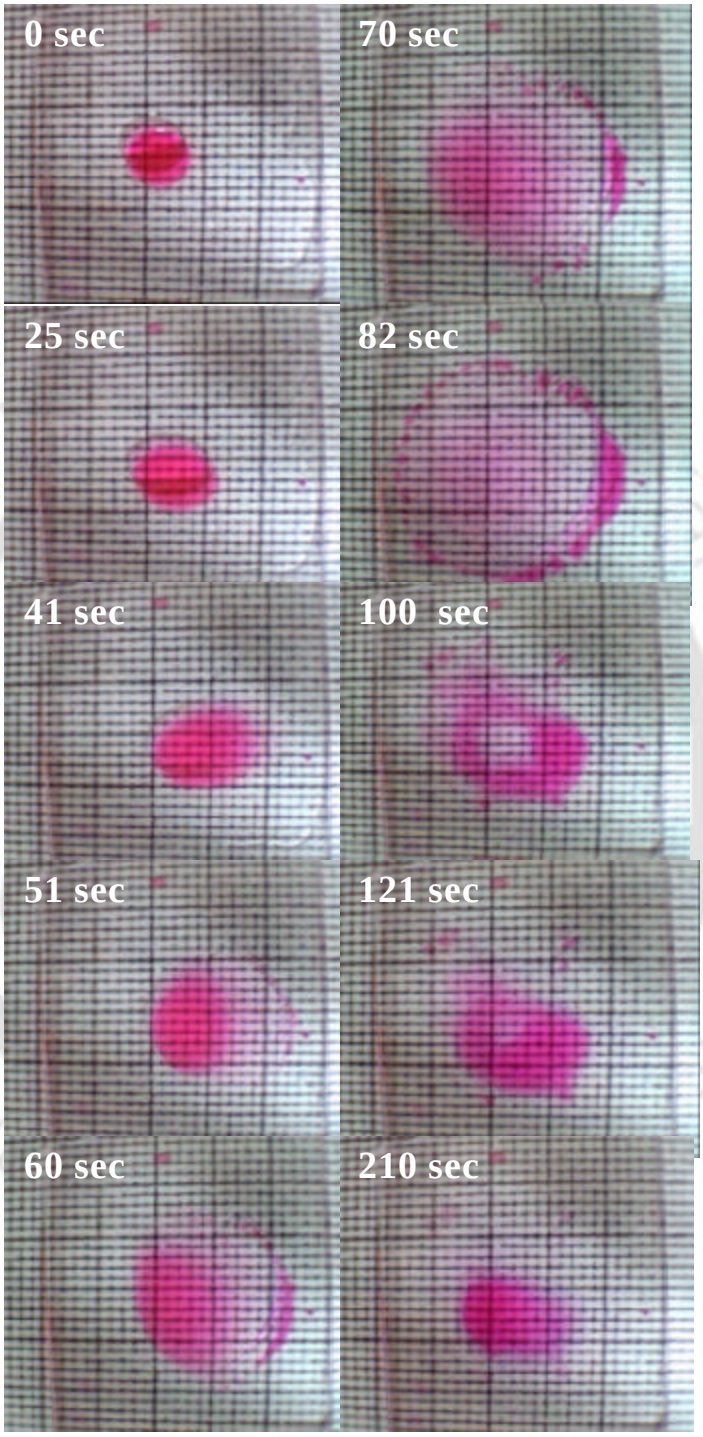

Figure 7.3: WEB camera shots of time dependent spread and recoil of an aqueous surfactant drop over i-PrOH film. The concentration of SDS in the drop was 32 mM. These are selected pictures representing the fate of the drop. The background squares are from an ordinary graph paper placed underneath the glass plate. *(Page 108)*

List of Publications

1. Spreading and Recoil of a Surfactant Containing Water Drop on Glass Supported Alcohol Films, **Devasish Chowdhury**, Surya Protim Sarkar, Dipankar Kalita, Tridib Kumar Sarma, Anumita Paul and Arun Chattopadhyay *Langmuir,* **2004**, 20, 1251.
2. Patterning Sub-micron scale Channel Structures on Glass by Chemical Etching, **Devasish Chowdhury,** Anumita Paul, Arun Chattopadhyay *Indian Journal of Physics* **2004** (in press).
3. Fabrication of Submicron Scale Patterned Plastic Thin Film Fluidic devices with controllable Thickness, Pompi Hazarika, **Devasish Chowdhury** and Arun Chattopadhyay *Lab on a chip,* **2003,** 3, 128.
4. Macroscopic and Mesoscopic Pattern Observed in Thin Films Formed due to Polymerization of Aniline at the Air-Water Interface **Devasish Chowdhury,** Anumita Paul **and** Arun Chattopadhyay**,** *Journal of Colloid and Interface Science* **2003,** 265, 70.
5. Spin Coating of Thin Films of Polystyrene as an Advanced Undergraduate Experiment, Mriganka Chakraborty**, Devasish Chowdhury** and Arun Chattopadhyay**,** *The Journal of Chemical Education* **2003,** 80, 806
6. Synthesis of Au nanoparticle-conductive polyaniline composite using H_2O_2 as oxidising as well as reducing agent**,** Tridib Kumar Sarma**, Devasish Chowdhury,** Anumita Paul and Arun Chattopadhyay**,** *Chemical Communication* **, 2002,** 1048.
7. Lithography by Simultaneous Chemical and Photochemical Polymerization of Aniline at the Air-Water Interface**, Devasish Chowdhury,** Anumita Paul, and Arun Chattopadhyay, *The Journal of Physical Chemistry B,* **May 2002,** 4343
8. Patterning Design in Color at the Submicron Scale**, Devasish Chowdhury,** Anumita Paul, and Arun Chattopadhyay **,** *Nano Letters,* **2001,** 409**.**

Patent

1. Filed a US patent in 2002 on the invention entitled " COLORED NANOLITHOGRAPHY ON GLASS AND PLASTIC SUBSTRATE " **Devasish Chowdhury,** Anumita Paul, and Arun Chattopadhyay